Delft University of Technology

On the dynamics of non-planar thin liquid films

Shah, M.S.

DOI
10.4233/uuid:d58185c6-1630-4e4a-a60a-be878f54e7fa

Publication date
2020

Document Version
Final published version

Citation (APA)
Shah, M. S. (2020). *On the dynamics of non-planar thin liquid films*. [Dissertation (TU Delft), Delft University of Technology]. https://doi.org/10.4233/uuid:d58185c6-1630-4e4a-a60a-be878f54e7fa

Important note
To cite this publication, please use the final published version (if applicable).
Please check the document version above.

Copyright
Other than for strictly personal use, it is not permitted to download, forward or distribute the text or part of it, without the consent of the author(s) and/or copyright holder(s), unless the work is under an open content license such as Creative Commons.

Takedown policy
Please contact us and provide details if you believe this document breaches copyrights.
We will remove access to the work immediately and investigate your claim.

This work is downloaded from Delft University of Technology.
For technical reasons the number of authors shown on this cover page is limited to a maximum of 10.

ON THE DYNAMICS OF NON-PLANAR THIN LIQUID FILMS

MAULIK SHAH

ON THE DYNAMICS OF NON-PLANAR THIN LIQUID FILMS

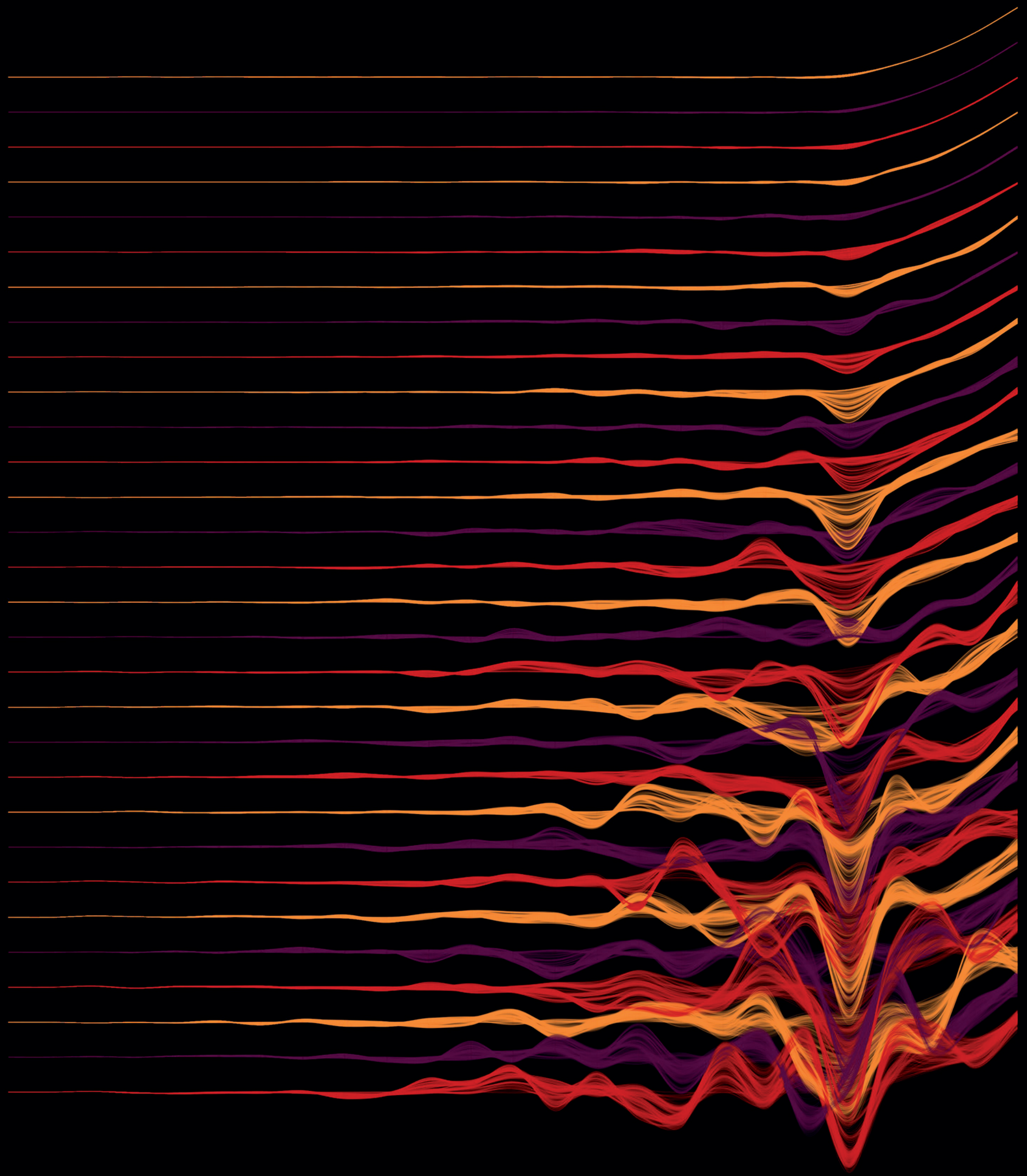

MAULIK SHAH

INVITATION

To the public defence of my doctoral thesis:

ON THE DYNAMICS OF NON-PLANAR THIN LIQUID FILMS

The defence ceremony is to be held on
September 8, 2020
(Tuesday)
at
1500 hrs
in the
Senaatszaal
of the
Aula,
TU Delft, Mekelweg 5, Delft.

*Prior to the defence, at **1430 hrs**, I will give a brief introduction to my PhD research.*

MAULIK SHAH
maulikshah1009@gmail.com

BK
547179-L-sub01-os-Shah
Processed on: 12-8-2020

Stellingen

behorende bij het proefschrift

On the dynamics of non-planar thin liquid films

Maulik S. Shah

1. Het berekenen van de deterministische dunnefilmvergelijking met een aanvankelijke witte ruisverstoring is een kosteneffectievere manier om de levensduur van de film te bepalen dan een stochastische dunne-filmoplosser.
   Hoofdstuk 3 van dit proefschrift
2. Het voorspellen van de filmlevensduur op basis van numerieke integratie van de stochastische dunnefilmvergelijking is sterk afhankelijk van de tijdstapgrootte wanneer de upwindingconcepten worden gebruikt in de convectieveruisterm.
   Grün et al., 2006
3. Schalingswetten uit de literatuur die de levensduur van dunne films relateren aan hun radii, zijn ongeldig voor films met grote radii.
   Manev et al., 1997
4. De sterkte van ruis is belangrijker dan zijn functionele vorm bij het in kaart brengen van een morfologisch fasediagram voor dunne films op substraten met periodieke heterogeniteiten.
   Thiele et al., 2003; Manu Vishal, MSc thesis, 2019
5. Meerdere oplossingsrealisaties van de deterministische dunnefilmvergelijking met pseudo-witte ruis als initiële voorwaarde tonen aan dat het systeem chaotisch is.
   Arvind Pari, MSc thesis, 2019
6. Een te grote nadruk op leiderschap verhult het belang van het spelen van tweede de viool.
7. Vasthouden aan oma's recepten levert meer op dan over stappen op superfoods.
8. Technische universiteiten zouden een minimum curriculum van geesteswetenschappen, kunst en sociale wetenschappen moeten hanteren om gevoelige, in plaats van koude ingenieurs de wereld in te sturen.
9. Het ongemak van analoog is esthetisch aantrekkelijker dan het gemak van digitaal.

Deze stellingen worden opponeerbaar en verdedigbaar geacht en zijn als zodanig goedgekeurd door de promotoren, prof. dr. ir. M.T. Kreutzer en prof. dr. ir. C.R. Kleijn.

Propositions

accompanying the thesis

On the dynamics of non-planar thin liquid films

Maulik S. Shah

1. Computation of the deterministic thin film equation with an initial white noise perturbation is a more cost-effective way to determine the film lifetimes compared to that by a stochastic thin film solver.
   Chapter 3 of this thesis
2. Film lifetimes predicted on the basis of numerical integration of the stochastic thin film equation strongly depend on the time step size when the upwinding concepts are used in the convective noise term.
   Grün et al., 2006
3. Scaling laws reported in the literature that relate the lifetime of thin films to their radii are invalid for films with large radii.
   Manev et al., 1997
4. The strength of noise is more important than its functional form in mapping a morphological phase diagram for thin films on substrates with periodic heterogeneities.
   Thiele et al., 2003; Manu Vishal, MSc thesis, 2019
5. Multiple solution realizations of the deterministic thin film equation with pseudo white noise as an initial condition show that the system is chaotic.
   Arvind Pari, MSc thesis, 2019
6. An over emphasis on leadership obscures the importance of playing second fiddle.
7. Sticking to grandma's recipes has more return on investment than switching to superfoods.
8. Technical universities should employ a minimum curriculum on humanities, art and social sciences to send sensitized, rather than cold, engineers out into the world.
9. The inconvenience of analog is aesthetically more appealing than the convenience of digital.

These propositions are considered opposable and defendable and as such have been approved by the promotors, prof. dr. ir. M.T. Kreutzer and prof. dr. ir. C.R. Kleijn.

On the dynamics of non-planar thin liquid films

Dissertation

for the purpose of obtaining the degree of doctor
at the Delft University of Technology,
by the authority of the RectorMagnificus Prof. dr. ir. T.H.J.J. van der Hagen,
chair of the Board of Doctorates,
to be defended publicly on Tuesday 8 September 2020 at 15:00 hrs
by

Maulik S. SHAH

Master of Science in Chemical Engineering, Delft University of Technology, The Netherlands
born in Mumbai, India

This dissertation has been approved by the promotors.
promotor: Prof. dr. ir. M.T. Kreutzer
promotor: Prof. dr. ir. C.R. Kleijn

Composition of the doctoral committee:

Rector Magnificus	chairperson
Prof. dr. ir. M.T. Kreutzer	Delft University of Technology, promotor
Prof. dr. ir. C.R. Kleijn	Delft University of Technology, promotor

Independent members

Prof. dr. U. Thiele	University of Münster, Germany
Prof. dr. ir. J. H. Snoeijer	University of Twente
Prof. dr. ir. J. T. Padding	Delft University of Technology
Prof. dr. ir. K. Vuik	Delft University of Technology

Other member

Dr. ir. V. van Steijn	Delft University of Technology

Dr. ir. V. van Steijn has, as supervisor, contributed significantly to the preparation of this dissertation.

This work was financially supported by the Netherlands Organization for Scientific Research (NWO) and Dutch Institute for Sustainable Process Technology (ISPT).

Keywords: thin liquid films, foams, (stochastic) simulations

Printed by: Ipskamp printing

Front & Back: Beautiful generative art by Dr. Siddhartha Mukherjee that captures the relevant physics studied in this thesis

ISBN 978-94-028-2159-8

Copyright ©2020 M.S. Shah

An electronic version of this dissertation is available at
`http://repository.tudelft.nl/`.

For my family

Nishaan chuk maaf, nahi maaf neechu nishaan

"To miss an aim is forgivable, setting a lower one isn’t"

- Anonymous
Often referred by beloved Dhiren Sir in his *Pathshala*

Contents

Summary **xi**

Samenvatting **xv**

1 Introduction **1**

1.1 Motivation 2

1.2 Field of research 2

1.3 Research questions 7

1.3.1 Lifetime of a semi-infinite non-planar film 7

1.3.2 Influence of thermal fluctuations 9

1.3.3 Dependence of film lifetimes on film radius and film thickness 10

1.4 Thesis outline 12

2 Evolution of nonconformal Landau-Levich-Bretherton films of partially wetting fluids **17**

2.1 Introduction 18

2.2 Experimental 19

2.3 Rupture time from Thin Film Equation 21

2.4 Flow regimes and pressure drop 26

2.5 Conclusions 27

3 Thermal fluctuations in capillary thinning of thin liquid films **31**

3.1 Introduction 32
3.2 Problem Formulation 34
3.3 Linear stability analysis 37
3.4 Numerical implementation 38
3.5 Results 40
  3.5.1 Transition between thinning mechanisms 40
  3.5.2 Influence of thermal fluctuations on film rupture at far limits of κ 42
  3.5.3 Influence of thermal fluctuations on rupture locations 45
  3.5.4 Influence of thermal fluctuations on rupture time 45
3.6 Conclusions 46

4 Influence of initial film radius and film thickness on the rupture of foam films 53

4.1 Introduction 54
4.2 Problem formulation 56
4.3 Numerical implementation 61
4.4 Results 61
  4.4.1 Characterisation of the film evolution for the governing parameter space 61
  4.4.2 Influence of initial film radius and film thickness on film lifetime 64
  4.4.3 Analytical model for dynamics of films with small radius . . . 64
4.5 Conclusions 70

5 Epilogue 83

5.1 Conclusions 84
5.2 Extensibility 86
5.3 Research opportunities 87
  5.3.1 Thermal nucleation in metastable films 87
  5.3.2 Fundamental topics in planar thin liquid films 89

List of publications 95

Acknowledgements 97

Curriculum Vitae 105

Summary

Thin liquid films are fluid structures with perpendicular length scale, typically of the O($< 10\,\mu$m), being much smaller than the lateral length scale, typically of the O(> 1 mm). From foams and emulsions to tear films on eyes, they widely occur in industrial processes and natural phenomena. Depending on the wetting energies between its different interfaces, it is susceptible to developing an instability which can lead to its subsequent rupture. It is a great example of how dynamics at microscopic scale influence large scale physical behaviour, with instabilities at micron scale influencing a foam collapse or the blinking action of an eye.

The subject of this thesis focuses on non-planar thin liquid films that are found, for instance, in between two foam bubbles or in partial wetting systems in microfluidic channels. The dynamics of such non-planar films is governed by two thinning mechanisms. The first mechanism involves drainage due to curvature differences, and results in a localized depression, commonly referred to as a dimple, at the connection between the planar and curved regions. The second thinning mechanism involves growth of a fluctuation originated instability arising from the competition between a stabilizing surface tension and destabilizing van der Waals forces. For this second thinning mechanism to manifest, the film's lateral length (radius) needs to be large enough to accommodate unstable waves to fit within the film. We study thin film dynamics, by performing numerical simulations that incorporate all these crucial physical processes in the thin film equation.

In chapter 2, we address one of the open questions of how the lifetime, t_r, of non-planar films depend on the fluid properties of the film. We use a semi-infinite film geometry with the planar part large enough so that it allows unstable waves to fit within the film. Together with the addition of a curved portion to a planar portion of the film, the semi-infiniteness of the planar portion, allows both the afore-mentioned thinning mechanisms to play a role in determining the thinning dynamics and lifetime of the film. Non-dimensionalizing the system yields one independent dimensionless parameter, κ, which is the ratio between the drainage pressure and the initial van der Waals pressure. In our numerical simulations, we find $t_r \sim \kappa^{-10/7}$, a result that is

in fair agreement with our mechanistic model based on analytical solutions and also with experimental results of lifetimes of non-planar films in partial wetting systems.

Having developed a framework to determine film lifetimes, in chapter 3 we add thermal fluctuations that naturally occur at the gas-liquid interface into the framework of the thin film equation. We do so to resolve a long standing debate on the relevance of thermal fluctuations in determining the lifetime of a non-planar thin film. Non-dimensionalizing the system yields two independent dimensionless parameters, namely the strength of drainage, κ and strength of thermal noise, θ. Our stochastic simulations show that there exists a temperature dependent transition value of $\kappa = \kappa_{tr}$, where both the afore-mentioned film thinning mechanisms are equally dominant. For large values of $\kappa \gg \kappa_{tr}$, films predominantly thin due to a localized dimple and their lifetimes are independent of θ. In this dimple-dominated regime, film lifetimes scale with the earlier reported scaling relation of $t_r \sim \kappa^{-10/7}$. For small values of $\kappa \ll \kappa_{tr}$, film thinning proceeds via growth of waves triggered by thermal fluctuations, and film lifetimes become independent of κ. In this fluctuation-dominated regime, film lifetimes scale with the strength of the thermal noise as $t_r \sim \ln(\sqrt{2\theta})^{\alpha}$, with $\alpha = 1.15$ explained based on a linear stability theory. Our simulations show, for the first time, if, when and why are thermal fluctuations relevant in determining lifetimes of non-planar thin liquid films.

After identifying the regime where thermal fluctuations are insignificant for the thinning dynamics and lifetimes of non-planar films, we next focused on the influence of initial film features, i.e. film radius and thickness on the lifetimes in the fluctuations-free regime. We therefore relax the semi-infinite film geometry and allow for finite film radius to be an independent parameter in our system. In this work, we resolve the debate on the various reported dependencies of lifetimes on the film radii, discrepancies that arise due to simplifying assumptions of the full thin film model. Our numerical simulations show distinctly different thinning dynamics and scaling relations for small and large radii films. For small radii films, film thinning occurs across the entire film length with a dimple at the connection between the planar and the curved portion of the film. The lifetimes scale with initial film features as, $t_r \sim h_o^0 R_{film}^{10/7}$. These numerical results for small films are in fair agreement with our mechanistic model. For large radii films, film thinning occurs as a localized dimple at the connection between the flat and the curved portion, akin to the film thinning observed for semi-infinite thin films. The lifetimes scale with initial film features as, $t_r \sim h_o^{5/7} R_{film}^0$, in line with the scaling relations obtained for semi-infinite films in chapters 2 and 3. Our work provides insight into the dynamics of film thinning and provides scaling rules on how film lifetimes depend on the initial film features for small and large films.

Overall, in this thesis, we developed a numerical framework to study the thinning dynamics and lifetimes of non-planar films and corroborated our numerical results using mechanistic models. We used this framework, firstly to determine how the film life-

times depend on fluid properties, and secondly, to resolve, at least to a certain extent, debates in the state-of-the-art literature. Although numerical simulations are often limited by the extent of the parameter space it can cover, one of the key advantage of them is that the many simplifications that are often necessary to provide analytical results, do not have to be made anymore. Furthermore, numerical simulations allowed us to systematically study and identify regimes, where one physical mechanism dominated over the other. We conclude this thesis with potential research opportunities to address other open questions in the literature, using our framework.

Samenvatting

Dunne vloeistoffilms zijn vloeistofstructuren waarbij de loodrechte lengteschaal, typisch van O($<$ 10 µm), veel kleiner is dan de laterale lengteschaal, typisch van O($>$ 1 mm). Ze komen voor in industriële processen en in de natuur: van schuimen en emulsies tot traanfilms op ogen. Afhankelijk van de bevochtigingsenergieën tussen de verschillende grensvlakken is het mogelijk dat een instabiliteit ontstaat die tot het barsten van de film kan leiden. Dit is een uitstekend voorbeeld van de invloed van dynamica op microscopische schaal op fysisch gedrag op grote schaal, gezien instabiliteiten op micrometerschaal het instorten van schuim of het knipperen van een oog beïnvloeden.

Het onderwerp van dit proefschrift richt zich op niet-vlakke vloeistoffilms die zich bijvoorbeeld voordoen tussen twee schuimbellen of in deels bevochtigde systemen in microfluïdische kanalen. De dynamica van dergelijke niet-vlakke films wordt bepaald door twee verdunningsmechanismen. Het eerste mechanisme omvat drainage door krommingsverschillen en resulteert in een lokale indrukking, ook wel een kuiltje genoemd, bij de verbinding tussen vlakke en gekromde delen. Het tweede verdunningsmechanisme omvat de groei van een instabiliteit die uit een fluctuatie is voortgekomen en die ontstaat uit de stabiliserende oppervlaktespanning aan de ene kant en de destabiliserende vanderwaalskrachten aan de andere kant. Dit tweede verdunningsmechanisme doet zich slechts voor als de laterale lengte van de film (radius) zo groot is dat onstabiele golven in de film passen. We bestuderen de dynamica van dunne films door numerieke simulaties uit te voeren waarin alle cruciale fysische processen in de dunnefilmvergelijking worden meegenomen.

In hoofdstuk 2 adresseren we de onbeantwoorde vraag hoe de levensduur, t_r, van niet-vlakke films afhangt van de vloeistofeigenschappen van de film. We beschouwen een half-oneindige filmgeometrie met een vlak deel dat dusdanig groot is dat onstabiele golven in de film passen. Samen met de toevoeging van een gekromd deel aan een vlak deel van de film zorgt de half-oneindigheid van het vlakke deel ervoor dat beide eerder genoemde verdunningsmechanismen een rol spelen in het bepalen van de verdunningsdynamica en de levensduur van de film. Het dimensieloos maken van het systeem levert een onafhankelijke dimensieloze parameter κ op die gelijk is aan de verhouding tussen de drainagedruk en de initiële vanderwaalsdruk. Uit onze numerieke simulaties bepalen we dat $t_r \sim \kappa^{-10/7}$, wat redelijk overeenkomt met ons mechanistische model dat gebaseerd is op zowel analytische oplossingen als experimentele resultaten van de levensduur van niet-vlakke films in deels bevochtigde systemen.

Nu we een raamwerk hebben ontwikkeld om de levensduur van de film te bepalen, voegen we in hoofdstuk 3 de thermische fluctuaties die natuurlijk voorkomen aan het gas-vloeistofgrensvlak toe aan dit raamwerk van de dunnefilmvergelijking. We doen dit om een langdurig debat over het belang van thermische fluctuaties voor de levensduur van een niet-vlakke vloeistoffilm te beslechten. Het non-dimensionaliseren van het systeem levert twee onafhankelijke dimensieloze parameters op: de drainagesterkte κ en de thermischeruissterkte θ. Onze stochastische simulaties tonen aan dat er een temperatuurafhankelijke transitiewaarde $\kappa = \kappa_{tr}$ bestaat waar beide eerdergenoemde filmverdunningsmechanismen even belangrijk zijn. Voor grote waarden van $\kappa \gg \kappa_{tr}$ verdunnen films vooral door een plaatselijk kuiltje en is hun levensduur onafhankelijk van θ. In dit kuitjes-gedomineerde regime schaalt de filmlevensduur met de eerdergenoemde schalingsrelatie $t_r \sim \kappa^{-10/7}$. Voor kleine waarden van $\kappa \ll \kappa_{tr}$ verloopt filmverdunning door de groei van golven die worden veroorzaakt door thermische fluctuaties en wordt de filmlevensduur onafhankelijk van κ. In dit door fluctuaties gedomineerde regime schaalt de levensduur van de film met de sterkte van de thermische ruis als $t_r \sim \ln(\sqrt{2\theta})^{\alpha}$, waar $\alpha = 1.15$ wordt verklaard met behulp van een lineaire stabiliteitstheorie. Onze simulaties tonen voor het eerst aan of, wanneer en waarom thermische fluctuaties relevant zijn voor de bepaling van de levensduur van niet-vlakke, dunne vloeistoffilms.

Na identificatie van het regime waarin thermische fluctuaties niet significant zijn voor de verdunningsdynamica en de levensduur van niet-vlakke films, richtten we ons op de invloed van de initiële filmkenmerken, dat wil zeggen de filmradius en de filmdikte, op de levensduur in het fluctuatieloze regime. Daartoe wijken we af van de half-oneindige filmgeometrie en nemen we de filmradius als een onafhankelijke systeemparameter. In dit onderzoek beslechten wij het debat tussen de verschillende gerapporteerde afhankelijkheden van de levensduur op de filmradii, waar de verschillen ontstonden door aannames ter versimpeling van het volledige dunnefilmmodel. Onze numerieke simulaties tonen duidelijk verschillende verdunningsdynamica en schalingsrelaties aan voor grote en kleine filmradii. Bij films met een kleine radius vindt verdunning over de gehele filmlengte plaats met een kuiltje bij de verbinding tussen het vlakke en het gekromde deel van de film. De levensduur schaalt met de initiële filmkenmerken als $t_r \sim h_o^0 R_{film}^{10/7}$. Deze numerieke resultaten voor kleine films zijn in redelijke overeenstemming met ons mechanistische model. Bij films met een grote radius vind verdunning lokaal plaats aan een kuiltje bij de verbinding tussen het vlakke en het gekromde deel, zoals bij de filmverdunning van half-oneindige dunne films. De levensduren schalen met de initiële filmeigenschappen als $t_r \sim h_o^{5/7} R_{film}^0$, wat in lijn ligt met de schalingsrelaties voor half-oneindige films uit hoofdstuk 2 en 3. Ons onderzoek schept inzicht in de filmverdunningsdynamica en levert schalingsregels op voor de afhankelijkheid van de levensduur van de film op de initiële filmkenmerken voor kleine en grote films.

Samenvattend hebben we in dit proefschrift een numeriek raamwerk ontwikkeld om de verdunningsdynamica en de levensduur van niet-vlakke films te besturen. Daarbij hebben mechanistische modellen onze numerieke resultaten bevestigd. We hebben dit raamwerk op de eerste plaats gebruikt om te bepalen hoe de filmlevensduur afhangt van de vloeistofeigenschappen, en op de tweede plaats om, tot op zekere hoogte, debatten in de huidige literatuur de beslechten. Hoewel numerieke simulaties vaak slechts een beperkte parameterruimte kunnen afdekken, hebben ze als groot voordeel dat er geen noodzaak meer is voor de vele vereenvoudigingen die bij analytische methoden vaak moeten worden toegepast. Bovendien konden we met numerieke simulaties systematisch regimes, waarin een bepaald fysisch mechanisme bepalend is, onderscheiden en bestuderen. We sluiten dit proefschrift af door voorstellen te doen voor vervolgonderzoek waarin met ons raamwerk andere open vragen in de literatuur kunnen worden beantwoord.

1. Introduction

1.1 Motivation

The presence of thin liquid films is ubiquitous in daily lives; be it in biological processes such as the removal of aqueous humour by the blinking of an eye, or in various industrial applications, such as in the production of foams and emulsions in food, and paints and coatings in consumer goods. The lifetime of the thin liquid films is of crucial importance, as it for example determines how the texture of food is preserved or how the multiphase mixture produced in oil and gas industries can be effeciently separated.

Research on the dynamics and stability of thin liquid films in natural and industrial settings has spanned for more than a century[1–5], including studies related to the coalescence of bubbles in foams[6–10]. Despite all research that has been performed, there are still important gaps and inconsistencies in existing understanding and predictive models. This was the reason for NWO, ISPT and various process technology companies to initiate a research project on the stability of liquid films, foams and emulsions within the NWO program “Process Technology Fundamentals”, funded by ISPT as a part of the water processing cluster.

The physics governing bubble coalescence occurs over a range of interconnected length scales. The bulk motion of bubbles occurs at macroscale, the approach of bubbles occurs at mesoscale and the evolution of the thin film that forms between the bubbles upon close contact occurs at micro to nanoscale. Within the NWO/ISPT project, the stability of foams and emulsions was studied at these three different scales in the form of three separate PhD projects. The research described in this thesis aimed at contributing towards the micro to nanoscale aspects of this particular area of scientific research.

1.2 Field of research

A key question pertaining to the stability of foams is whether the thin liquid film between bubbles is stable, and if not, a logical follow-up question is how the thinning dynamics and lifetime of the film depend on fluid properties and process conditions. This section introduces the basic physics that governs the stability and dynamics of thin liquid films as a background to this thesis. The most well studied configuration is a film of uniform thickness, referred to as a planar film (see left schematic in Fig. 1.1), such that we use this configuration as a starting point. Thereafter, we continue with the configuration of interest in this thesis: non-planar films (see right schematic in Fig. 1.1), that are thicker at the edges than in the center. Besides the basic physics, this section also presents the state-of-the-art, revealing the gaps in current understanding.

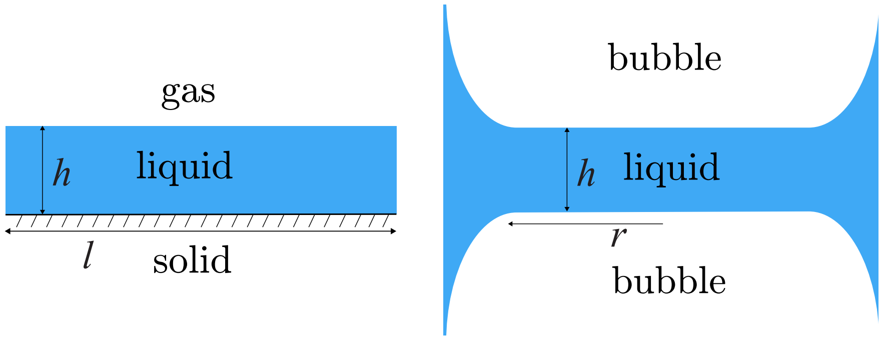

Figure 1.1 Two thin liquid film configurations commonly encountered in literature: (left) planar film on a solid substrate and (right) non-planar film between two bubbles.

Dynamics of thin films: A distinctive feature of thin liquid films is that their perpendicular length scale, h (thickness), is much smaller than their lateral length scale, l (length in Cartesian, radius in cylindrical coordinates, respectively). This slenderness of the films makes it possible to describe the flow in them by simplifying the Navier-Stokes equation using the lubrication approximation. On integrating the approximated Navier-Stokes equation over the local film thickness, and on taking into account the pressure contributions arising from surface tension and intermolecular van der Waals forces, the well known 'thin film equation' is obtained that describes the evolution of the free interface in time and space[2,3]. The thin film equation, for a two dimensional Cartesian system, is given as

$$\frac{\partial h}{\partial t} = -\frac{1}{3\mu}\left(\frac{\partial}{\partial x}\left(h^3\frac{\partial P}{\partial x}\right)\right) \tag{1.1}$$

with,

$$P = \gamma\frac{\partial^2 h}{\partial x^2} - \frac{A}{6\pi h^3} \tag{1.2}$$

where, μ, γ, A and P are fluid viscosity, interfacial tension, Hamaker constant and pressure in the thin liquid film.

Planar films: Planar thin liquid films have been extensively studied in the context of (de-)wetting of films on solid substrates[2,5,11,12]. Their stability is governed by the competition between stabilizing surface tension forces that try to minimize the additional interfacial area created by thickness perturbations, and destabilizing attractive van der Waals forces that bring the free gas-liquid interface closer to the solid substrate, and thus enhances thickness perturbations. This competition may result in the amplification of perturbations that are naturally present on the interface due to the

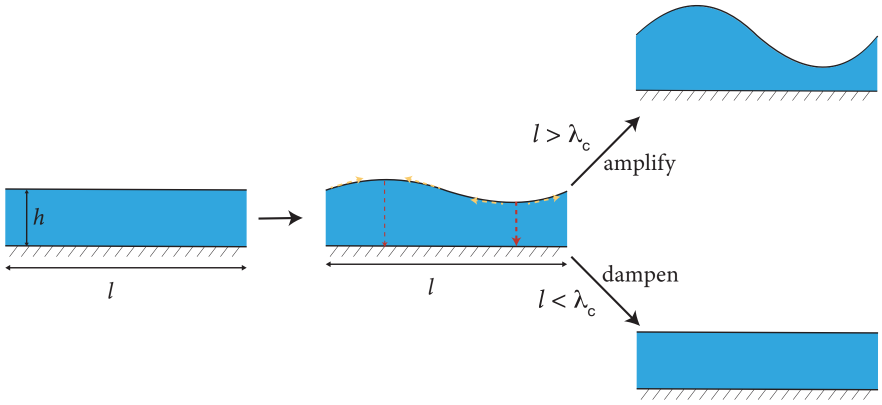

Figure 1.2 (colour online) Schematic of an evolution of a planar thin liquid film. The leftmost figure corresponds to a film of uniform thickness. When perturbed, the next schematic shows the competition between stabilizing surface tension forces (yellow dashed arrows) and destabilizing van der Waals forces (red dashed arrows, with different thicknesses of the arrows signifying that van der Waals forces increase with decreasing film thickness). The rightmost schematics show dampening (amplification) of perturbations for films with lateral length scale smaller (larger) than the critical film length delineating the neutral stability of the film.

thermal motion of molecules[13], resulting in the growth of waves, leading to an instability, that induces rupture of the film. Whether a film is stable against such thermal fluctuations has been studied in the literature using several approaches, including linear stability analysis[6,14] and non-linear simulations[15–17]. As schematically shown in Fig. 1.2, these studies teach us that if the length of the planar film is larger than the length scale of the afore-mentioned instability, then the film is inherently unstable and ruptures with patterns that are characterized by the length scale associated with the fastest growing wave of the instability[12,18,19].

Although morphological patterns found in experiments are well-described by linear stability theory and simulations, there is a mismatch between the lifetimes of the films found in experiments and in simulations that do not include the continuous presence of thermal fluctuations at the interface of these films. Grün et al.[20] showed that the lifetimes of planar films predicted by simulations that accounted for thermal fluctuatons were an order of magnitude smaller than the ones without and were much closer to those found in experiments[12]. Diez et al.[21] emphasized the relevance of spatial correlations in thermal noise on determining the film lifetimes and morphology in metallic planar films. Upon dewetting of a planar film, in the subsequent stages of film evolution, Nesic et al.[22] showed that thermal fluctuations play an important role in determining the time scales for coarsening of droplets. These first accounts

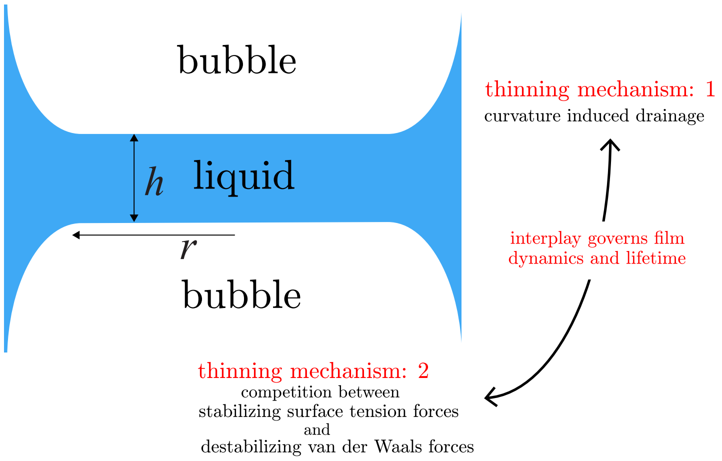
bubble
h
liquid
r
bubble
thinning mechanism: 1
curvature induced drainage
interplay governs film dynamics and lifetime
thinning mechanism: 2
competition between stabilizing surface tension forces and destabilizing van der Waals forces

Figure 1.3 Thinning mechanisms in non-planar thin liquid films. The thinning of the planar portion of the film is governed by the competition between the surface tension and van der Waals forces, as discussed in Fig. 1.2. The curved edges ensure an additional thinning mechanism due to drainage from the planar portion of the film to the low pressure curved portions. The interplay between these two thinning mechanisms governs the film dynamics and its lifetime.

on planar films point towards the importance of including thermal fluctuations in the description of planar film evolution.

Non-planar films: Many industrial applications and natural phenomena involve films that are not planar, but are curved near their edges. Typical examples include the film that form between two bubbles, the wetting film between an elongated bubble and the walls of non-circular capillaries[23], the tear film on an eye lid[24] and the soap film held on a wire frame[25]. The presence of curved regions imposes a localized pressure gradient that drains the fluid from the planar portion of the film towards this low pressure curved portion, often leading to a localised depression called a dimple[44,45]. The dynamics of such non-planar films is hence governed by two thinning mechanisms, namely, (1) drainage due to curvature differences and (2) growth of a fluctuations-originated instability, which arises from the competition between the stabilizing surface tension forces and the destabilizing van der Waals forces. One of the unresolved aspect pertaining to non-planar films lies in developing an approach to combine the afore-mentioned two thinning mechanisms and subsequently determine the lifetime of a non-planar film as a function of its fluid and geometrical properties.

A second unresolved aspect in the context of non-planar films lies in the relevance of thermal fluctuations. Unlike for planar films, whether and when thermal fluctuations determine the film lifetime of non-planar films is debated. The classical paper by Vrij[6] postulates that a non-planar film thins uniformly up to a certain critical thickness. This critical thickness marks the neutral stability of the film against the instability arising from the competition between stabilizing surface tension forces and destabilizing van der Waals forces. On further thinning, long-wavelength pertubations at the film interface amplify, and their growth outruns uniform thinning due to drainage. In addition to the seminal work by Vrij[6], which highlights the role of thermal fluctuations in determining film lifetime, more recent experiments[26,27] and molecular dynamic simulations[28] emphasized the role of thermal fluctuations in droplet coalescence. In contrast, Vakarelski et al.[29] showed that their fluctuations-free theory was sufficient to explain coalescence times for small microbubbles in AFM experiments. In small radii films found in their experiments, the unstable waves (in addition to the fastest growing wave) did not fit within the film radii. This has been identified in the literature[29,30] as one of the reasons for the lack of relevance of fluctuations. In order to resolve whether or not the afore-mentioned results in the literature on the role of thermal fluctuations in film thinning are conflicting, it therefore seems important to take the lateral dimension of the film into account. We here distinguish between small (finite) and large (semi-infinite) film radius, where the largeness and smallness of the film radius signifies whether or not the film radius encompasses at least one wavelength of the fastest growing wave. Furthermore, for films with finite radius, the film dynamics do depend on the film radius, whereas the film dynamics become independent of the film radius for a film with semi-infinite lateral length.

Apart from the debate on the role of thermal fluctuations in determining film lifetimes, a third unresolved aspect of non-planar films lies in developing a simple theoretical model that includes all relevant physical mechanisms, i.e. drainage due to dimple formation and subsequent thinning due to van der Waals forces, in order to predict how the film dynamics and lifetime depend on the film features. For films with finite-sized radii found in Scheludko cell experiments[31–33], a variety of conflicting scaling rules for the film lifetime, t_r, on the initial film radius, R_{film}, have been reported[1,34,35],

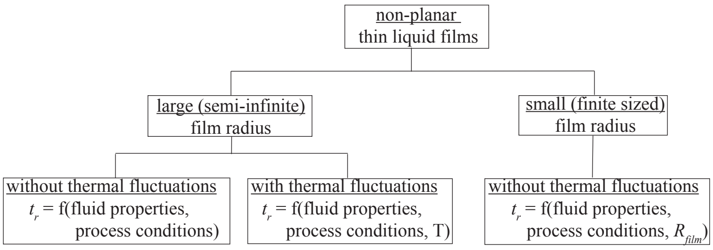
non-planar thin liquid films
large (semi-infinite) film radius
small (finite sized) film radius
without thermal fluctuations
t_r = f(fluid properties, process conditions)
with thermal fluctuations
t_r = f(fluid properties, process conditions, T)
without thermal fluctuations
t_r = f(fluid properties, process conditions, R_{film})

Figure 1.4 Schematic representation of the research topics investigated in this thesis within an overarching research field of non-planar thin liquid films.

with $t_r \sim R_{film}^{\alpha}$, where α has been found to be 2[1], $4/5$[34] and $3/4$[35]. The underlying assumptions in these works include the plane-parallel nature of the drainage[1] and some refinements that superimpose translatory[35] or quasi-static[34] oscillations on the plane-parallel interface that sustain throughout the film evolution. These assumptions have been challenged in the literature[30] based on their esoteric nature and the lack of applicability of these results to experimental systems other than those performed in Scheludko-cells.

In the next section, we postulate research questions that this thesis addresses with respect to the three unresolved aspects discussed above in the context of semi-infinite non-planar films (sections §1.3.1, without thermal fluctuations and §1.3.2 with thermal fluctuations) and finite-sized films (section §1.3.3). Fig. 1.4 shows the overarching research topic that has been studied in this thesis. To keep the problem simple, we first develop a framework to study the dynamics and lifetime of a non-planar film in the absence of thermal fluctuations. Upon developing such a framework, we add thermal fluctuations at the film interface in the problem description and identify when they play a role. Based on these insights, we retrospectively justify our choice of leaving out thermal fluctuations to answer the research questions in section §1.3.1. For films with finite radius studied in section §1.3.3, we leave out thermal fluctuations since the unstable waves do not fit within the radius of the film[29,30].

1.3 Research questions

1.3.1 Lifetime of a semi-infinite non-planar film

To be able to appreciate why predicting lifetime of a semi-infinite non-planar thin liquid film is important, we first highlight its significance in digital microfluidics, and subsequently discuss the relevant state-of-the-art followed by postulating the research question.

The understanding of the motion of elongated bubbles (or droplets) in microfluidic channels is crucial for designing lab-on-a-chip devices[36]. In such multiphase flows, a thin liquid film of the carrier fluid may surround the bubbles[23,37,38]. The physics behind the (de-)wetting of these films is well understood for circular channels wherein the films are conformal (of uniform thickness) with respect to the shape of the channels[2,39,40] but not for non-circular channels[41,42] as often encountered in the field of microfluidics.

For rectangular (and in general: non-circular) channels, bubbles do not conform to the underlying channel shape at the sharp corners of the channel. This results in the thin liquid film being non-planar (i.e. of non-uniform thickness). The initial thickness (at $t = 0$) of the film that gets formed depends on the speed of the bubble, the channel

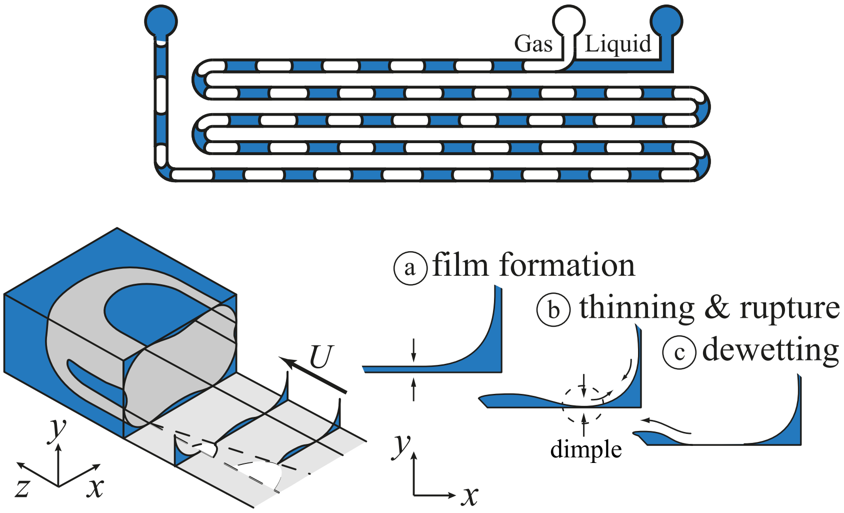

Figure 1.5 Top schematic: a regular multiphase flow pattern in a microfluidic channel is shown. Bottom left schematic: three-dimensional isometric view of the bubble and the film at the channel walls is shown. The cross-sectional cutout in the x-y plane shows the film at the channel walls. Bottom right: evolution of thin liquid film upon its (a) formation, (b) thinning due to dimple formation and its subsequent rupture and (c) growth of the dewetting front (not studied in this thesis) is shown. Figure adapted from Kreutzer et al.[43].

dimensions and the capillary speed (ratio of interfacial tension and viscosity, i.e. γ/μ) of the carrier fluid[23], and is typically less than O(1 µm). The lateral length scale of the film is approximately the width of the microfluidic channel (typically O(100 µm)), and is large enough for the fastest growing wave to feature within its length, thereby forming a semi-infinite film. Predicting the lifetime of such non-planar films can help in predicting the transition from a regular multiphase flow pattern of bubbles and droplets within the carrier fluid, to more chaotic flow patterns resulting from partial wetting of the two fluids with the channel walls[41].

Film drainage in semi-infinite non-planar films has been shown to proceed via the formation of a localised dimple[44,45]. Inspired by previous work[44], Aradian et al.[25] calculated the shape of the dimple, and developed a scaling rule that captures how film thinning due to dimpling proceeds in time. In the absence of any van der Waals forces, this scaling rule, however, cannot be used to predict the lifetime of the film, because the film thickness asymptotically approaches rupture in time. Zhang and Lister[46], on the other hand, developed scaling rules for film thinning in time in the presence of surface tension and van der Waals forces, but in the absence of drainage.

Thus, significant progress has been made to understand the film dynamics in the two limiting cases, viz (i) drainage via the formation of a dimple, but in the absence of van der Waals forces[25] and (ii) film thinning in the presence of surface tension and van der Waals forces, but in the absence of drainage[46]. However, a comprehensive analysis that combines the afore-mentioned cases in order to predict film lifetime is still lacking. To address this research gap, the questions that we ask ourselves are: how can we predict the lifetime of a semi-infinite non-planar thin liquid film by combining the dynamics of dimple formation during the drainage process and of rapid rupture in the presence of van der Waals forces? What scaling rule governs the film lifetime as a function of the fluid properties and the process conditions?

1.3.2 Influence of thermal fluctuations

Next, we study the relevance of thermal fluctuations on film lifetimes. In the last decade, thermal fluctuations have been shown to be of relevance in planar thin film rupture, bringing simulated film lifetimes[20] closer to experiments[12]. However, their role in the dynamics of non-planar thin liquid films has not yet been elucidated.

Important seminal works[6,7] exploring the stability of thin films attributed a crucial role to the presence of thermal fluctuations in determining the film lifetime. Vrij[6] postulated that the film first drains uniformly with a thinning rate governed by the classical Reynolds' law[1] (wherein drainage is assumed to proceed in a plane-parallel manner), until a stage is reached when a fastest growing wave fits within the film radius, and the growth of this wave outruns Reynolds' thinning rate. However, experimental evidences show a deviation from the Reynolds' thinning rate due to significant fluctuations (thermal[31] or hydrodynamic[34], in origin) in film thickness. Furthermore, as shown in Fig. 1.6, Aarts and Lekkerkerker[27] reported illustrative experiments of interfaces with ultra-low interfacial tension, and demonstrated the large role of thermal fluctuations on inducing rupture[47]. In contrast, Vakarelski et al.[29] showed that thermal fluctuations play no significant role in the rupture of small film radii films, and that film thinning due to drainage is sufficient to explain their lifetimes. Therefore, the dominant rupture mechanism has been a subject of debate in the literature, with some studies[6,26–28] emphasizing the relevance of thermal fluctuations in film thinning, whereas other studies[29,30] show no significant role of thermal fluctuations in determining film lifetimes.

The question we pose is: what role do thermal fluctuations play in determining the dynamics and lifetimes of non-planar films? Are there any distinct regimes where thermal fluctuations are relevant, and if so, what bounds those regimes? How do the film evolution and lifetime depend on the strength of thermal fluctuations?

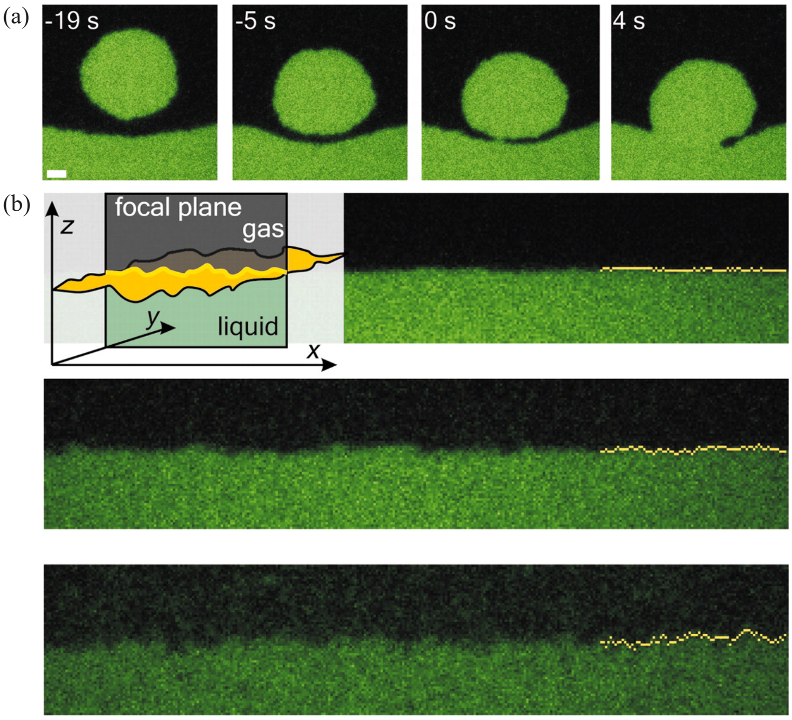

Figure 1.6 (a) Confocal microscopy images of droplet coalescence in an ultra-low interfacial tension system is shown, wherein the crucial role of thermal fluctuations leading to film breakup on a random location can be observed. (b) Zoomed view of the interface, wherein experimental evidence of thermal fluctuations can be seen. Figures taken from Aarts et al.[26].

1.3.3 Dependence of film lifetimes on film radius and film thickness

The questions in the previous two sections dealt with films that were sufficiently large in the lateral dimension for it to not influence the film dynamics and its lifetimes. We now consider films with finite radius (lateral dimensions), wherein the thinning dynamics and hence the film lifetimes, t_r depend on the initial film radius, R_{film} and film thickness, h_o.

The evolution of small radii films has been studied using several approaches (see Fig. 1.7 for schematic representation of these approaches). Under a quasi-steady assumption (in Eqs. 1.1 and 1.2), classical theory[1] fixes the shape of the interface to be plane-parallel during the entire film thinning process, and predicts $t_r \sim R^2_{film}$. Re-

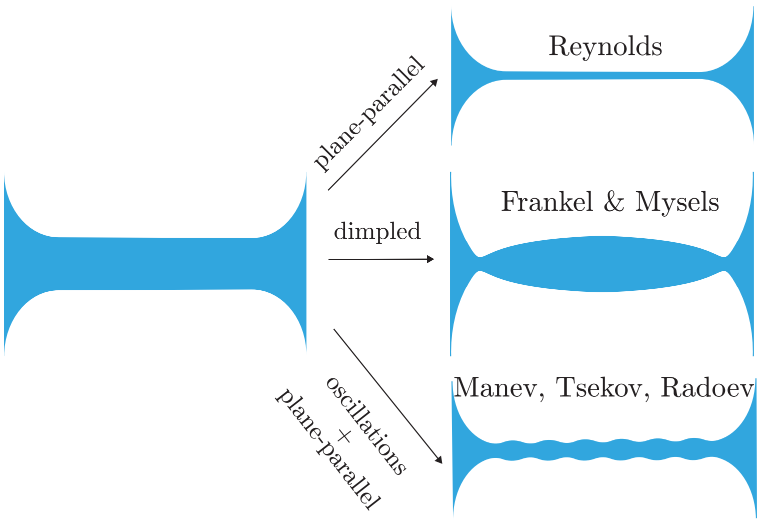

Figure 1.7 Schematic of different approaches used in the literature to describe thinning of a non-planar thin liquid film. Reynolds[1] theory assumes drainage in a plane-parallel manner. Frankel and Mysels[44] developed a theory on the film drainage that proceeds through the formation of a dimple. Manev et al.[34] superimposed quasi-static fluctuations on plane-parallel film, and developed a theory (commonly referred as MTR thinning law) assuming these fluctuations are sustained throughout the film evolution.

laxing the quasi-steady assumption[1], Sharma and Ruckenstein[48] included the stabilizing effect of film drainage on the growth of fluctuations in a plane-parallel film to show that $t_r \sim R^1_{film}$. Hydrodynamic simulations that solved exclusively for the flow in the Plateau border, while assuming the film to remain essentially plane-parallel showed $t_r \sim R^{4/5}_{film}$, independent of h_o. However, experimental evidences have shown that the film thinning is not necessarily plane-parallel[31,34,45]. To corroborate with this finding, several other approaches were undertaken that included quasi-stationary non-homogeneities[34,49] or translatory oscillations[35] superimposed over a plane-parallel interface, leading to $t_r \sim R^{\alpha}_{film}$, where $\alpha = 4/5$ (commonly referred as MTR thinning law) and $3/4$ respectively.

However, the assumptions in the above approaches have been challenged in the literature[30] as they fail to capture the pronounced dimple shape commonly observed in experiments[45,50,51]. Frankel and Mysels[44] used a quasi-steady approach to calculated the shape of the dimple and developed a scaling rule for the film thickness, h_{min} at the periphery, of the dimple ($h_{min} \sim t^{-1/2}$) and h_c at the centre of the film ($h_c \sim t^{-1/4}$). Without including any van der Waals forces, their theory does not predict film rupture in finite time. Taken altogether, it is not yet clear how the film lifetime depends on the initial film radius and film thickness, when all relevant physics is accounted for in the problem description.

Based on this research gap, the question pertaining to small radii films that we have is: How do film lifetimes depend on the initial film radii and film thicknesses when all the relevant physics, i.e. drainage due to dimple formation, surface tension and van der Waals forces, is included in the problem description? Furthermore: Can a simple model that accounts for the dynamics of dimpling and thinning due to van der Waals forces explain this dependency of film lifetime on the initial features of the film?

1.4 Thesis outline

In the subsequent chapters, we address each of these open research questions, viz

- Chapter-2: What scaling rule governs the film lifetime as a function of the fluid properties and the process conditions for semi-infinite non-planar films, as for instance encountered around elongated bubbles and droplets traveling through micro-channels with a rectangular cross section?
- Chapter-3: What role do thermal fluctuations play in determining lifetimes of semi-infinite non-planar films? Are there any distinct regimes where thermal fluctuations are relevant, and if so, what bounds those regimes? What are the observable differences in film evolution and final rupture as thermal fluctuations become relevant?
- Chapter-4: How do film lifetimes depend on the initial film radius and film thickness for finite sized non-planar thin films, as for example encountered in Scheludko cell experiments?

These are self-contained chapters that are either published in, or are submitted to, peer-reviewed journals. We conclude the thesis with an epilogue where we discuss the broader applicability of our findings and present opportunities for future research.

Bibliography

[1] O. Reynolds. On the theory of lubrication and its application to Mr. Beauchamp tower's experiments, including an experimental determination of the viscosity of olive oil. Phil. Trans. Roy. Soc. Lon., 177:157–234, 1886. doi: 10.1098/rstl.1886.0005.

[2] A. Oron, S. H. Davis, and S. G. Bankoff. Long-scale evolution of thin liquid films. Rev. Mod. Phys., 69(3):931–980, 1997. doi: 10.1103/RevModPhys.69.931.

[3] G. K. Batchelor. An Introduction to Fluid Dynamics. Cambridge Mathematical Library. Cambridge University Press, 2000.

[4] L. G. Leal. Advanced transport phenomena: fluid mechanics and convective transport processes. Cambridge University Press, 2007.

[5] R. V. Craster and O. K. Matar. Dynamics and stability of thin liquid films. Rev. Mod. Phys., 81: 1131–1198, Aug 2009. doi: 10.1103/RevModPhys.81.1131.

[6] A. Vrij. Possible mechanism for the spontaneous rupture of thin, free liquid films. Discuss. Faraday Soc., 42:23–33, 1966. doi: 10.1039/DF9664200023.

[7] A. Scheludko. Thin liquid films. Adv. Colloid Interface Sci., 1(4):391–464, 1967. doi: 10.1016/0001-8686(67)85001-2.

[8] R. J. Pugh. Foaming, foam films, antifoaming and defoaming. Adv. Colloid Interface Sci., 64:67 – 142, 1996. doi: 10.1016/0001-8686(95)00280-4.

[9] D. Exerowa and P. M. Kruglyakov. Foam and foam films: theory, experiment, application. Elsevier, 1997.

[10] V. Bergeron. Forces and structure in thin liquid soap films. J. Phys. Condens. Matter, 11(19):R215, 1999.

[11] G. Reiter. Dewetting of thin polymer films. Phys. Rev. Lett., 68:75–78, 1992. doi: 10.1103/PhysRevLett.68.75.

[12] J. Becker, G. Grün, R. Seemann, H. Mantz, K. Jacobs, K. R. Mecke, and R. Blossey. Complex dewetting scenarios captured by thin-film models. Nat. Mater., 2(1):59, 2003. doi: 10.1038/nmat788.

[13] A Vrij. Light scattering by soap films. J. Colloid Sci., 19(1):1 – 27, 1964. doi: 10.1016/0095-8522(64)90003-0.

[14] E. Ruckenstein and R. K. Jain. Spontaneous rupture of thin liquid films. J. Chem. Soc., Faraday Trans. 2, 70:132–147, 1974. doi: 10.1039/F29747000132.

[15] R. Khanna and A. Sharma. Pattern formation in spontaneous dewetting of thin apolar films. J. Colloid Interface Sci., 195(1):42 – 50, 1997. doi: 10.1006/jcis.1997.5134.

[16] K. Kargupta and A. Sharma. Templating of thin films induced by dewetting on patterned surfaces. Phys. Rev. Lett., 86:4536–4539, 2001. doi: 10.1103/PhysRevLett.86.4536.

[17] R. Seemann, S. Herminghaus, and K. Jacobs. Dewetting patterns and molecular forces: A reconciliation. Phys. Rev. Lett., 86:5534–5537, 2001. doi: 10.1103/PhysRevLett.86.5534.

[18] A. Sharma and R. Khanna. Pattern formation in unstable thin liquid films. Phys. Rev. Lett., 81: 3463–3466, 1998. doi: 10.1103/PhysRevLett.81.3463.

[19] A. Sharma and R. Khanna. Pattern formation in unstable thin liquid films under the influence of antagonistic short- and long-range forces. J. Chem. Phys., 110(10):4929–4936, 1999. doi: 10.1063/1.478378.

[20] G. Grün, K. Mecke, and M. Rauscher. Thin-film flow influenced by thermal noise. J. Stat. Phys., 122(6):1261–1291, 2006. doi: 10.1007/s10955-006-9028-8.

[21] J. A. Diez, A. G. González, and R. Fernández. Metallic-thin-film instability with spatially correlated thermal noise. Phys. Rev. E, 93:013120, 2016. doi: 10.1103/PhysRevE.93.013120.

[22] S. Nesic, R. Cuerno, E. Moro, and L. Kondic. Fully nonlinear dynamics of stochastic thin-film dewetting. Phys. Rev. E, 92:061002, 2015. doi: 10.1103/PhysRevE.92.061002.

[23] H. Wong, C. J. Radke, and S. Morris. The motion of long bubbles in polygonal capillaries .1. thin

films. J. Fluid Mech., 292:71–94, 1995. doi: 10.1017/S0022112095001443.

[24] H. Wong, I. Fatt, and CJ Radke. Deposition and thinning of the human tear film. J. Colloid Interface Sci., 184(1):44–51, 1996. doi: 10.1006/jcis.1996.0595.

[25] A. Aradian, E. Raphael, and P. G. de Gennes. Marginal pinching in soap films. Europhys. Lett., 55 (6):834–840, 2001. doi: 10.1209/epl/i2001-00356-y/fulltext/.

[26] D. G. A. L. Aarts, M. Schmidt, and H. N. W. Lekkerkerker. Direct visual observation of thermal capillary waves. Science, 304(5672):847–850, 2004. doi: 10.1126/science.1097116.

[27] D. G. A. L. Aarts and H. N. W. Lekkerkerker. Droplet coalescence: drainage, film rupture and neck growth in ultralow interfacial tension systems. J. Fluid Mech., 606:275–294, 2008. doi: 10.1017/S0022112008001705.

[28] S. Perumanath, M. K. Borg, M. V. Chubynsky, J. E. Sprittles, and J. M. Reese. Droplet coalescence is initiated by thermal motion. Phys. Rev. Lett., 122:104501, 2019. doi: 10.1103/PhysRevLett.122.104501.

[29] I. U. Vakarelski, R. Manica, X. Tang, S. J. O'Shea, G. W. Stevens, F. Grieser, R. R. Dagastine, and D. Y. C. Chan. Dynamic interactions between microbubbles in water. Proc. Nat. Acad. Sci., 107(25): 11177–11182, 2010. doi: 10.1073/pnas.1005937107.

[30] D. Y. C. Chan, E. Klaseboer, and R. Manica. Film drainage and coalescence between deformable drops and bubbles. Soft Matter, 7:2235–2264, 2011. doi: 10.1039/C0SM00812E.

[31] B. P. Radoev, A. D. Scheludko, and E. D. Manev. Critical thickness of thin liquid films: Theory and experiment. J. Colloid Interface Sci., 95(1):254 – 265, 1983. doi: 10.1016/0021-9797(83)90094-2.

[32] E.D. Manev, S.V. Sazdanova, and D.T. Wasan. Emulsion and foam stability - the effect of film size on film drainage. J. Colloid Interface Sci., 97(2):591 – 594, 1984. doi: 10.1016/0021-9797(84)90334-5.

[33] J. L. Joye, G. J. Hirasaki, and C. A. Miller. Dimple formation and behavior during axisymmetrical foam film drainage. Langmuir, 8(12):3083–3092, 1992. doi: 10.1021/la00048a038.

[34] E. Manev, R. Tsekov, and B. Radoev. Effect of thickness non-homogeneity on the kinetic behaviour of microscopic foam film. J. Dispersion Sci. Technol., 18(6-7):769–788, 1997. doi: 10.1080/01932699708943771.

[35] E. Ruckenstein and A. Sharma. A new mechanism of film thinning: Enhancement of Reynolds' velocity by surface waves. J. Colloid Interface Sci., 119(1):1 – 13, 1987. doi: 10.1016/0021-9797(87)90239-6.

[36] V.S. Ajaev and G.M. Homsy. Modeling shapes and dynamics of confinded bubbles. Annu. Rev. Fluid Mech., 38:227–307, 2006. doi: 10.1146/annurev.fluid.38.050304.092033.

[37] F. P. Bretherton. The motion of long bubbles in tubes. J Fluid. Mech., 10:166–88, 1961. doi: 10.1017/S0022112061000160.

[38] H. Wong, C. J. Radke, and S. Morris. The motion of long bubbles in polygonal capillaries. 2. drag, fluid pressure and fluid-flow. J Fluid. Mech., 292:95–110, 1995. doi: 10.1017/S0022112095001455.

[39] D. Bonn, J. Eggers, J. Indekeu, J. Meunier, and E. Rolley. Wetting and spreading. Rev. Mod. Phys., 81:739–805, 2009. doi: 10.1103/RevModPhys.81.739.

[40] J. H. Snoeijer and B. Andreotti. Moving contact lines: Scales, regimes, and dynamical transitions. Ann. Rev. Fluid Mech., 45(1):269–292, 2013. doi: 10.1146/annurev-fluid-011212-140734.

[41] R. Dreyfus, P. Tabeling, and H. Willaime. Ordered and disordered patterns in two-phase flows in microchannels. Phys. Rev. Lett., 90(14):144505, 2003. doi: 10.1103/PhysRevLett.90.144505.

[42] B. M. Jose and T. Cubaud. Formation and dynamics of partially wetting droplets in square microchannels. RSC Adv., 4:14962–14970, 2014. doi: 10.1039/C4RA00654B.

[43] M. T. Kreutzer, M. S. Shah, P. Parthiban, and S. A. Khan. Evolution of nonconformal landau-levich-

bretherton films of partially wetting liquids. Phys. Rev. Fluids, 3:014203, 2018. doi: 10.1103/PhysRevFluids.3.014203.

[44] S. P. Frankel and K. J. Mysels. On the dimpling during the approach of two interfaces. J. Phys. Chem., 66(1):190–191, 1962. doi: 10.1021/j100807a513.

[45] D Platikanov. Experimental investigation on the dimpling of thin liquid films. J. Phys. Chem., 68 (12):3619–3624, 1964. doi: 10.1021/j100794a030.

[46] W. W. Zhang and J. R. Lister. Similarity solutions for van der waals rupture of a thin film on a solid substrate. Phys. Fluids, 11(9):2454–2462, 1999. doi: 10.1063/1.870110.

[47] Y. Hennequin, D. G. A. L. Aarts, J. H. van der Wiel, G. Wegdam, J. Eggers, H. N. W. Lekkerkerker, and D. Bonn. Drop formation by thermal fluctuations at an ultralow surface tension. Phys. Rev. Lett., 97(24):244502, 2006. doi: 10.1103/PhysRevLett.97.244502.

[48] A. Sharma and E. Ruckenstein. Stability, critical thickness, and the time of rupture of thinning foam and emulsion films. Langmuir, 3(5):760–768, 1987. doi: 10.1021/la00077a033.

[49] R. Tsekov. The r4/5-problem in the drainage of dimpled thin liquid films. Colloids Surf. A: Physicochem. Eng. Asp., 141(2):161 – 164, 1998. doi: 10.1016/S0927-7757(97)00253-7.

[50] E. Klaseboer, J.Ph. Chevaillier, C. Gourdon, and O. Masbernat. Film drainage between colliding drops at constant approach velocity: Experiments and modeling. J. Colloid Interface Sci., 229(1): 274 – 285, 2000. doi: 10.1006/jcis.2000.6987.

[51] A.N. Zdravkov, G.W.M. Peters, and H.E.H. Meijer. Film drainage between two captive drops: Peo-water in silicon oil. J. Colloid Interface Sci., 266(1):195 – 201, 2003. doi: 10.1016/S0021-9797(03)00466-1.

2. Evolution of nonconformal Landau-Levich-Bretherton films of partially wetting fluids[†]

We experimentally and theoretically describe the dynamics of evolution and eventual rupture of Landau-Levich-Bretherton films of partially-wetting liquids in microchannels in terms of non-planar interface curvatures and disjoining pressure. While both the early-stage dynamics of film evolution and near-collapse dynamics of rupture are understood, we match these regimes and find theoretically that the dimensionless rupture time, T_r, scales with $\kappa^{-10/7}$. Here, κ is the dimensionless curvature given by the ratio of the Laplace-pressure discontinuity that initiates film thinning to initial strength of the disjoining pressure that drives the rupture. We experimentally verify the rupture times and highlight the crucial consequences of early film rupture in digital microfluidic contexts: pressure drop in segmented flow and isolation of droplets from the walls.

[†] Published as: M. T. Kreutzer, M. S. Shah, P. Parthiban, S. A. Khan Evolution of nonconformal Landau-Levich-Bretherton films of partially wetting fluids. Phys. Rev. Fluids 3, 014203, 2018, doi: 10.1103/PhysRevFluids.3.014203. While I contributed to this work mainly by performing numerical simulations, the experimental details and theoretical model in this chapter is presented as they appeared in the journal for the sake of completeness of the work.

2.1 Introduction

Rain droplets running on windows or over surface of leaves are everyday examples of the delicate interplay of forced wetting, stability and dewetting of thin liquid films deposited on repelling surfaces. A crucial question is whether a film of uniform thickness can coat the repelling surface without any gradients in film curvature. Such *conformal* films are found on flat plates, cylinders, spheres, and even on such simple surfaces, interesting transitions between coating and non-wetting states emerge with rich dynamics and transitions that typically involve careful analysis of the contact line and stability analysis involving perturbations of both the contact line shape and film curvature[1]. The general physics of what happens to coating conformal thin films is now well understood. Briefly, for flat plates or cylindrical objects that are withdrawn at sufficient speed from a liquid bath, the Landau-Levich-Bretherton (LLB) theory[2] teaches that conformal films are pulled along. The deposited film thickness then scales as $h \sim \mathscr{C}^{2/3}$, where the capillary number $\mathscr{C}=\mu U/\gamma$, with viscosity μ, velocity U and surface tension γ, signifies the ratio of viscous stress ($\sim\mu U/h$) to capillary pressure ($\sim\gamma/h$). The eventual fate of these wetting films, on partially wetting surfaces, is to form droplets. Small perturbations of film thickness grow and lead to rupture of the film and dewetting to droplets, with a dramatic height dependence of rupture time, $t \sim h^5$, such that a 1 µm film ruptures in one week and a 1 nm film ruptures in a second[3]. In contrast, on non-flat surfaces, e.g. near acute corners, in channels with rectangular cross-sections or on topographically pre-patterned surfaces, even the static case without external flow is attended by polymorphism and topological bifurcations[4]. If, in addition, flow deposits non-conformal films, then sharp localized curvature gradients cause fluid flow and even in a fully-wetting context profoundly influence the final shape of the deposited film[5,6]. Non-conformal partially-wetting films exhibit accelerated film thinning and rupture with dramatic consequences: while moving elongated bubbles or drops in circular microchannels are surrounded by long-lasting thin films of the carrier liquid on the confining walls, in square channels such a well-behaved scenario is not observed for partially-wetting fluids: in contrast, the flow is characterized by chaotic dynamics that are poorly understood[7].

In this paper, we address the open question of predicting the rupture time from a well-defined initial film shape, by studying a representative problem of confined long bubbles flowing in channels of rectangular cross section, such that the distance from the nose of the bubble directly relates to lifetime of the film. While significant progress has been made in understanding the evolution of such films in various limiting cases[8], a comprehensive analysis that encompasses all the stages of film evolution, and which ultimately predicts the rupture time is still lacking. Briefly, the early stages of thinning have been studied in the context of marginal soap pinching and ophthalmology[6,9], while the main features of the final collapse are also understood[10]. We analyze the full dynamic evolution of such thin films, from deposition to thinning to rupture, with theoretical rupture times that can be compared to experiment. These rupture times find application beyond the time required to blink an eye to rewet it, as mentioned above. We highlight the consequences of partial wetting in the context of digital microfluidics, using the rupture time to delineate regimes with markedly different behaviour.

2.2 Experimental

We recorded top-view micrographs of elongated bubbles coflowing with liquid (Fig. 2.1(a)) in a microchannel ($h_c \times w_c = 127\,\mu\mathrm{m} \times 300\,\mu\mathrm{m}$) that was manufactured using standard lithographic techniques such that all walls consisted of smooth polydimethylsiloxane (PDMS). Speed U and length l of monodisperse bubbles were independently varied by adjusting the gas and liquid feed rates into a T-junction[11]. The channel was trans-illuminated by reflection from a white background and the microscope objective was focussed on the bottom wall, such that droplets and film curvature were visible in high contrast (Fig.2.1(b)). The partially wetting liquid was ethanol (>99.9%) of viscosity $\eta = 1.09\,\mathrm{mPa\,s}$, surface tension $\gamma = 21.8\,\mathrm{mN\,m^{-1}}$, equilibrium contact angle $\theta_0 = 8°$ with air, and PDMS-ethanol-air Hamaker constant $A = 2 \cdot 10^{-21}$ J calculated from the literature[12].

Flows at low speeds ($\mathscr{C}<2.5 \cdot 10^{-5}$) showed no deposition of fluid on the wall (Fig 2.1(c)). This image clearly shows the contact line between the liquid in the corners of the channel (black) and the bare wall in the $x - z$ plane. The z-component of the velocity of this contact line is given by $U \cos\alpha$, where α is the angle of the normal of the contact line with the z-axis, as shown in Fig. 2.1(e). Increasing the bubble speeds first resulted in a wetting film, first near the centerline of the channel where $\cos\alpha \approx 1$. This film is so thin that it immediately ruptures into the small droplets that are clearly visible in the image. Increasing the bubble velocity further increases the distance from the centerline where a film is deposited. Analysis of the data in Fig. 2.1(d-g) revealed that the highest value of α for which a film was deposited was given by $\alpha \approx \cos^{-1}(\mathscr{C}_c/\mathscr{C})$ with the critical capillary number for the onset of forced wetting $\mathscr{C}_c \approx 3 \cdot 10^{-5}$, which is in reasonable agreement, assuming a slip length of 1 nm, with[13]. At even higher bubble speeds when $\alpha \sim \pi/2$, a film was deposited that spanned the entire cross section of the channel between the menisci at the sides (Fig. 2.1(h-j)). This film ruptured, always at the edge where the deposited film met the meniscus. We measured the distance z_r of unruptured film, as shown in Fig. 2.1(j) at five different locations on the microchip. With increasing $\mathscr{C}$, z_r increased from $z_r \approx 100\,\mu\mathrm{m}$ at $\mathscr{C} = 1.8 \cdot 10^{-4}$ to $z_r \approx 7.5\,\mathrm{mm}$ at $\mathscr{C} = 2 \cdot 10^{-3}$, provided the bubble was long enough to observe any rupture at all. The standard deviation of the measurements at the five locations was 20-25% for all experiments. At low speeds, the main source of uncertainty was the location of film deposition, i.e. the point where the

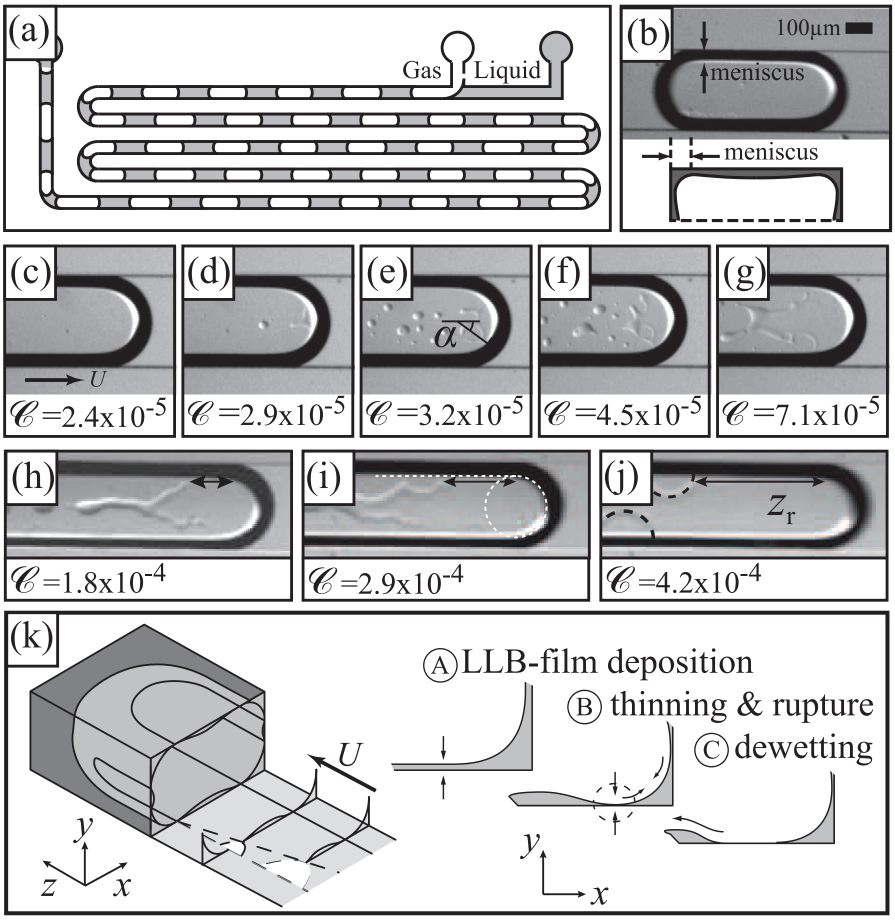
(a)
Gas
Liquid
(b)
100μm
meniscus
meniscus
(c)
U
$\mathscr{C}$=2.4x10^{-5}
(d)
$\mathscr{C}$=2.9x10^{-5}
(e)
α
$\mathscr{C}$=3.2x10^{-5}
(f)
$\mathscr{C}$=4.5x10^{-5}
(g)
$\mathscr{C}$=7.1x10^{-5}
(h)
$\mathscr{C}$=1.8x10^{-4}
(i)
$\mathscr{C}$=2.9x10^{-4}
(j)
z_r
$\mathscr{C}$=4.2x10^{-4}
(k)
Ⓐ LLB-film deposition
Ⓑ thinning & rupture
Ⓒ dewetting
U
y
z
x
y
x

Figure 2.1 (a) Sketch of the experimental setup. (b) Top-view micrograph of a flowing bubble; dark regions in the image indicate corner menisci. (c)-(g) Microscope observations of Landau-Levich-Bretherton (LLB) film deposition dynamics; films are deposited at capillary numbers $\mathscr{C} > 2.5 \cdot 10^{-5}$. (h)-(j) Observations of dewetting dynamics - films rupture at the corners and move along circular fronts; z_r is a speed-dependent length of unruptured film. (k) Schematic 3D cut-out near the nose of the bubble (left) and $x - y$ cross-sections of the lubricating film at increasing distance from the nose, depicting the important events, including film deposition, rupture and dewetting (right).

curvature in the z-direction has vanished, determined by fitting a circle and straight line to the inner black shadow of the micrographs (Fig.2.1(i)). At higher speeds, the main source of uncertainty was the interpolation between two frames to find the moment of rupture. We did this interpolation as follows: after rupture of the film near the meniscus, a dewetting front developed that spread out radially at $2.2\,\mathrm{mm\,s^{-1}}$, independent of film thickness in agreement with theory[14]. We measured the radius of this front in several frames after rupture, as shown by the black dotted circles in Fig.2.1(j). Then, we extrapolated the time evolution of this front to zero to achieve sub-frame resolution of the time and location of rupture. In turn, this sub-frame resolution of the rupture time straightforwardly allowed interpolation of the location of the nose at the rupture between two frames to find z_r.

The sequence of images in Fig. 2.1(c-j) shows that there are three distinct regimes: a fully dewetted regime without a LLB film, (Fig. 2.1(c)), a partially wetted regime where the LLB film ruptures, but such that the dewetting front cannot 'catch-up' with the nose (Fig. 2.1(d-j)), and finally a fully wetted regime in which the lifetime of the LLB film is longer than the convective time l/U of the bubble. Jose and Cubaud[8] observed this last regime as a 'lubricated' regime and observed droplets (bubbles) that at least partially wet the walls in the other two regimes. Their experimental data for different silicon oils with water droplets collapsed onto a regime boundary as $l/w = \zeta U^{1/3}\mathscr{C}^{2/3}$, where ζ is a dimensional constant. In the following, we derive this regime boundary from the evolution of the LLB film.

2.3 Rupture time from Thin Film Equation

A bubble moving through a rectangular microchannel, besides depositing thin films, also leaves liquid 'gutters' along the channel edges, with a meniscus of radius $r^{-1} = (2w_c^{-1} + 2h_c^{-1})$ (Fig 2.1(b)). Axial flow in these gutters can be ignored, but a Laplace pressure difference $p = \gamma/r$ causes transverse flow, which is balanced by viscous drag in the deposited film. Where the meniscus meets the flat part of the film, the film thins out by liquid drainage into a localized dimple, where long-range forces eventually induce a rapid collapse.

The evolution of the film thickness $h(x,t)$ in the dimple near the meniscus is described by the thin-film equation[1]

$$\partial_t h + \partial_x \left(\frac{\gamma}{3\mu} h^3 \partial_{xxx} h + \frac{A}{6\pi\mu h} \partial_x h \right) = 0. \tag{2.1}$$

in a region around $x{=}0$ where the meniscus meets the thin film. We use the disjoining pressure approximation, in which the long-range intermolecular forces between the phases are replaced by a disjoining pressure $\Pi = A/6\pi h_0^3$ applied at the film boundary[15]. For negative x, the dimple region will match onto the stagnant meniscus of constant curvature, i.e.

$$h = h_0 + \frac{x^2}{2r}, \quad \partial_{xx} h = r^{-1} \quad \text{for} \quad x \ll 0. \tag{2.2}$$

The film deposited by the nose is not flat and decreases in thickness from $h_0 \sim h_c \mathscr{C}^{2/3}$ near the centerline to $h_0 \sim h_c \mathscr{C}$ near the menisci at the sides, where h_c is the microchannel height[6]. Then, the initial slope and curvature for small and positive x are $\partial_x h \sim \mathscr{C}^{2/3}$ and $\partial_{xx} h \sim \mathscr{C}^{2/3}/w_c$ respectively, and for small $\mathscr{C}$ we may use

$$h = h_0, \quad \partial_x h = 0 \quad \text{for} \quad x \gg 0 \tag{2.3}$$

to complete the boundary conditions. A suitable choice of scales for time, transverse coordinate and height is

$$t^* = \frac{12\pi^2 \mu \gamma h_0^5}{A^2}, \qquad x^* = h_0^2 \sqrt{2\pi\gamma/A}, \qquad h^* = h_0. \tag{2.4}$$

Scaling with $H{=}h/h^*$, $T{=}t/t^*$, $X{=}x/x^*$ removes all parameters from (2.1) to get

$$\partial_T H + \partial_X \left(H^3 \partial_{XXX} H + \frac{1}{H} \partial_X H \right) = 0, \tag{2.5}$$

$$H = 1{+}\frac{1}{2}\kappa X^2, \quad \partial_{XX} H = \kappa \quad \text{for} \quad X \ll 0, \text{ and} \quad H = 1, \quad \partial_X H = 0 \quad \text{for} \quad X \gg 0 \tag{2.6}$$

and leaves only a dimensionless curvature

$$\kappa = \frac{\pi h_0^3 \gamma}{A} r^{-1} \tag{2.7}$$

in the boundary conditions. This last remaining parameter, κ, signifies the relative strength of the initial Laplace pressure jump (γ/r) at $x = 0$ to the disjoining pressure Π_0 at the initial film thickness.

Fig. 2.2(a) shows a numerical solution of (2.1) for $\kappa = 50$, starting from $H = 1{+}\kappa X^2$ $(x < 0)$, $H = 1$ $(x \geq 0)$. A depression in the film develops having a minimum film thickness $H_{\min}$ near $x = 0$. First, a self-similar film profile develops, up to $H_{\min} \approx 0.2$ at $T = 2.3 \cdot 10^{-3}$, which marks the depth of the dimple region where long-range forces become prominent. From that moment onwards, the film thins out in a region $|X| < 0.1$, leading to rupture at $T = 2.5 \cdot 10^{-3}$. In this short time, the dimple profile is hardly affected outside the fast-pinching region, indicating how fast the final pinch is in comparison to the earlier thinning.

At early times, h is large and the dimple slope $\partial_x h$ is small, such that the disjoining pressure term in (2.1) may be ignored. Variables associated with this early stage are denoted by the symbol $\hat{}$. Characteristic scales for time, height and width of the dimple are

$$\hat{t}^* = \frac{3\mu r^4}{\gamma h_0^3}, \quad \hat{h}^* = h_0, \quad \hat{x}^* = \frac{x}{r}. \tag{2.8}$$

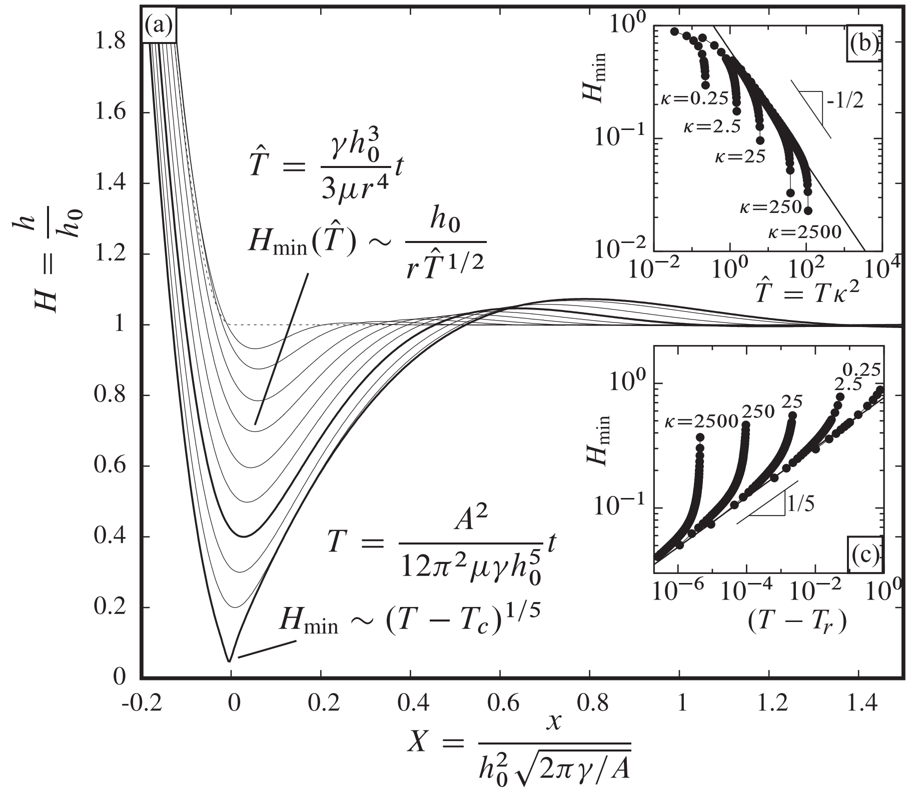

Figure 2.2 (a) Dimensionless film height profiles H in the dimple region at various times T=(0.01, 0.03, 0.08, 0.15, 0.27, 0.45, 0.75, 1.28, 2.0, 2.5) $\cdot\ 10^{-3}$ from numerical solutions of (2.1) for $\kappa = 50$. The highlighted profile indicates a transition from an early drainage dominated regime[9] to a long range force induced rupture regime[10]. (b)-(c) Minimum film height $H_{\min}$ values extracted from numerical solutions of (2.1) for various κ are well described by the two self-similar expressions for minimum film height $H_{\min}$ provided in (a) at early and late times respectively.

Now rescaling allows a self-similar solution[9], where the width of the dimple grows as $\hat{W} \sim h_0/r\hat{T}^{1/4}$ and the height of film decreases as $\hat{H}_{\min} \sim h_0/r\hat{T}^{1/2}$. Fig. 2.2(b) shows that the evolution of the minimum in film thickness for $0.25 < \kappa < 2.5 \cdot 10^3$ all collapse onto a single master-curve of $\hat{H}_{\min} \approx 0.6\hat{T}^{-1/2}$ of a monotonically decreasing thinning rate. This master-curve describes the evolution of films that are still so thick that the disjoining pressure need not be taken into account. Films that are initally already so thin that the disjoining pressure is relevant from the start, such as that of $\kappa = 0.25$, never fully experience this regime. As soon as the long-range intermolecular term becomes dominant, however, the thinning rate increases, rapidly, as the early and late time scales are related as $\hat{T} = \kappa^2 T$: for large κ the time scale of the problem changes by orders of magnitude as the dimple moves through progressive stages of thinning. Close to the time of rupture T_r, the evolution of the minimum film thickness is also amenable to a self-similar analysis[10], which predicts that $H_{\min}$=$0.7681(T - T_r)^{1/5}$, independent of κ. We find indeed that for all κ, the final evolution of the minimum film height collapse onto this curve (Fig 2.2(c)). Here too, note that for $\kappa = 0.25$, the film is initially so thin that its entire evolution collapses onto this curve.

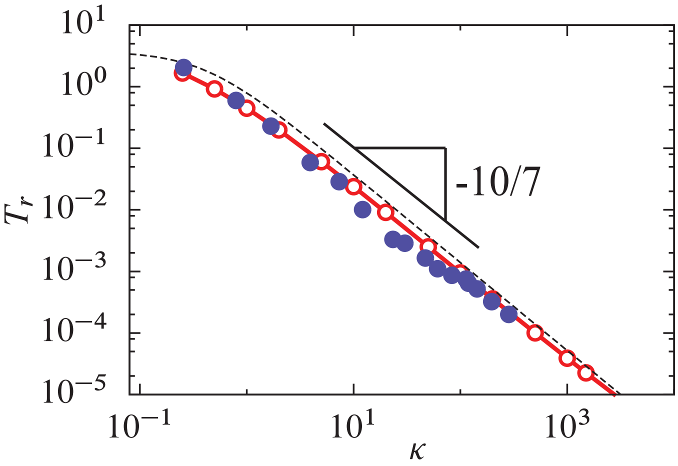

Figure 2.3 (colour online) Film rupture time versus dimensionless meniscus curvature κ. The red markers are numerical calculations. The dotted line is the theoretical prediction $T_r = 3.92[1 + 3.74\kappa^{10/7}]^{-1}$ obtained by matching the two self-similar solutions from Fig. 2.2. The blue markers represent experimental data of rupture times of ethanol films deposited around long bubbles on a PDMS surface.

We now explore whether we can match these two asymptotic descriptions to describe the entire evolution. The crudest matching is using the early curve for the minimal film height $H_{\min}$ up to a given H' at T' and then instantaneously switching to the other curve. This matching amounts to requiring that $H_{\min}$ and $\partial_T H_{\min}$ are continuous at T' and is, in fact, identical to calculating the value of H' for which the rupture is fastest, $\partial_{H'} T_r = 0$, as proposed by Vrij[16]. After some algebra, one finds that the cross-over occurs at $T' = 0.913\kappa^{-10/7}$, with $H' = 0.627\kappa^{-2/7}$, and the film ruptures at $T_r = 1.278\kappa^{-10/7}$. Of course, when the film is initially so thin that rupture is dominated by van der Waals forces from the beginning, only the last asymptotic description is needed. One expects this to happen for $\kappa \ll 1$ and, indeed, we find $T_r = 13.0$ for all $\kappa < 0.196$. We find that this matching systematically overestimates the numerical rupture times, because at the cross-over both capillary thinning and long-range forces are important. Following the structure of equation (2.1), in which the capillary term

$\partial_X(H^3\partial_{XXX}H)$ and long-range term $\partial_X(H^{-1}\partial_X H)$ contribute additively to the rate of thinning $\partial_T H$, it is better to add the thinning rates of both regimes. We begin by rewriting the rate of thinning $\partial_T H$ in terms of H. For the early regime with $\partial_T H = -0.3\kappa^2(\kappa^2 T)^{-3/2}$ we use the $H = 0.6(\kappa T)^{-1/2}$ to eliminate T, to obtain $\partial_T H = -1.388\kappa^2 H^3$. Likewise for the late regime, we recast $\partial_T H = -0.1536(T_r - T)^{-4/5}$ into $\partial_T H = -0.053H^{-4}$. We then add these contributions to obtain the overall $\partial_T H$ and integrate the resulting $\partial_H T = (\partial_T H)^{-1}$ from initial to final height to obtain the rupture time. The rupture time is then given by

$$T_r = \int_0^1 \left(1.38\kappa^2 H^3 + 0.053H^{-4}\right)^{-1} dH \approx 3.92[1 + 3.74\kappa^{10/7}]^{-1}. \tag{2.9}$$

The integral can be evaluated analytically to an impractically long expression, and the approximate solution is compact and captures the relevant physics, as it is based on the limiting values $T_r \to 3.92$ for $\kappa \to 0$ and $T_r \to 1.048\kappa^{-10/7}$ for $\kappa \to \infty$ of the full analytical solution. Fig. 2.3 shows how well this prediction of rupture time agrees with the numerical simulations. For large κ, the analytical result tends to the numerical value. As can be seen in Fig. 2.2(b), for $\kappa \gg 1$ the two thinning regimes are well separated and the evolution of $H_{\min}$ runs closely along the asymptotic master curves. For smaller values of κ, the separation of the regimes is less pronounced and $H_{\min}$ does not evolve on the capillary master curve, which accounts for the small difference in analytical and numerical result. Nevertheless, the matching of the two regimes does identify the proper scaling of the rupture time with the only parameter of the problem, and the numerical results corroborate the $-10/7$ exponent derived above.

Returning to our experiments, we could easily vary the deposited film thickness by adjusting the bubble speed, with negligible impact on the meniscus curvature. We measured the time of rupture accurately as $t_r = z_r/U$. With experimental Capillary numbers in the range $10^{-4} < \mathscr{C} < 3 \cdot 10^{-3}$, we used $h_0 \approx 0.5 h_c \mathscr{C}^6$ to estimate the initial film thickness in the range h_0 in $[6 - 180]$ nm, such that our experiments spanned three orders of magnitude of κ and four decades of rupture time, $T_r = t_r/t^* = (8z_r A^2)/(3\pi^2\gamma^2 h_c^5 \mathscr{C}^6)$. Fig.2.3 shows that the time needed to rupture elongated bubbles in microchannels agrees very well with theory. In dimensional quantities, the large-κ limit of the rupture length, as measured from the nose of the bubble, is given by

$$z_r = 1.73\left(\frac{h_c^3 w_c^2}{(h_c + w_c)^2}\right)^{5/7}\left(\frac{\mu^3 U^3}{A\gamma^2}\right)^{4/7} \tag{2.10}$$

where for clarity we have isolated the geometric parameters from the flow parameters. The distance from the nose where dewetted patches of the lubricating film begin to grow is proportional to $U^{12/7}$, which is larger than the linear scaling $z_r \propto U$ that Jose and Cubaud[8] found. In our analysis, the time needed to rupture t_r increases with initial film thickness, which requires that $z_r = Ut_r$ increases more than linearly with velocity.

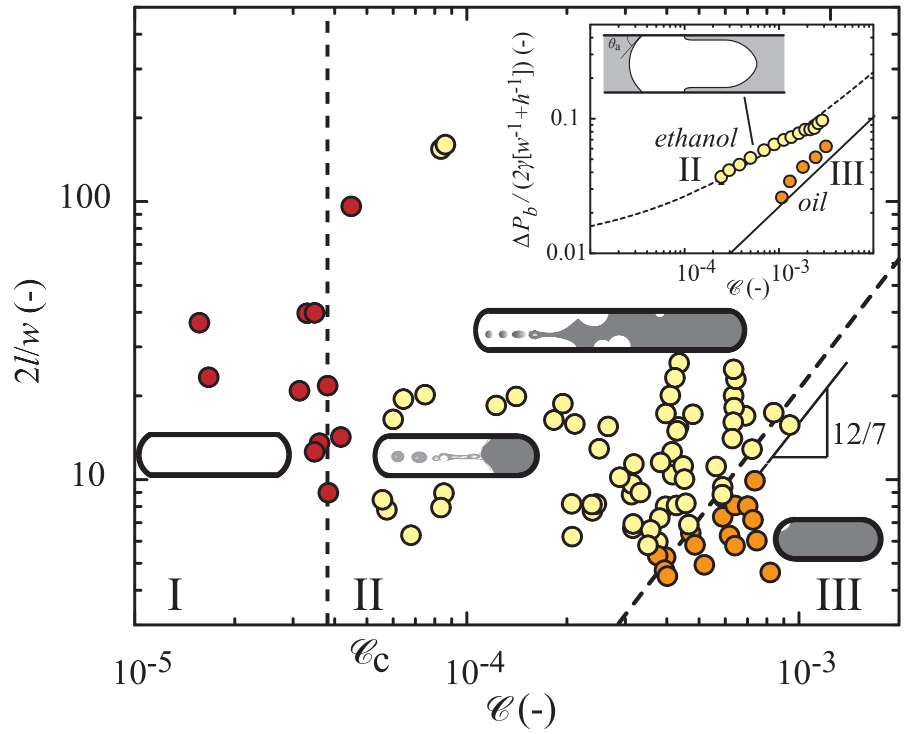

Figure 2.4 Map of observed topological regimes, for PDMS-ethanol-air, arising from the dynamics of film deposition and rupture: (I) no film deposition below a threshold $\mathscr{C}$, (II) simultaneous film deposition and dewetting - a speed dependent unruptured length of film exists in all cases, and (III) completely lubricated bubbles encapsulated in intact thin films. (Inset) Measured pressure drop across bubbles depends strongly on the topological regime.

2.4 Flow regimes and pressure drop

In the context of digital microfluidics, droplets contain analytes and reagents that should remain isolated from each other and have no interaction, chemical or otherwise, with the wall. We consolidate our experimental observations in a topological map of dimensionless bubble length versus capillary number (Fig. 2.4), featuring two boundaries. The first, corresponding to a critical capillary number $\mathscr{C}_c \sim 3\cdot 10^{-5}$ indicates the minimum speed to observe films at all. The second boundary shows how short the bubble must be to ensure complete surrounding by wetting films. This boundary is well predicted by our analysis of rupture times (Fig. 2.3) with $z_r \sim \mathscr{C}^{12/7}$ as shown in Fig 2.4. The preceding analysis neglects the fluid above the lubricating film in the fluid-mechanical problem, which is appropriate for the bubbles we analyzed experimentally. For liquid droplets, however, this may not be the case, and effects on Hamaker constant and viscous drag need to be accounted for. However, we note that the latter effect may not be dominant, especially when droplet viscosity is lower than that of the carrier fluid, as is typically the case in microfluidic experiments.

To highlight the importance of partial wetting for the overall fluid mechanics of digital microflows, even at small contact angles, we now examine the implications of differences in film topologies on the frictional drag of bubble motion. We calculate the friction experienced by a flowing bubble, expressed as the pressure jump across the bubble, as $\Delta p_{\mathrm{B}} = (\Delta p - RUwh)/n$, where n is the total number of bubbles in the device. The hydrodynamic resistance, R, in the liquid segments, is equivalent to flow without bubbles, and given by $R = \mu[12/(1-0.63\,hw^{-1})](L_{\mathrm{liq}}/h^3 w)$. In experiments using fully-wetting silicone oil (μ=10 mPa s, γ=20.1 mN m^{-1}, θ_0=0°) at $\mathscr{C} = O(10^{-3})$, we find indeed that the pressure jump per bubble is a few percent of (γ/r), and scales as predicted, finding $\Delta p = 2.1\mathscr{C}^{2/3}(\gamma/r)$ within 25% of the theoretical value[6,17]. In the second regime in Fig. 2.4, the front of the bubble is lubricated by a wetting film that ruptures, and the rear is an advancing contact line. In this case, the net pressure jump over the bubble can be written in terms of curvature differences ΔC as $\Delta p_{\mathrm{B}} \sim \gamma\Delta C$. The curvature at the (lubricated) nose is $r^{-1}\cos\theta_e + \beta\mathscr{C}^{2/3}$[6], and that at the rear can be written as $r^{-1}\cos\theta_a$ in terms of an advancing dynamic contact angle $\theta_a^3 = \theta_e^3 + 9\ln(r/\ell_m)\mathscr{C}$, where ℓ_m is a microscopic slip length[18]. In the inset of Fig. 2.4, we calculate the pressure drop for the partially-lubricated bubbles. Interestingly, for $\mathscr{C} > 10^{-3}$, the pressure drop scales again as $\Delta p_{\mathrm{B}} \sim \mathscr{C}^{2/3}$ (which follows from expanding $1 - \cos\mathscr{C}^{1/3} \approx \frac{1}{2}\mathscr{C}^{2/3}$), but the pressure drop per bubble is a factor 2-3 higher, even at the small contact angle $\theta_e = 8°$ of ethanol on PDMS. Recent experiments of pressure drop of bubbles in rectangular PDMS channels[19] did obey the $\Delta p \sim \mathscr{C}^{2/3}$ scaling, but also exhibited higher proportionality constants for aqueous surfactant solutions than those predicted by theory[6], which may well have been caused by partial wetting with small contact angles, in agreement with our experiments.

2.5 Conclusions

In conclusion, in this paper we explain the full evolution of nonconformal thin films under the action of surface-tension and intermolecular forces. These nonconformal films exhibit LLB flat films connected to gutters that are akin to Plateau borders. The films first thin out due to capillary suction at the boundary between gutter and flat film to create a dimple, until intermolecular forces take over to rapidly thin out this dimple.

The ratio of capillary and intermolecular forces, as expressed in a dimensionless parameter κ, determines how much of the thinning occurs in the first regime and how much in the second. We predict and experimentally verify the dimensionless moment of rupture as $T_r \sim \kappa^{-10/7}$. The present analysis offers a glimpse into the phenomena that mark the transition from regular droplet and pearl-type flows to chaotic flows in partially wetting channels[7,8].

Acknowledgements

It is a pleasure to acknowledge Michiel Musterd, Volkert van Steijn, Chris Kleijn and Jacco Snoeijer for fruitful discussions and comments on earlier version of this manuscript.

Bibliography

[1] A. Oron, S. H. Davis, and S. G. Bankoff. Long-scale evolution of thin liquid films. Rev. Mod. Phys., 69(3):931–980, 1997. doi: 10.1103/RevModPhys.69.931.
D. Bonn, J. Eggers, J. Indekeu, J. Meunier, and E. Rolley. Wetting and spreading. Rev. Mod. Phys., 81:739–805, 2009. doi: 10.1103/RevModPhys.81.739.
J. H. Snoeijer and B. Andreotti. Moving contact lines: Scales, regimes and dynamical transitions. Ann. Rev. Fluid Mech., 45:269–92, 2013. doi: 10.1146/annurev-fluid-011212-140734.
P. G. de Gennes, F. Brochard-Wyard, and D. Quéré. Capillary and Wetting Phenomena: Bubbles, Pearls, Waves. Springer, New York, NY 10013, 2004.
P. G. De Gennes. Wetting - statics and dynamics. Rev. Mod. Phys., 57(3):827–863, 1985. doi: 10.1103/RevModPhys.57.827.
J. Ziegler, J. H. Snoeijer, and J. Eggers. Film transitions of receding contact lines. Eur. Phys. J.-Spec. Top., 166(1):177–180, 2009. doi: 10.1140/epjst/e2009-00902-3.
M. Galvagno, D. Tseluiko, H. Lopez, and U. Thiele. Continuous and discontinuous dynamic unbinding transitions in drawn film flow. Phys. Rev. Lett., 112(13):137803, 2014. doi: 10.1103/PhysRevLett.112.137803.
J. H. Snoeijer, B. Andreotti, G. Delon, and M. Fermigier. Relaxation of a dewetting contact line. part 1. a full-scale hydrodynamic calculation. J Fluid. Mech., 579:63–83, 2007. doi: 10.1017/s0022112007005216.

[2] L. Landau and B. Levich. Dragging of a liquid by a moving plate. Acta Physicochim. URSS, 17(42), 1942.
F. P. Bretherton. The motion of long bubbles in tubes. J. Fluid. Mech., 10:166–88, 1961. doi: 10.1017/S0022112061000160.
D. Quere, J. M. Dimeglio, and F. Brochard-Wyard. Spreading of liquids on highly curved surfaces. Science, 249(4974):1256–1260, 1990. doi: 10.1126/science.249.4974.1256.
H. A. Stone. Batchelor prize lecture interfaces: in fluid mechanics and across disciplines. J. Fluid Mech., 645(1):25, 2010. doi: 10.1017/S0022112009994186.

[3] A. Vrij and J. T. G. Overbeek. Rupture of thin liquid films due to spontaneous fluctuations in thickness. J. Am. Chem. Soc., 90(12):3074–3078, 1968. doi: 10.1021/ja01014a015.

[4] R. Seemann, M. Brinkmann, E. J. Kramer, F. F. Lange, and R. Lipowsky. Wetting morphologies at microstructured surfaces. Proc. Nat. Acad. Sci. USA, 102(6):1848–1852, 2005. doi: 10.1073/pnas.0407721102.
R. Mukherjee, D. Bandyopadhyay, and A. Sharma. Control of morphology in pattern directed dewetting of thin polymer films. Soft Matter, 4:2086–2097, 2008. doi: 10.1039/B806925E.
Stephan Herminghaus, Martin Brinkmann, and Ralf Seemann. Wetting and dewetting of complex surface geometries. Annu. Rev. Mater. Res., 38:101–121, 2008.

[5] A. De Lozar, A. Juel, and A. L. Hazel. The steady propagation of an air finger into a rectangular tube. J Fluid. Mech., 614:173–195, 2008. doi: 10.1017/S0022112008003455.

[6] H. Wong, C. J. Radke, and S. Morris. The motion of long bubbles in polygonal capillaries .1. thin films. J Fluid. Mech., 292:71–94, 1995. doi: 10.1017/S0022112095001443.
H. Wong, C. J. Radke, and S. Morris. The motion of long bubbles in polygonal capillaries .2. drag, fluid pressure and fluid-flow. J Fluid. Mech., 292:95–110, 1995. doi: 10.1017/S0022112095001455.

[7] R. Dreyfus, P. Tabeling, and H. Willaime. Ordered and disordered patterns in two-phase flows in microchannels. Phys. Rev. Lett., 90(14):144505, 2003. doi: 10.1103/PhysRevLett.90.144505.

[8] B. M. Jose and T. Cubaud. Formation and dynamics of partially wetting droplets in square microchannels. RSC Adv., 4:14962–14970, 2014. doi: 10.1039/C4RA00654B.

[9] A. Aradian, E. Raphael, and P. G. de Gennes. Marginal pinching in soap films. Europhys. Lett., 55 (6):834–840, 2001. doi: 10.1209/epl/i2001-00356-y/fulltext/.

[10] W. W. Zhang and J. R. Lister. Similarity solutions for van der waals rupture of a thin film on a solid substrate. Phys. Fluids, 11(9):2454–2462, 1999. doi: 10.1063/1.870110.

[11] P. Garstecki, M. J. Fuerstman, H. A. Stone, and G. M. Whitesides. Formation of droplets and bubbles in a microfluidic t-junction - scaling and mechanism of break-up. Lab Chip, 6(3):437–446, 2006. doi: 10.1039/B510841A.
V. van Steijn, C. R. Kleijn, and M. T. Kreutzer. Flows around confined bubbles and their importance in triggering pinch-off. Phys. Rev. Lett., 103:214501, Nov 2009. doi: 10.1103/PhysRevLett.103.214501.

[12] J. Léopoldès and P. Damman. From a two-dimensional chemical pattern to a three-dimensional topology through selective inversion of a liquid–liquid bilayer. Nature Mat., 5(12):957–961, 2006. doi: 10.1038/nmat1787.

[13] T. Shing Chan, T. Gueudré, and J. H. Snoeijer. Maximum speed of dewetting on a fiber. Phys. Fluids, 23(11):112103, 2011. doi: 10.1063/1.3659018.

[14] C. Redon, F. Brochard-Wyard, and F. Rondelez. Dynamics of dewetting. Phys. Rev. Lett., 66(6): 715–718, 1991. doi: 10.1103/PhysRevLett.66.715.

[15] B. Dai, L. G. Leal, and A. Redondo. Disjoining pressure for nonuniform thin films. Phys. Rev. E, 78:061602, Dec 2008. doi: 10.1103/PhysRevE.78.061602.

[16] A. Vrij. Possible mechanism for the spontaneous rupture of thin, free liquid films. Discuss. Faraday Soc., 42:23–33, 1966. doi: 10.1039/DF9664200023.

[17] A.L. Hazel and M. Heil. The steady propagation of a semi-infinite bubble into a tube of elliptical or rectangular cross-section. J Fluid. Mech., 470:91–114, 2002.

[18] E. Rio, A. Daerr, B. Andreotti, and L. Limat. Boundary conditions in the vicinity of a dynamic contact line: Experimental investigation of viscous drops sliding down an inclined plane. Phys. Rev. Lett., 94(2):024503, 2005. doi: 10.1103/PhysRevLett.94.024503.

[19] M. J. Fuerstman, A. Lai, M. E. Thurlow, S. S. Shevkoplyas, H. A. Stone, and G. M. Whitesides. The pressure drop along rectangular microchannels containing bubbles. Lab Chip, 7(11):1479–1489, 2007.

3. Thermal fluctuations in capillary thinning of thin liquid films[§]

Thermal fluctuations have been shown to influence the thinning dynamics of planar thin liquid films, bringing predicted rupture times closer to experiments. Most liquid films in nature and industry are, however, non-planar. Thinning of such films not just results from the interplay between stabilizing surface tension forces and destabilizing van der Waals forces, but also from drainage due to curvature differences. This work explores the influence of thermal fluctuations on the dynamics of thin non-planar films subjected to drainage, with their dynamics governed by two parameters: the strength of thermal fluctuations, θ, and the strength of drainage, κ. For strong drainage ($\kappa \gg \kappa_{tr}$), we find that the film ruptures due to the formation of a local depression called a dimple that appears at the connection between the curved and flat parts of the film. For this *dimple-dominated* regime, the rupture time, t_r, solely depends on κ, according to the earlier reported scaling, $t_r \sim \kappa^{-10/7}$. By contrast, for weak drainage ($\kappa \ll \kappa_{tr}$), the film ruptures at a random location due to the spontaneous growth of fluctuations originating from thermal fluctuations. In this *fluctuations-dominated* regime, the rupture time solely depends on θ as $t_r \sim -(1/\omega_{max}) \ln(\sqrt{2\theta})^{\alpha}$, with $\alpha = 1.15$. This scaling is rationalized using linear stability theory, which yields ω_{max} as the growth rate of the fastest-growing wave and $\alpha = 1$. These insights on if, when and how thermal fluctuations play a role are instrumental in predicting the dynamics and rupture time of non-flat draining thin films.

[§] Published as: M. .S. Shah, V. van Steijn, C. R. Kleijn, M. T. Kreutzer, Thermal fluctuations in capillary thinning of thin liquid films. Journal of Fluid Mechanics 876, 1090-1107, 2019, doi: 10.1017/jfm.2019.595.

3.1 Introduction

The dynamics of thin planar liquid films on solid surfaces has been extensively studied in the context of free-surface instabilities[1,2]. The stability of such films depends on the interplay between surface tension on the one hand, that always stabilizes the film, and intermolecular forces on the other hand, that may destabilize it. The evolution of unstable planar films starts from minute corrugations on the free interface originating from stochastic thermal motion of molecules. In the absence of destabilizing intermolecular forces, the film is stable and dynamically perturbed by corrugations of amplitude $\sim \sqrt{k_B T/\gamma}$, with k_B the Boltzmann constant, T the absolute temperature and γ the interfacial tension[3]. For unstable films, these corrugations spontaneously grow until the film ruptures. In the last decade, thermal fluctuations have been explicitly incorporated into the thin film equation using a stochastic term, bringing simulations[4] closer to experiments for planar films[5].

Many films encountered in natural and industrial settings are, however, not planar. Typically, highly curved regions exist at the edges immediately after film formation, examples being the film between two foam bubbles, the wetting film between an elongated bubble and the walls of a non-circular capillary, the curved edges of a soap film supported on a wire frame, and the tear film on eye lids. These curved regions impose a localized pressure gradient that drains the film towards the curved edges. The dynamics of non-planar films is hence governed by two thinning mechanisms: (1) capillary thinning, i.e. drainage due to curvature differences and (2) spontaneous growth of fluctuations originating from thermal fluctuations. The interplay of these two thinning mechanisms is the subject of this paper.

Theory on the dynamics of films solely governed by drainage (and not by the spontaneous growth of fluctuations) goes back to Reynolds[6], who modelled the drainage of a planar film as spatially uniform thinning caused by a prescribed pressure jump at the edge of the film. It is, by now, known that non-planar films do not thin out uniformly, unless they are, in some sense, small[7–9]. Larger films develop a local depression called a *dimple* near the film edge that eventually leads to rupture[10]. Joye et al.[11] determined a criterion for the thinning predominantly due to the formation of a dimple by comparing the curvature of the dimple with that of the meniscus. For many practical systems, this criterion teaches that films with a radius larger than about 50 μm have dimples[12,13]. For such large films, our recent work[14] provides a scaling rule for the rupture times of unstable films with the relative strength of drainage and intermolecular forces as the key governing parameter. Here, we focus on this large-film limit, where thinning is non-uniform and confined to a dimple at the edge of the film.

How the dynamics of non-planar films alters when, on top of drainage, thinning also occurs through the spontaneous growth of fluctuations is not yet fully understood.

Vrij[15] and Scheludko[16] attribute a crucial role to thermal fluctuations in the spontaneous growth of unstable waves leading to rupture. One of the seminal papers by Vrij[15] postulates that a film initially thins uniformly while all fluctuations are dampened until the stability flips as predicted from linear stability analysis. After this flip, a wave with growing amplitude fits within the length of the film such that the film ruptures at the trough of the wave. However, experimental observations have noted significant fluctuations in film thickness already from the onset of drainage, whether thermal[17] or hydrodynamic[13] in origin. Manev et al.[13] show in their experiments that these fluctuations do not dampen out if they are large enough, and attribute this to the large nonlinearities in the thin film equation. To account for the observed deviations between experiments and Reynolds' theory, several theories have been developed that semi-empirically incorporate non-uniform thinning together with fluctuations in the description of planar film thinning[13,18–20]. Although these theories are in reasonable agreement with experiments, they do not teach if and when rupture occurs through the formation of a dimple or due to the spontaneous growth of waves originating from thermal fluctuations, or are due to both. This lack of clarity is also reflected in the more recent literature; some studies emphasize the relevance of thermal fluctuations resulting in stochasticity in film rupture[21–23], whereas other studies argue that the influence of this stochastic phenomenon is insignificant[24,25]. Aarts and Lekkerkerker[21] reported illustrative experiments of interfaces with ultra-low interfacial tension, which visually reveal the role of thermal fluctuations in inducing rupture. Rio and Biance[22] in their review compare the order of magnitude of the time scales of drainage and of the spontaneous growth of thermal fluctuations, and suggest that stochastic rupture due to thermal fluctuations is relevant in determining film rupture times. Perumanath et al.[23] show using molecular dynamics simulations that, in the absence of film drainage, the onset of coalescence is a stochastic phenomenon triggered by thermal fluctuations. In contrast, Vakarelski et al.[24] and Chan et al.[25] argue that thermal fluctuations play no significant role in the rupture of films in parameter ranges typical for the coalescence of droplets and bubbles.

The aim of this work is to systematically study the dynamics of thin liquid films subjected to curvature-induced drainage for a wide parameter space in terms of drainage strength and thermal noise strength and to resolve when one of the two abovementioned thinning mechanisms is dominant. The model geometry considered in this numerical study is a semi-infinite planar film connected to a curved film of constant curvature, known as a Plateau border. We incorporate thermal fluctuations at the gas-liquid interface using a stochastic term in the thin film equation[4,26], which allows us to study the effect of different strengths of thermal noise. Contrary to large films of finite size, as for the example found in Scheludko-cell experiments e.g.[17,27,28] in which dimple formation and thinning of the planar part of the film occur simultaneously leading to a complex dependency of rupture time on film size, we consider this semi-infinite geometry which evolves in the limit of full dimple formation, also known as *marginal pinching*[29]. The selected geometry and a wide parameter space in terms of

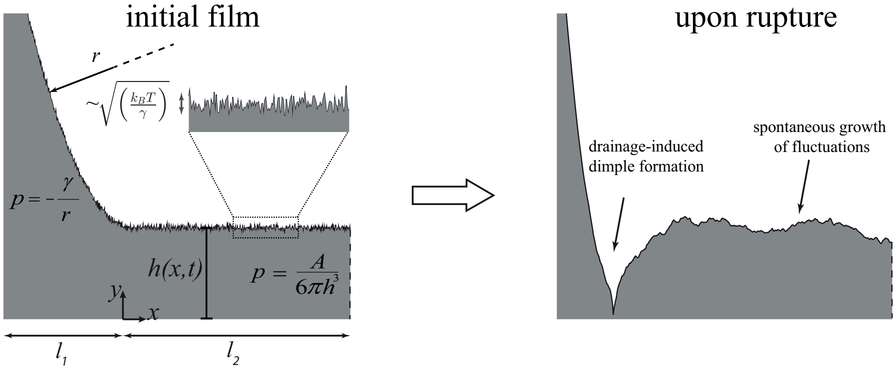

Figure 3.1 Schematic of a non-flat draining thin film subjected to thermal fluctuations, with the film thickness parameterized by $h(x,t)$. (left) The initial film shows a curved part extending from $-l_1 \leq x < 0$ with the pressure given by the Laplace pressure, $p = -\gamma/r$, with $1/r$ as the curvature imposed at the edge. This curved part is connected to a flat part extending from $0 \leq x \leq l_2$ with the pressure given by the van der Waals component of the disjoining pressure, $p = A/6\pi h^3$. Besides curvature-induced drainage, the film is also subjected to thermal fluctuations of the free interface, resulting in thickness variations of amplitude $\sim \sqrt{k_B T/\gamma}$. The dashed line at $x = l_2$ signifies the symmetry in the system. (right) Shape upon rupture, highlighting that film thinning stems from two competing mechanisms: (1) the formation of a localised dimple due to curvature-induced drainage and (2) the spontaneous growth of waves originating from thermal fluctuations.

drainage strength and thermal noise strength defines the problem in its simplest form and allows us to resolve when, if and how thermal fluctuations are relevant in dimpled film rupture.

3.2 Problem Formulation

We study the evolution of non-flat thin liquid films with viscosity μ and surface tension γ, with the spatio-temporal film thickness parameterized by $h(x,t)$, as shown in figure 3.1. The film is comprised of a curved part ($-l_1 \leq x < 0$), with a curvature $1/r$ corresponding to a Plateau border, connected to a flat part ($0 \leq x \leq l_2$). Considering the pressure in the gas phase to be uniform and setting it equal to zero, the pressure p in the curved part of the liquid film, where intermolecular forces play an insignificant role, is dictated primarily by the Laplace pressure and is equal to $p = -\gamma/r$. Conversely, the pressure in the thin flat part is dictated by intermolecular forces, which in this paper, are considered as attractive van der Waals forces, such that $p = A/6\pi h^3$, with $A < 0$ being the Hamaker constant. The difference in pressure drains the liquid from the flatter part of the film to the more curved part. On top of this capillary thinning mechanism arising from curvature differences, a second thinning mechanism arises from the interplay between stabilizing surface tension forces and destabilizing van der Waals forces leading to the spontaneous growth of perturbations. These perturbations originate from thermal fluctuations at the gas-liquid interface causing corrugations of amplitude $\sim \sqrt{k_B T/\gamma}$. Depending on the relative strength between these two thinning mechanisms, the former may result in the formation of a dimple at the connection between the flat and curved part, while the later may result in the growth of unstable waves on the film interface.

The stochastic thin film equation that describes the evolution of non-planar thin films subjected to thermal fluctuations can be derived by applying a long-wave approximation on the incompressible Navier-Stokes equations with thermal noise[4]. This yields

$$\frac{\partial h}{\partial t} = -\frac{\partial}{\partial x}\left(\frac{\gamma}{3\mu}h^3\frac{\partial^3 h}{\partial x^3} + \frac{A}{6\pi\mu h}\frac{\partial h}{\partial x}\right) + \frac{\partial}{\partial x}\left(\frac{1}{3\mu}\sqrt{3h^3}\xi(x,t)\right), \tag{3.1}$$

with the first term on the right-hand side arising from surface tension forces and the second term from long-ranged attractive van der Waals forces. Together with the transient term on the left-hand side, they comprise the well known deterministic thin film equation[1,30]. The functional form of the noise term, i.e. the third term on the right-hand side, has been independently derived by Davidovitch et al.[26] and Grün et al.[4] using different approaches, with $\xi(x,t)$ constituting spatio-temporal Gaussian white noise consistent with the fluctuation-dissipation theorem. It possesses the following properties

$$\left.\begin{aligned} \langle \xi(x,t)\rangle &= 0, \\ \langle \xi(x,t)\xi(x',t')\rangle &= 2\mu k_B T\delta(x-x')\delta(t-t'), \end{aligned}\right\} \tag{3.2}$$

with $\delta(x-x')$ in units $1/\mathrm{m}^2$, resulting from the reduction of the two-dimensional fluctuating hydrodynamics equations to one dimension[4,31].

The initial film profile consists of a flat film connected to a parabola with constant curvature $(1/r)$, akin to a Plateau border. This yields the following initial condition

$$h(x<0,t=0) = h_o + \frac{x^2}{2r}, \text{ and, } h(x \geq 0, t=0) = h_o. \tag{3.3}$$

As left far-field boundary conditions, we impose an interface shape with a constant curvature similar to the system studied by Aradian et al.[29]. We impose the boundary conditions at $x = -l_1$, with l_1 chosen such that the profile remains essentially constant in time for $x \ll 0$, ensuring that the region of interest is connected to a practically static far-field profile. Note that, as usually tacitly assumed for thin-film dynamics between two far-field static profiles, the lubrication approximation needs to only hold in the transition region in-between the far-field limits[31]. As right far-field boundary condition, we have zero gradients in thickness and pressure (at $x = l_2$), such that the problem is mirror symmetric around $x = l_2$. The boundary conditions hence read

$$\left.\begin{aligned} h(x=-l_1,t) = h_o + \frac{x^2}{2r},\ \frac{\partial^2 h}{\partial x^2}(x=-l_1,t) = \frac{1}{r}, \\ \frac{\partial h}{\partial x}(x=l_2,t) = 0,\ \frac{\partial^3 h}{\partial x^3}(x=l_2,t) = 0. \end{aligned}\right\} \tag{3.4}$$

Using a height scale $h^* = h_o$, an axial length scale $x^* = h_0^2\sqrt{2\pi\gamma/A}$ and a time scale $t^* = 12\pi^2\mu\gamma h_0^5/A^2$, we obtain the dimensionless variables $\tilde{h} = h/h^*$, $\tilde{x} = x/x^*$ and $\tilde{t} = t/t^*$ together with the following dimensionless equations

$$\frac{\partial \tilde{h}}{\partial \tilde{t}} = -\frac{\partial}{\partial \tilde{x}}\left(\tilde{h}^3\frac{\partial^3 \tilde{h}}{\partial \tilde{x}^3} + \frac{1}{\tilde{h}}\frac{\partial \tilde{h}}{\partial \tilde{x}}\right) + \sqrt{2\theta}\frac{\partial}{\partial \tilde{x}}\left(\tilde{h}^{3/2}\tilde{\xi}(\tilde{x},\tilde{t})\right), \tag{3.5}$$

$$\left.\begin{aligned} \langle\tilde{\xi}(\tilde{x},\tilde{t})\rangle &= 0, \\ \langle\tilde{\xi}(\tilde{x},\tilde{t})\tilde{\xi}(\tilde{x}',\tilde{t}')\rangle &= \delta(\tilde{x}-\tilde{x}')\delta(\tilde{t}-\tilde{t}'), \end{aligned}\right\} \tag{3.6}$$

$$\tilde{h}(\tilde{x} < 0, \tilde{t} = 0) = 1 + \kappa\tilde{x}^2, \text{ and, } \tilde{h}(\tilde{x} \geq 0, \tilde{t} = 0) = 1, \tag{3.7}$$

$$\left.\begin{aligned} \tilde{h}(\tilde{x}=-\tilde{l}_1,\tilde{t}) = 1 + \kappa\tilde{x}^2,\ \frac{\partial^2 \tilde{h}}{\partial \tilde{x}^2}(\tilde{x}=-\tilde{l}_1,\tilde{t}) = 2\kappa, \\ \frac{\partial \tilde{h}}{\partial \tilde{x}}(\tilde{x}=\tilde{l}_2,\tilde{t}) = 0,\ \frac{\partial^3 \tilde{h}}{\partial \tilde{x}^3}(\tilde{x}=\tilde{l}_2,\tilde{t}) = 0, \end{aligned}\right\} \tag{3.8}$$

where ξ was made dimensionless using $\tilde{\xi} = \xi/[\gamma(h_o/x^*)^3\sqrt{2\theta/3h_o}]$ and l_1 and l_2 using x^*. This analysis shows that, besides the two parameters characterizing the domain length ($\tilde{l}_1$ and $\tilde{l}_2$), the problem is fully governed by two dimensionless control parameters, the strength of drainage, $\kappa = \pi h_o^3\gamma/Ar$, and the strength of thermal noise, $\theta = k_B T/\gamma h_o^2$. The former describes the ratio between the imposed Laplace pressure that induces drainage and the initial disjoining pressure arising from attractive van der Waals forces. The latter describes the square of the ratio between the amplitude of interface corrugations due to thermal fluctuations ($\sqrt{k_B T/\gamma}$) and the initial film thickness (h_0). We scan a wide range of values for κ ($10^{-5} - 10^3$) and θ ($4 \cdot 10^{-5} - 4 \cdot 10^{-2}$) with corresponding corrugations in thickness of $O(\sqrt{2\theta})$. While typical experimental values for κ are $\kappa \geq 10^{-1}$ and for θ are $10^{-5} - 10^{-3}$, we do not restrict ourselves to this parameter space but perform a full parametric study.

Having formulated the problem, we describe the domain considerations to capture the relevant physics. The extent of l_1 needs to be larger than the transition region in which the curvature changes from practically zero at the flat part of the film to $1/r$ in the Plateau border. The dimensional length of this transition region is estimated to be $\sim \sqrt{h_o r}$[32,33], where h_o is the initial film thickness. This gives the lower limit, $l_1 \gg \sqrt{h_o r}$. The upper limit to the extent of l_1 is dictated by the geometric constraint of the long-wave approximation, i.e., $\partial_x h \ll 1$. More specifically, the curvature as defined by $\partial_x^2 h/(1+(\partial_x h)^2)^{3/2} = 1/r$ in the parabolic description of the Plateau border should be approximately equal to $\partial_x^2 h \approx 1/r$ as assumed in the boundary condition, Eq. (3.4). Estimating $\partial_x h$ as x/r from Eq. (3.3) and setting $x = l_1$, this directly gives the upper limit, $l_1 \ll r$. Taken together, $\sqrt{1/2\kappa} \ll l_1 \ll \sqrt{r/2h_o\kappa}$ gives the lower and upper limit to l_1 in dimensionless form. The extent of l_2 is chosen such that at least one fastest-growing wave, arising from the interplay between the stabilizing surface tension forces and destabilizing van der Waals forces, fits within the film, i.e. $l_2 \geq \lambda_{max}$, with the wavelength of the fastest-growing wave (λ_{max}) estimated in the next section. All parameters and variables are made dimensionless from this point on and we therefore drop the tilde in the rest of the paper.

We conclude this section by noting that the chosen geometry allows us to study two types of systems: (1) the film between two two-dimensional bubbles with rigid interfaces (as may be encountered in surfactant-rich systems) * and (2) the film between a surfactant-free bubble and a solid wall, as for example encountered between an elongated bubble and the walls of a non-circular microchannel. In that case, a nearly flat film in the central part of the channel connects to a meniscus at the corners of the channel, with the curvature of the meniscus primarily imposed by the dimensions of the channel[34,35]. In the first system, the free interface at $y = h(x,t)$ is described by the commonly encountered tangentially immobile boundary condition[25], i.e. no-slip, while a symmetry boundary condition, i.e. no-shear, is used at $y = 0$. In the second system, the free interface is described by a no-shear condition and the wall by a no-slip condition. Although the boundary conditions for the velocity at the top and bottom of the domain are reversed for these two systems, their dynamics is described by one and the same thin film equation and the results presented throughout this paper are equally valid for both types of system.

3.3 Linear stability analysis

As an input to our numerical implementation in choosing a film large enough to accommodate a fastest-growing wave, we study how small perturbations develop on a planar thin film using linear stability theory. We consider a film of initially uniform thickness $h(x, t = 0) = 1$, subjected to perturbation of amplitude $\epsilon \ll 1$. Its response to these perturbations, represented by waves of wavelength λ, wave number $k = 2\pi/\lambda$

---

[*] For this problem description to be strictly applicable to the case of thin films between two two-dimensional bubbles, one needs to use the thickness, 2h, between the two gas-liquid interfaces instead of the currently used h in the disjoining pressure in the current problem formulation. This introduces an extra factor 8 in the denominator of the second term of Eq. 3.1.

and growth rate ω, is found by substituting $h(x,t) = h(x,t=0) + \epsilon e^{ikx+\omega t}$ in the noise-free equivalent of Eq. (3.5). In this analysis, $h(x,t)$ was made dimensionless using h^*, λ using x^*, k using $1/x^*$, and ω using $1/t^*$. Linearizing the resulting expression to $O(\epsilon)$ yields the dimensionless dispersion relation

$$\omega = -k^2\left(k^2 - 1\right). \tag{3.9}$$

The film is unstable for all ks corresponding to $\omega > 0$, and stable otherwise. The wave that grows fastest and dominates the other waves has a wavenumber $k_{max} = 1/\sqrt{2}$, with corresponding wavelength $\lambda_{max} = 2\pi/k_{max} = 2\sqrt{2}\pi \approx 8.8$ and growth rate $\omega_{max} = 1/4$. The time, t_r required for the film to rupture due to the spontaneous growth of the perturbations is hence of order of magnitude, $t_r \sim 1/\omega_{max} = 4$. How this time depends on the magnitude of the initial perturbations is estimated by considering when the magnitude of the perturbation due to the fastest-growing wave, i.e. $\epsilon e^{\omega_{max} t_r}$, is of the order of $h(x,t=0) = 1$. As the initial perturbations originate from thermal noise, such that ϵ can be approximated with the amplitude $\sqrt{2\theta}$ in Eq. (3.5), the time t_r required for the film to rupture due to the spontaneous growth of thermal fluctuations is hence of order of magnitude

$$t_r \approx (1/\omega_{max})\ln(\sqrt{2\theta})^{-1} = -4\ln(\sqrt{2\theta}). \tag{3.10}$$

3.4 Numerical implementation

We numerically solved the one-dimensional stochastic thin film equation (Eq. 3.5) along with its initial and boundary conditions (Eq. 3.7-3.8) using a finite difference method. We discretized the domain into an equidistant mesh of size, Δx, using a second-order central differencing scheme for spatial discretization and an implicit-explicit time differencing scheme of a constant time step size, Δt, with a theoretical order of accuracy of $O(\Delta t^{0.5})$[36]. The curved part extends from $-l_1 \leq x < 0$ and the flat part from $0 \leq x \leq l_2$, resulting in $N = (l_1 + l_2)/\Delta x + 1$ grid points.

We discuss the domain considerations based on the constraints described in §2. For the parabolic film profile at $-l_1 \leq x < 0$, we require $\sqrt{1/2\kappa} \ll l_1 \ll \sqrt{r/2h_o\kappa}$. We confirm that rupture times and rupture locations are insensitive to the chosen value when chosen within this range. For $\kappa \leq 0.1$, we used $l_1 = 300$, while smaller values were used for larger κ. For the flat part, we used $l_2 = 240$, which is much larger compared to the wavelength of the fastest-growing wave ($\lambda_{max} = 8.8$), as determined using a linear stability analysis. We note that, for large $\kappa \gg 1$, shorter l_2 captures the relevant physics as well, so long as at least one fastest-growing wave can be expressed in it. For small $\kappa \ll 1$, we will show later that the results weakly depend on l_2, even though $l_2 \gg \lambda_{max}$.

Time discretization of the stochastic thin film equation (Eq. 3.5) is performed using an implicit-explicit scheme, wherein the fourth-order term describing the capillary forces is discretized implicitly. The terms describing the nonlinear van der Waals forces and the stochastic noise are discretized explicitly. The mobility term in the deterministic part (h^3) is discretized as per the positivity-preserving scheme described by Diez et al.[37]. Such a scheme is not required in discretizing the square root of the mobility term in the stochastic part ($h^{3/2}$)[4], and therefore we discretize it using a standard central differencing scheme.

The stochastic term, $\xi(x,t)$, is expanded as per separation of variables in the Q-Wiener process, and further based on the lemmas given in Grün et al.[4], as follows

$$\xi(x,t) = \frac{\partial W(x,t)}{\partial t} = \sum_{q\to-\infty}^{q\to\infty} \chi_q \dot{\beta}_q(t) g_q(x) \approx \sum_{q=-\frac{N-1}{2}}^{q=\frac{N-1}{2}} \chi_q \dot{\beta}_q(t) g_q(x), \tag{3.11}$$

$$\dot{\beta}_q \approx \frac{\Delta\beta_q}{\Delta t} = \frac{\beta_q(t_{n+1}) - \beta_q(t_n)}{t_{n+1} - t_n} = \frac{\mathcal{N}_q^n \sqrt{\Delta t}}{\Delta t} = \frac{\mathcal{N}_q^n}{\sqrt{\Delta t}}. \tag{3.12}$$

where χ_q is a measure of spatial correlation (with $\chi_q = 1$ for spatially uncorrelated systems, as considered in this paper). $\dot{\beta}_q$ corresponds to white-noise processes in time, where the term $\beta_q(t_{n+1}) - \beta_q(t_n)$ is normally distributed with variance given by the time increment, Δt[4,36]. $\mathcal{N}_q^n$ are computer-generated normally distributed random numbers (using the randn MATLAB routine), which are approximately distributed with a mean of 0 and standard deviation of 1. $g_q(x)$ corresponds to the set of orthonormal eigenfunctions [4,31] according to

$$g_q(x) = \begin{cases} \sqrt{\frac{2}{L}} sin\left(\frac{2\pi q x}{L}\right), & \text{for } q < 0 \\ \sqrt{\frac{1}{L}}, & \text{for } q = 0 \\ \sqrt{\frac{2}{L}} cos\left(\frac{2\pi q x}{L}\right), & \text{for } q > 0 \end{cases} \tag{3.13}$$

with L the dimensionless domain size equal to $l_1 + l_2$. The resulting discrete noise term equals

$$\xi(x,t) = \frac{1}{\sqrt{\Delta t}} \sum_{q=-\frac{N-1}{2}}^{q=\frac{N-1}{2}} \mathcal{N}_q^n g_q(x). \tag{3.14}$$

We note here that in our finding an upwind discretization of the noise term, as proposed in Grün et al.[4], led to time step size dependent results of the rupture times. Therefore we used a central differencing scheme to discretize the stochastic term. Using $\Delta x = 0.05$ and $\Delta t = \Delta x^{2.75}$ for $\kappa \leq 10^{-1}$, and $\Delta x = 0.005$ and $\Delta t = \Delta x^{3.25}$ for $\kappa > 10^{-1}$, the presented simulation results for rupture times are grid and time step size independent within 5%, as can be seen from figure 3.7 in the appendix for the smallest and the largest value of κ considered in this work. The number of realizations for noise-inclusive simulations obtained for different values of the governing parameters κ and θ is 400, with different seeds for every realization. This yields a sampling error in mean and standard deviation of reported rupture times below $1/\sqrt{400} \triangleq 5\%$, see figure. 3.8 in the appendix. Error bars in figures 3.5 - 3.7 represent one standard deviation.

3.5 Results

3.5.1 Transition between thinning mechanisms

A signifying feature of draining thin films as compared to their non-draining counterparts is the formation of a local depression. This so-called *dimple*[11,29] results from the localized non-zero pressure gradient at the location where the flat part of the film connects to the curved part (in this study, at $x = 0$). We start with an estimate of the dimensionless curvature, κ_{tr} at which the time scale for film rupture as a result of curvature-induced drainage is comparable to the time scale for film rupture as a result of the growth of fluctuations due to the interplay between surface tension and van der Waals forces. An estimate for κ_{tr} is obtained by comparing the time scale for the dimple formation and that for the growth of fluctuations. The former is calculated as $t_r \sim 1.05\kappa^{-10/7}$ for $\kappa \gg \kappa_{tr}$ in Kreutzer et al.[14] and the latter is calculated as $t_r \approx -4\ln(\sqrt{2\theta})$ (see §3.3), independent of κ. Matching these two time scales, for realistic noise strengths of $\theta = 10^{-5} - 10^{-3}$, gives $\kappa_{tr} \approx 0.1$ at which the transition between the two thinning mechanisms occurs.

We first analyse film rupture at $\kappa \approx \kappa_{tr}$. Figure 3.2a shows the film evolution for a (noise-free) deterministic simulation ($\theta = 0$). The film profiles $h(x,t)$ illustrate the formation of a dimple at $x \sim 0$, while the film remains flat far from the dimple. Further characterizing the film dynamics based on the minimum film height, $h_{min}(t)$, as shown in the inset, we observe that its evolution consists of two stages: (i) an early stage primarily governed by drainage, roughly between $1 \geq h_{min} \gtrsim 0.8$, with a thinning rate that decreases in time as discussed in Aradian et al.[29], and (ii) a late stage governed by the disjoining pressure, for $h_{min} \lesssim 0.8$, with the thinning rate rapidly increasing prior to rupture as discussed in Zhang and Lister[38].

How the addition of thermal noise alters the film dynamics is shown in figure 3.2b for a single realization of a noise-inclusive simulation with a noise strength $\theta = 0.001$. The film evolves with the formation of a dimple at $x \sim 0$, similar to what is seen in figure 3.2a for the deterministic counterpart. However, it also illustrates the growth of fluctuations, resulting in the formation of a wave in the flat portion of the film, thereby

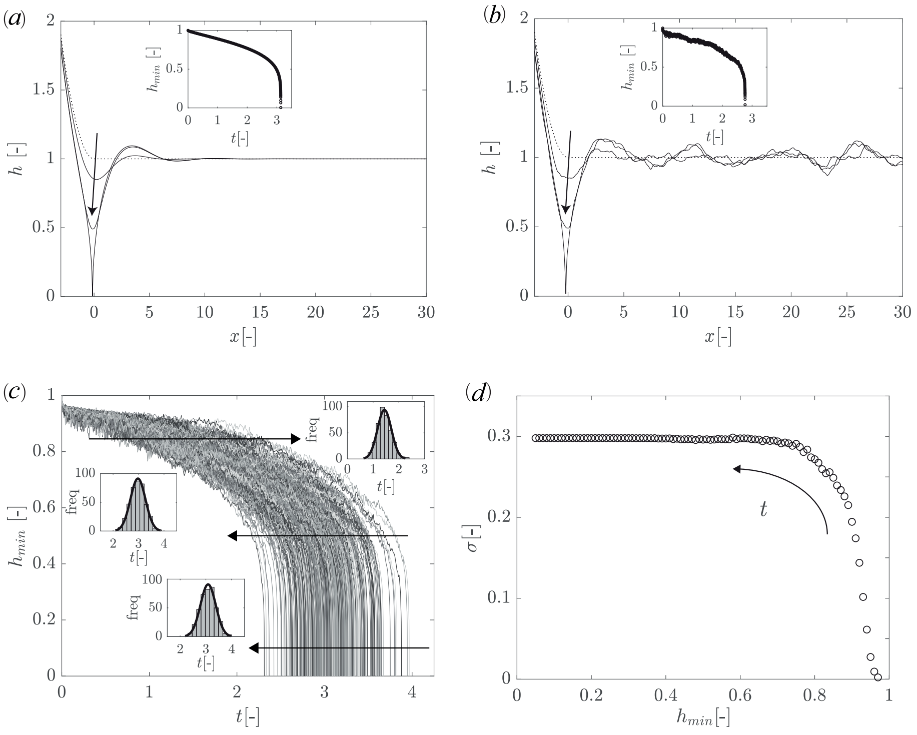

Figure 3.2 Film dynamics for $\kappa = 0.1$, i.e. close to the transition curvature where the time scale for rupture due to drainage is comparable to the time scale for rupture due to the spontaneous growth of fluctuations. (a) Film evolution in space (zoomed here close to $x \sim 0$) and time (for $t = 0$, 1.37, 3.00, 3.14) for noise-free (deterministic) simulation ($\theta = 0$). (b) Single realisation of the noise-inclusive counterpart of (a) for $\theta = 0.001$. The insets in (a) and (b) show the time evolution of the minimum film height, h_{min}. (c) Film evolution for 400 realizations of the same simulations as in (b), with the minimum film heights being extrapolated from their last recorded ($h_{min} \lesssim 0.05$) values to 0. The insets represent the distributions of times required to reach the three indicated heights, one in early drainage-governed stage, a second at the late disjoining pressure-governed stage, and a third at the crossover of these stages. (d) Standard deviation in the time required to reach a given minimum height as obtained from the 400 realizations of (c).

indicating a competition between the two thinning mechanisms. The minimum film height shown in the inset decreases similarly to the deterministic counterpart, but with the noise superimposed over it. An additional consequence of the inclusion of noise is the spread in film evolution as shown for 400 realizations in figure 3.2c. The curves show that most of the spread occurs in the early drainage stage. This is more clearly seen from the three insets, which show histograms of the time required to reach the three indicated minimum heights. These distributions appear normal and were used to further characterize the spread in evolution by computing the standard deviation as a function of h_{min}, as shown in figure 3.2d. The rupture times, t_r, of all realizations were calculated as the time at which the minimum film height first reaches $h_{min}(t = t_r) = 0.05$. We note that the reported results for t_r are insensitive to our chosen value of 0.05, because of the rapid evolution prior to rupture. For the presented case with $\kappa = 0.1$, we find $t_r = 3.11 \pm 0.32$ (mean ± standard deviation) for the noise-inclusive simulation with $\theta = 0.001$, with the mean value close to the noise-free ($\theta = 0$) rupture time, $t_r = 3.14$.

3.5.2 Influence of thermal fluctuations on film rupture at far limits of κ

Having analysed film rupture for $\kappa \approx \kappa_{tr}$, we now proceed to understand how thermal fluctuations influence the film break-up in the limit of high ($\gg \kappa_{tr}$) and low ($\ll \kappa_{tr}$) κ, comparing these limits without ($\theta = 0$) and with realistic ($\theta = 0.001$) thermal noise. For strong drainage ($\kappa = 50$), we find that the film ruptures due to the formation of a dimple, with the spatio-temporal film profiles being almost indistinguishable for the noise-inclusive and noise-free case, see figure 3.3a and 3.3b, respectively. This negligible influence of thermal fluctuations is as expected, because the time scale for dimple formation is much smaller compared to the time scale for the spontaneous growth of fluctuations for $\kappa \gg \kappa_{tr}$, as explained before. In this *dimple-dominated* regime, the resulting rupture time is insensitive to the addition of noise, with rupture times $t_r = 2.5 \cdot 10^{-3} \pm 8.7 \cdot 10^{-5}$ for the noise-inclusive case and $t_r = 2.5 \cdot 10^{-3}$ for the noise-free counterpart. Further characterization of the thinning dynamics in terms of h_{min} shows that the height of the dimple initially decreases as $h_{min} \sim t^{-1/2}$ for both the noise-free and noise-inclusive case, see the insets in figure 3.3a and 3.3b, in agreement with earlier theoretical work[29].

For weak drainage ($\kappa = 0.001$), rather than through the formation of a dimple, film rupture is initiated by the growth of unstable waves on the planar portion of the film, akin to what is observed for de-wetting of thin planar films[4,31]. In this *fluctuations-dominated* regime, the film evolution exhibits the growth of a dominant unstable wave, which grows fastest close to $x = 0$ due to the small dimple that still forms there which triggers the accelerated growth of the wave at that location. For the noise-free case, rupture occurs at $x \approx -2.5$ (figure 3.3c), i.e. within half a wavelength

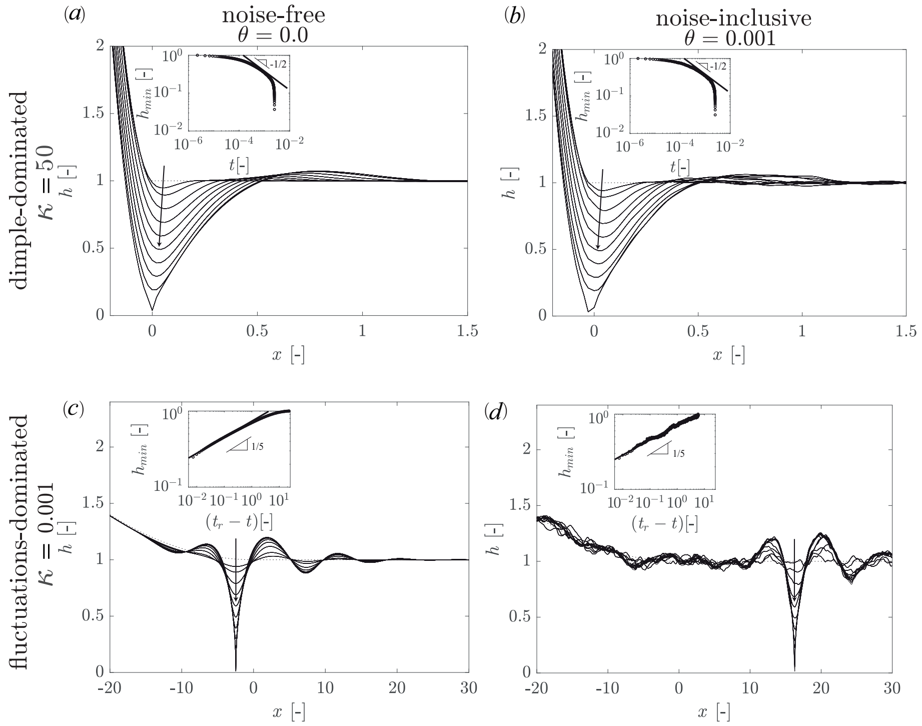

Figure 3.3 Comparison between films with high ($\kappa \gg \kappa_{tr}$, dimple-dominated) and low ($\kappa \ll \kappa_{tr}$, fluctuations-dominated) curvature, without ($\theta = 0$) and with realistic ($\theta = 0.001$) noise. (a) Evolution of film heights in the dimple region for $\kappa = 50$ for a deterministic simulation, at various dimensionless times $t = (0.01, 0.03, 0.08, 0.16, 0.28, 0.45, 0.75, 1.3, 2.1, 2.5) \cdot 10^{-3}$ (also reported in[14]); (b) Evolution of film heights in the dimple region for $\kappa = 50$ for a single realization of a stochastic simulation, at various dimensionless times $t = (0.01, 0.02, 0.07, 0.14, 0.28, 0.5, 0.87, 1.4, 2.0, 2.3) \cdot 10^{-3}$. (c) Evolution of film heights for $\kappa = 0.001$ for deterministic simulations, at various dimensionless times, $t = (7, 10, 13.6, 14.7, 15.2, 15.5, 15.55, 15.58, 15.6)$; (d) Evolution of film heights for $\kappa = 0.001$ for a single realization of a stochastic simulation at various dimensionless times, $t = (1.6, 3, 5.04, 5.7, 6.16, 6.27, 6.37)$. The insets in (a-d) show the corresponding time evolutions of the minimum film height.

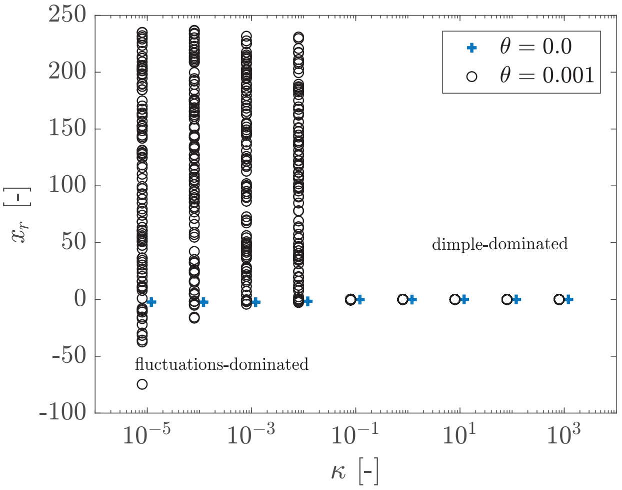

Figure 3.4 Comparison of rupture location between noise-free ($\theta = 0$) and noise-inclusive ($\theta = 0.001$) evolutions as a function of curvature. The rupture locations for the noise-inclusive evolutions are illustrated as individual data points for 100 out of 400 realizations. The rupture locations for $\theta = 0$ and $\theta = 0.001$ are shifted horizontally for better visibility.

of the fastest-growing wave ($\lambda_{max} = 8.8$) from $x = 0$. The inset shows an almost dormant initial evolution of the film, with little decrease in film height due to drainage for $(t_r - t) > 5$, followed by a rapid decrease in film height due to the van der Waals forces. In this stage, the film height evolves with the earlier reported theoretical scaling, $h_{min} \sim (t_r - t)^{1/5}$[38], see the inset of figure 3.3c. Interestingly, the addition of thermal noise to films exhibiting weak drainage results in rupture locations away from $x = 0$, see figure 3.3d. The film instability is initiated due to the growth of an unstable dominant wave, like the noise-free evolution. However, due to the presence of noise everywhere along the film, rupture can occur at any of the valleys of the wave that grows fastest. Comparing the dynamics of the film evolution for the noise-inclusive case with that of the noise-free case, we see no dormant initial phase in the inset of figure 3.3d. This is because the amplitude of the corrugations resulting from thermal noise is orders of magnitude larger compared to the initial perturbation in the noise-free case, where spontaneous growth of unstable waves originates from the non-uniform initial shape of the film. This leads to shorter rupture times for the noise-inclusive case yielding $t_r = 6.95 \pm 0.68$ versus $t_r = 15.6$ for noise-free case.

3.5.3 Influence of thermal fluctuations on rupture locations

Having established that the film ruptures through the formation of a dimple at $x \sim 0$ for strong drainage ($\kappa \gg \kappa_{tr}$) and through the spontaneous growth of fluctuations at a random location for weak drainage ($\kappa \ll \kappa_{tr}$), we now further detail the influence of thermal fluctuations on rupture location for the whole range of curvatures. Without noise, the film ruptures through the formation of a dimple at $x_r \approx 0$ within one grid point, see the crosses in figure 3.4. With noise, the film also ruptures at $x_r \approx 0$ for strong drainage, while rupture occurs at a random location for weak drainage, with x_r being uniformly distributed over the flat portion of the film without any preference for the location where the dimple would otherwise grow. The differences in rupture locations between films with strong and weak drainage can be used to explain the experimental observations of films being ruptured always at the rim[10] or at random locations[21]. As expected based on the earlier presented analysis of time scales, figure 3.4 clearly illustrates that $\kappa_{tr} \approx 0.1$ marks the transition between the dimple-dominated regime ($\kappa \gg \kappa_{tr}$) and the fluctuations-dominated regime ($\kappa \ll \kappa_{tr}$). We note that for the lowest values of κ, the film not only ruptures at the flat portion of the film, but also occasionally at the curved portion ($x < 0$) in the Plateau border.

3.5.4 Influence of thermal fluctuations on rupture time

We now study how thermal fluctuations influence the rupture time for different strengths of drainage. Figure 3.5a shows that the presence of noise does not significantly affect the rupture time and its earlier reported scaling with curvature[14] for $\kappa \gg \kappa_{tr}$. By contrast, rupture times for $\kappa \ll \kappa_{tr}$ depend strongly on noise strength and not on drainage strength, with higher noise strength resulting in shorter rupture times. Since the dominant thinning mechanism for low κ is through the spontaneous growth of fluctuations and not through the formation of a dimple, there is no fundamental mechanistic difference between non-planar films with weak drainage $\kappa \ll 1$ and flat films without drainage $\kappa = 0$, with the rupture times for low κ approaching those of flat films (with periodic boundary conditions). We note here that the rupture times in the fluctuations-dominated regime depend weakly on the choice of l_2, see figure 3.6 in Appendix. This is easily understood from the fact that, with increasing l_2, the number of valleys of the dominant wave increases, thereby increasing the probability for the fastest possible rupture. An estimate for the rupture time for a truly semi-infinite film, i.e., $l_2 \to \infty$, is hence obtained by considering the minima of rupture times in a sufficiently large ensemble of evolutions for the fluctuations-dominated regime.

How rupture times depend on noise strength for a given value of κ is next examined. We rationalized that the rupture time scales with noise strength according to $\omega_{max} t_r \sim \ln(\sqrt{2\theta})^{-1}$, see Eq. (3.10). This prediction agrees well with sim-

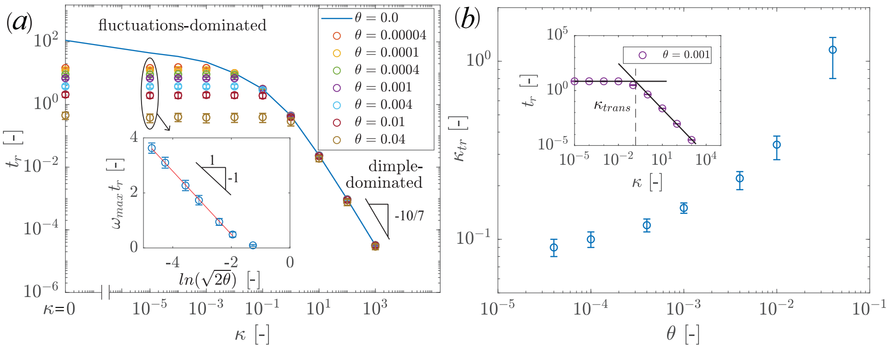

Figure 3.5 (a) Dependence of rupture time on drainage (κ) and noise strength (θ). Two clearly separated regimes are visible wherein film thinning is dominated by dimple formation for high curvatures ($\kappa \gg \kappa_{tr}$) or by the growth of fluctuations for low curvatures ($\kappa \ll \kappa_{tr}$). Inset: rupture times rescaled with $1/\omega_{max}$ at $\kappa = 1 \cdot 10^{-5}$ (highlighted by the ellipse) for different noise strengths. The observed slope is close to -1 as indicated by the triangle. We excluded the rupture time for the noise strength of $\theta = 0.04$ in the fit, because the fluctuations of the interface $\sim \sqrt{2\theta}$ are approximately 30% of the initial film thickness and the time for them to develop into the fastest growing wave with $\omega_{max} = 1/4$ is significantly longer than the film rupture time itself. (b) Transition curvature, κ_{tr}, from dimple-dominated rupture to fluctuations-dominated rupture versus noise strength, with the inset showing how κ_{tr} is calculated based on the film rupture times.

ulation results for which we obtain $\omega_{max} t_r \sim \ln(\sqrt{2\theta})^{-1.15\pm0.04}$ for $\kappa = 10^{-5}$, see the inset of figure 3.5a. We attribute this small difference primarily to the overprediction of the rupture time by applying linear theory to a full nonlinear problem. Finally, figure 3.5b shows how the transition curvature κ_{tr}, marking the transition from the dimple-dominated regime to the fluctuations-dominated regime depends on noise strength, with κ_{tr} calculated as shown in the inset. For realistic θ between $10^{-5} - 10^{-3}$, this transition only weakly depends on θ, and the earlier estimated transition $\kappa_{tr} = 0.1$ provides a good estimate for most experimentally relevant conditions.

3.6 Conclusions

We studied the evolution of draining non-planar thin films under the influence of thermal fluctuations for the large-film limit, where drainage is confined to a dimple. The central question answered in this paper is what role thermal fluctuations play in determining lifetimes of such films. The two key parameters governing this problem are the strength of drainage (κ) and the strength of thermal noise (θ). For strong drainage, $\kappa \gg \kappa_{tr}$, our simulations show that the film ruptures deterministically due to rupture in the thinnest part of the dimple, regardless of κ and θ. The rupture time then is as reported earlier[14], leaving no room for thermal fluctuations to grow and moderate the rupture process, in contrast to the concept of thermally induced rupture from some critical moment onwards. By contrast, for weak drainage, $\kappa \ll \kappa_{tr}$, the film ruptures through the spontaneous growth of waves originating from thermal fluctuations. Rupture occurs at one of the valleys of the dominant wave, anywhere along the planar portion of the film. The mean rupture times are found to be independent of κ and are well predicted by linear stability analysis as $t_r \approx 1/\omega_{max} \ln(\sqrt{2\theta})^{-1}$. The transition between the dimple-dominated regime ($\kappa \gg \kappa_{tr}$) and the fluctuations-dominated regime ($\kappa \ll \kappa_{tr}$) is around $\kappa_{tr} = 0.1$, with a weak dependence on noise strength.

Our work explains if, when and why it is important to include thermal fluctuations in the dynamics of draining thin films to predict where and when they rupture. We reiterate that our work focuses on the large film limit. Experimental data sets obtained in Scheludko cells e.g.[17,20,27] are for films in which drainage in the planar portion of the film occurs simultaneously with dimpled thinning. A direct comparison to those experiments requires including the film size as an additional parameter, which is beyond the scope of the present paper.

Acknowledgements

This work is supported by the Netherlands Organization for Scientific Research (NWO) and the Dutch Institute for Sustainable Process Technology (ISPT) as part of the project COFILM.

Appendix

Figure 3.6 shows how rupture times for the fluctuations-dominated (low κ) regime depend on the extent of flat portion of the film, l_2, with its mean and standard deviation decreasing by about 22% and 84%, respectively, when l_2 is increased from 60 to 960. Figure 3.7 shows a grid and time step size dependency study, for $\kappa = 10^{-5}$ and $\kappa = 10^{3}$. In the spirit of Grün et al.[4], we used a time step $\Delta t = \Delta x^{\alpha}$, for which we determined the values of α empirically, varying α between 2.25 and 3 for the fluctuations-dominated regime and between 3.25 and 4 for the dimple-dominated regime. In the fluctuations-dominated regime, i.e. at low κ, the analysis shows that a combination of a grid size of $\Delta x = 0.05$ and a time step size of $\Delta t = \Delta x^{2.75}$

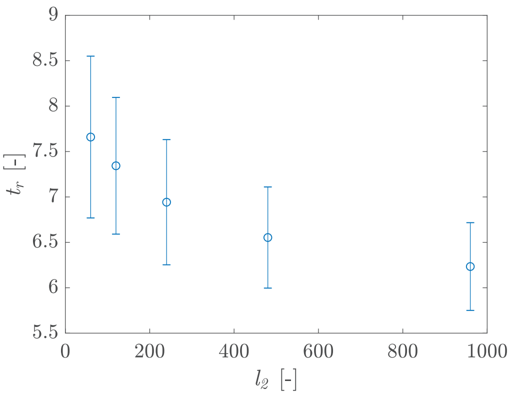

Figure 3.6 Dependence of rupture time on the extent of flat portion of the film, l_2 for $\theta = 0.001$ and $\kappa = 10^{-5}$.

provides a rupture time within 5% of the smallest grid and time step size used. For the dimple-dominated (high κ) regime, a similar accuracy is obtained for $\Delta x = 0.005$ and $\Delta t = \Delta x^{3.25}$. Figure 3.8 shows how the mean and standard deviation of the rupture time depend on the number of realisations, again for $\kappa = 10^{-5}$ and $\kappa = 10^3$. It shows that after about 300 realizations, the mean and the standard deviation are within 2% and 5%, respectively, of the values obtained for all 400 realizations.

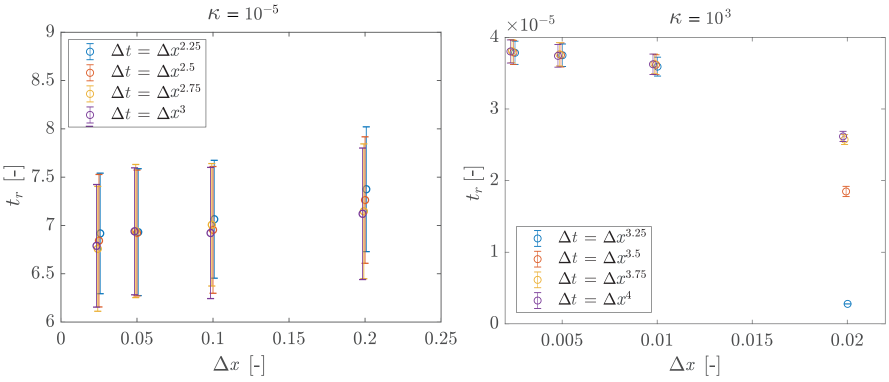

Figure 3.7 (colour online) Dependence of rupture time on grid and time step size for noise-inclusive simulations ($\theta = 0.001$) for (left) $\kappa = 10^{-5}$ and (right) $\kappa = 10^3$. Error bars were horizontally shifted for better visibility.

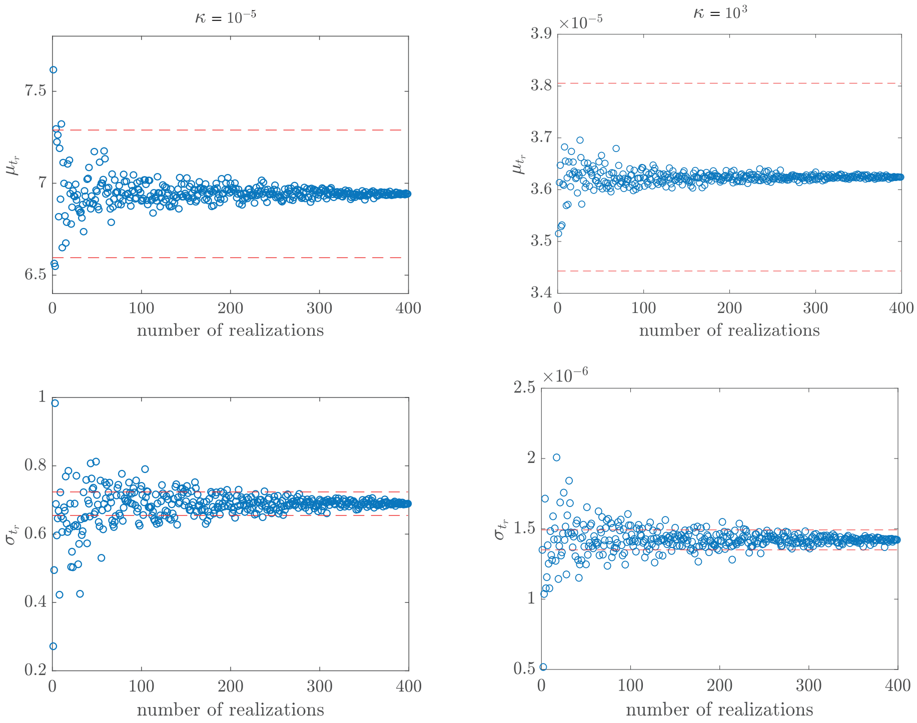

Figure 3.8 (colour online) Statistical significance based on the number of realizations. Mean rupture times (μ_{tr}) (top) and corresponding standard deviation (σ_{tr}) (bottom) as a function of the number of realizations randomly picked from a pool of 400 noise-inclusive simulations ($\theta = 0.001$) for $\kappa = 10^{-5}$ (left) and $\kappa = 10^{3}$ (right). The dashed red lines indicate 5% deviation from the values of mean and standard deviation for the entire pool.

Bibliography

[1] A. Oron, S. H. Davis, and S. G. Bankoff. Long-scale evolution of thin liquid films. Rev. Mod. Phys., 69(3):931–980, 1997. doi: 10.1103/RevModPhys.69.931.

[2] R. V. Craster and O. K. Matar. Dynamics and stability of thin liquid films. Rev. Mod. Phys., 81: 1131–1198, Aug 2009. doi: 10.1103/RevModPhys.81.1131.

[3] D. G. A. L. Aarts, M. Schmidt, and H. N. W. Lekkerkerker. Direct visual observation of thermal capillary waves. Science, 304(5672):847–850, 2004. doi: 10.1126/science.1097116.

[4] G. Grün, K. Mecke, and M. Rauscher. Thin-film flow influenced by thermal noise. J. Stat. Phys., 122(6):1261–1291, 2006. doi: 10.1007/s10955-006-9028-8.

[5] J. Becker, G. Grün, R. Seemann, H. Mantz, K. Jacobs, K. R. Mecke, and R. Blossey. Complex dewetting scenarios captured by thin-film models. Nat. Mater., 2(1):59, 2003. doi: 10.1038/nmat788.

[6] O. Reynolds. IV. on the theory of lubrication and its application to mr. beauchamp tower's experiments, including an experimental determination of the viscosity of olive oil. Phil. Trans. Roy. Soc. Lon., 177:157–234, 1886. doi: 10.1098/rstl.1886.0005.

[7] D. Platikanov. Experimental investigation on the "dimpling" of thin liquid films. J. Phys. Chem., 68 (12):3619–3624, 1964. doi: 10.1021/j100794a030.

[8] Yu. A. Buevich and E. Kh. Lipkina. Draining of liquid from thin axially symmetric films. J. App. Mech. Tech. Phys., 16(2):217–222, 1975. doi: 10.1007/BF00858916.

[9] G. Singh, C. A. Miller, and G. J. Hirasaki. On dimple formation in foam films. J. Colloid Interface Sci., 187(2):334 – 337, 1997. doi: https://doi.org/10.1006/jcis.1996.4703.

[10] S. P. Frankel and K. J. Mysels. On the "dimpling" during the approach of two interfaces1. J. Phys. Chem., 66(1):190–191, 1962. doi: 10.1021/j100807a513.

[11] J. L. Joye, G. J. Hirasaki, and C. A. Miller. Dimple formation and behavior during axisymmetrical foam film drainage. Langmuir, 8(12):3083–3092, 1992. doi: 10.1021/la00048a038.

[12] A. K. Malhotra and D. T. Wasan. Effect of film size on drainage of foam and emulsion films. AIChE journal, 33(9):1533–1541, 1987. doi: 10.1002/aic.690330913.

[13] E. Manev, R. Tsekov, and B. Radoev. Effect of thickness non-homogeneity on the kinetic behaviour of microscopic foam film. J. Dispersion Sci. Technol., 18(6-7):769–788, 1997. doi: 10.1080/01932699708943771.

[14] M. T. Kreutzer, M. S. Shah, P. Parthiban, and S. A. Khan. Evolution of nonconformal landau-levich-bretherton films of partially wetting liquids. Phys. Rev. Fluids, 3:014203, 2018. doi: 10.1103/PhysRevFluids.3.014203.

[15] A. Vrij. Possible mechanism for the spontaneous rupture of thin, free liquid films. Discuss. Faraday Soc., 42:23–33, 1966. doi: 10.1039/DF9664200023.

[16] A. Scheludko. Thin liquid films. Adv. Colloid Interface Sci., 1(4):391–464, 1967. doi: 10.1016/0001-8686(67)85001-2.

[17] B. P. Radoev, A. D. Scheludko, and E. D. Manev. Critical thickness of thin liquid films: Theory and experiment. J. Colloid Interface Sci., 95(1):254 – 265, 1983. doi: https://doi.org/10.1016/0021-9797(83)90094-2.

[18] A. Sharma and E. Ruckenstein. Stability, critical thickness, and the time of rupture of thinning foam and emulsion films. Langmuir, 3(5):760–768, 1987. doi: 10.1021/la00077a033.

[19] R. Tsekov and E. Ruckenstein. Effect of thermal fluctuations on the stability of draining thin films. Langmuir, 9(11):3264–3269, 1993. doi: 10.1021/la00035a082.

[20] E. D. Manev and A. V. Nguyen. Critical thickness of microscopic thin liquid films. Adv. Colloid Interface Sci., 114-115:133 – 146, 2005. doi: 10.1016/j.cis.2004.07.013.

[21] D. G. A. L. Aarts and H. N. W. Lekkerkerker. Droplet coalescence: drainage, film rupture and neck growth in ultralow interfacial tension systems. J. Fluid Mech., 606:275–294, 2008. doi: 10.1017/S0022112008001705.

[22] E. Rio and A. L. Biance. Thermodynamic and mechanical timescales involved in foam film rupture and liquid foam coalescence. ChemPhysChem, 15(17):3692–3707, 2014. doi: 10.1002/cphc.201402195.

[23] S. Perumanath, M. K. Borg, M. V. Chubynsky, J. E. Sprittles, and J. M. Reese. Droplet coalescence is initiated by thermal motion. Phys. Rev. Lett., 122:104501, 2019. doi: 10.1103/PhysRevLett.122.104501.

[24] I. U. Vakarelski, R. Manica, X. Tang, S. J. O'Shea, G. W. Stevens, F. Grieser, R. R. Dagastine, and D. Y. C. Chan. Dynamic interactions between microbubbles in water. Proc. Nat. Acad. Sci., 107(25): 11177–11182, 2010. doi: 10.1073/pnas.1005937107.

[25] D. Y. C. Chan, E. Klaseboer, and R. Manica. Film drainage and coalescence between deformable drops and bubbles. Soft Matter, 7:2235–2264, 2011. doi: 10.1039/C0SM00812E.

[26] B. Davidovitch, E. Moro, and H. A. Stone. Spreading of viscous fluid drops on a solid substrate assisted by thermal fluctuations. Phys. Rev. Lett., 95:244505, 2005. doi: 10.1103/PhysRevLett.95.244505.

[27] E. D. Manev, S. V. Sazdanova, and D. T. Wasan. Emulsion and foam stability - The effect of film size on film drainage. J. Colloid Interface Sci., 97(2):591 – 594, 1984. doi: 10.1016/0021-9797(84)90334-5.

[28] J. E. Coons, P. J. Halley, S. A. McGlashan, and T. Tran-Cong. A review of drainage and spontaneous rupture in free standing thin films with tangentially immobile interfaces. Adv. Colloid Interface Sci., 105(1):3 – 62, 2003. doi: https://doi.org/10.1016/S0001-8686(03)00003-4.

[29] A. Aradian, E. Raphael, and P. G. de Gennes. Marginal pinching in soap films. Europhys. Lett., 55 (6):834–840, 2001. doi: 10.1209/epl/i2001-00356-y/fulltext/.

[30] G. K. Batchelor. An Introduction to Fluid Dynamics. Cambridge Mathematical Library. Cambridge University Press, 2000.

[31] J. A. Diez, A. G. González, and R. Fernández. Metallic-thin-film instability with spatially correlated thermal noise. Phys. Rev. E, 93:013120, 2016. doi: 10.1103/PhysRevE.93.013120.
FP Bretherton. The motion of long bubbles in tubes. J Fluid. Mech., 10:166–88, 1961. doi: 10.1017/S0022112061000160.

[32] C. J. W. Breward and P. D. Howell. The drainage of a foam lamella. J. Fluid Mech., 458:379–406, 2002. doi: 10.1017/S0022112002007930.

[33] I. Cantat, S. Cohen-Addad, F. Elias, F. Graner, R. Höhler, O. Pitois, F. Rouyer, and A. Saint-Jalmes. Foams: structure and dynamics. OUP Oxford, 2013.

[34] H. Wong, C. J. Radke, and S. Morris. The motion of long bubbles in polygonal capillaries .1. thin films. J. Fluid Mech., 292:71–94, 1995. doi: 10.1017/S0022112095001443.

[35] S. Khodaparast, O. Atasi, A. Deblais, B. Scheid, and H. A. Stone. Dewetting of thin liquid films surrounding air bubbles in microchannels. Langmuir, 34(4):1363–1370, 2018. doi: 10.1021/acs.langmuir.7b03839.

[36] G. J. Lord, C. E. Powell, and T. Shardlow. An introduction to computational stochastic PDEs. Number 50. Cambridge University Press, 2014.

[37] J. A. Diez, L. Kondic, and A. Bertozzi. Global models for moving contact lines. Phys. Rev. E, 63: 011208, 2000. doi: 10.1103/PhysRevE.63.011208.

[38] W. W. Zhang and J. R. Lister. Similarity solutions for van der waals rupture of a thin film on a solid substrate. Phys. Fluids, 11(9):2454–2462, 1999. doi: 10.1063/1.870110.

4. Influence of initial film radius and film thickness on the rupture of foam films[¶]

The initial thickness and radius of the film that forms upon close contact of two foam bubbles are known to influence the thinning dynamics and lifetime of the film. Various scalings of lifetime, t_r, with initial radius, R_{film}, and thickness, h_o, have been proposed in literature. In this paper, we present a hydrodynamic thin film model that includes both surface tension, van der Waals forces and drainage and that clarifies the various proposed scalings of lifetime. Our model equations were solved numerically for a range of R_{film} and h_o as direct input parameters. Films with a large radius are found to thin locally at a dimple, while films with a small radius thin across the entire film. The observed dynamics and lifetime were interpreted by developing a simplified model that describes the early stage dimpled drainage and the late stage van der Waals thinning, using known similarity solutions. For large radii films, our simulations confirm earlier theoretical work on semi-infinite films that predicts $t_r \sim R^{0}_{film} h_0^{5/7}$. For small radii films, our numerical simulations show the opposite trend with lifetime being solely dependent on R_{film}, in fair agreement with the simplified model that predicts $t_r \sim R^{10/7}_{film} h_0^{0}$.

[¶] Under review: M. .S. Shah, C. R. Kleijn, M. T. Kreutzer, V. van Steijn, Influence of initial film radius and film thickness on the rupture of foam films. Physical Review Fluids.

4.1 Introduction

The stability of foams and emulsions is largely determined by the lifetime of the thin liquid film that forms between two bubbles or droplets upon close contact. Thinning of this film is mediated by drainage induced by the pressure difference between the film and the Plateau border. Once the film gets thinner than O(100 nm), destabilizing van der Waals forces overtake the thinning process and induce rupture of the film. Together, the early stage drainage and late stage rupture, which partially overlap, determine the lifetime of the film.

Classical theory by Reynolds[1] describes the thinning of the film between the two bubbles by considering a fluid between two plane-parallel rigid discs subjected to drainage. It teaches that the approaching velocity of the discs is constant in time and depends on the imposed suction pressure and disc radius. Vrij[2] extended Reynolds' theory by postulating that the film thins uniformly with the velocity predicted by Reynolds' theory down to a critical thickness. This critical thickness marks the neutral stability of waves on the film due to the interplay between stabilizing surface tension forces and destabilizing van der Waals forces. Upon further thinning, these waves, which originate from thermal fluctuations, exhibit an exponential growth that outruns the Reynolds' velocity, perturbing the interface until rupture occurs randomly at one of the troughs on the surface of the film. However, earliest experiments in so-called Scheludko cells are at odds with this picture: instead of uniform initial thinning, a local depression immediately develops near the Plateau border, and this so-called 'dimple' thins out more rapidly than the central part of the film[3–5]. The formation of a dimple was first studied theoretically by Frankel and Mysels[6], who developed scaling rules for film thinning at the center and at the periphery of the film. A criterion that describes whether and when a film primarily thins uniformly or locally through a dimple was developed by Joye et al.[7] and Singh et al.[8] based on a comparison between the curvature in the dimple and in the Plateau border. For many practical systems, this criterion teaches us that films with a radius larger that about 50 µm develop dimples in the film thinning process. Taken altogether, the film thinning process comprises of an early drainage stage, that has been found to proceed via the formation of a dimple, and a late rupture stage, where destabilizing van der Waals forces induce rupture that may be enhanced through the amplification of perturbations on the interface.

A well-established theoretical description of film thinning is rooted in the thin film equation, which has been shown to accurately describe spatio-temporal profiles of the film and its lifetime as reported for controlled drainage experiments between two bubbles or two droplets[9–12] and between a bubble or droplet and a solid substrate[13–17]. Being a fourth order non-linear partial differential equation, it is commonly solved numerically. An important aspect to be considered is how to incorporate the approach of two initially spherical bubbles, and the resulting shape of the thin film that subsequently forms between the flattened bubbles[18–20], into the thin film description.

More specifically, the extent over which the film is flattened, referred to as the film radius, has been shown to depend on the approach velocity in AFM measurements[19] and on the rate at which liquid is withdrawn between two bubbles in Scheludko cell experiments[7,18]. A common way to incorporate these effects in the thin film description is to introduce an external force that drives the initially spherical interfaces together, which is switched off once a flattened film has formed in order to study the thinning dynamics in the absence of this external force[9]. In order to single out the effect of the initial features of the flattened film, i.e. its radius and its thickness, we developed a simplified description that allows to immediately start from a flattened film with prespecified radius and thickness. We use this approach to resolve the debated question how initial film radius and thickness influence thinning dynamics and film lifetime. This debate stems from the various simplifications to the classical thin film equation that have been used to answer the question using analytical techniques.

Assuming the film to be planar and to thin quasi-statistically, Reynolds' theory and later refinements to the same analytically predict the lifetime to scale with film radius as $t_r \sim R_{film}^2$[1,21]. Relaxing the quasi-steady assumption to include the influence of drainage on the growth of waves in a plane-parallel film, and using experimentally observed thinning rates, Sharma and Ruckenstein[22] predicted $t_r \sim R_{film}^1$. Malhotra and Wasan[23] performed numerical simulations using the thin film equation that solved exclusively for the flow in the Plateau border, while assuming that the film remains essentially plane-parallel, to find $t_r \sim R_{film}^{4/5}$. Although this model is in reasonable agreement with experimentally observed lifetimes, photographic techniques have shown that draining films are not plane-parallel[5,24,25]. This finding inspired the development of several theories that either take into account quasi-stationary non-homogeneities on a plane-parallel interface resulting in $t_r \sim R_{film}^{4/5}$[24–26], or assume the translatory and oscillatory motion of hydrodynamic waves on a plane-parallel interface resulting in $t_r \sim R_{film}^{3/4}$[27]. With the inclusion of the afore-mentioned non-homogeneities, these theories address the notion that film thinning is not strictly plane-parallel in nature. However, they fail to capture the pronounced dimple shapes observed in the experiments[5,11,12,28]. Besides the development of steady and non-steady plane-parallel models, with and without non-homogeneities, models have been developed on quasi-steady non-planar films featuring dimples. With the interface shape no longer fixed, but freely deformable, an analysis of the spatio-temporal film profiles is significantly simplified when assuming that the flow at the periphery of the film is independent of its radial location. Using such a quasi-steady approach, Frankel and Mysels[6] calculated the shape of a dimple close to rupture. Aradian et al.[29] developed a comprehensive model for dimpling that extended the model of Frankel and Mysels[6] for infinitely large films. However, both of these works do not include van der Waals forces. Without their inclusion, films do not rupture (i.e. reach a zero thickness asymptotically) such that the lifetime of the film and its dependency on film radius and thickness cannot be predicted by these models.

In the present work, we clarify the variety of scaling rules in the literature, stemming from various applied simplifications, by numerically solving the thin film equation without such simplifications, using initial film radius and thickness as direct input parameters. To mechanistically explain the numerically obtained dependency of the lifetime of the film on its initial radius and thickness, we combined earlier-reported analytical models for dimpling in the early stage[6] and rupture through van der Waals forces in the late stage[30]. While these models were obtained through simplification of the full thin film equation, the combined model presented here does corroborate the dependency found in our simulations of the full thin film equation.

4.2 Problem formulation

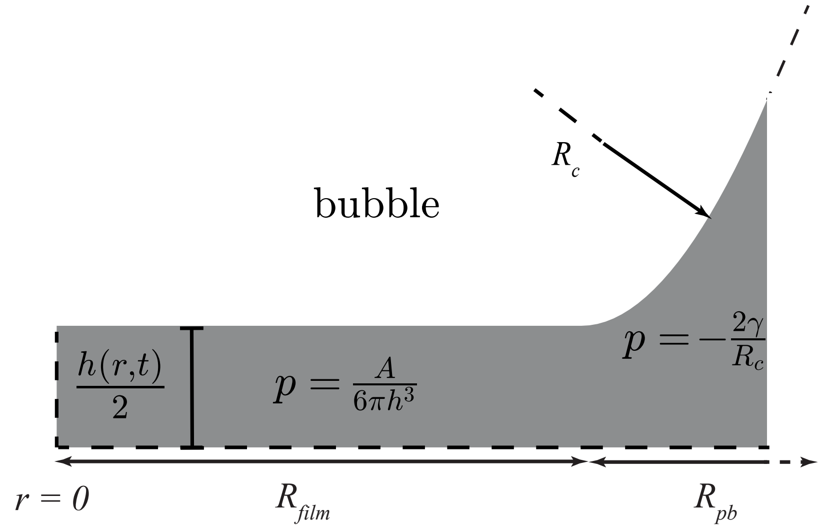

Figure 4.1 Schematic of an axisymmetric non-planar thin liquid film between two gas bubbles with the film thickness parameterized by $h(r,t)$. Since the geometry is mirror symmetric, we here display the upper half. The initial film shows a flat part extending from $0 < r \leq R_{film}$ with the pressure primarily given by the van der Waals component of the disjoining pressure, $p \sim A/6\pi h^3$. This flat part is connected to a curved part extending from $R_{film} < r \leq R_{film} + R_{pb}$ with the pressure primarily given by the Laplace pressure, $p \sim -2\gamma/R_c$, with $2/R_c$ as the curvature imposed at the edge. The dashed line at $r = 0$ signifies the second symmetry of the problem, viz. the axisymmetry in the system.

We study the evolution of an axisymmetric non-planar thin liquid film with viscosity

μ and surface tension γ between two gas bubbles. The spatio-temporal thickness of the film is parameterized by $h(r,t)$. Since the geometry of the problem is mirror-symmetric, we consider only one half of the film as shown in Fig. 4.1. Throughout this work, the term 'thickness' is used to refer to the full film thickness, $h(r,t)$. The film comprises of a flat part between $0 < r \leq R_{film}$ of initial thickness h_o, connected to a curved part between $R_{film} \leq r \leq R_{film}+R_{pb}$, with a curvature $2/R_c$ corresponding to a Plateau border. Considering the pressure in the gas phase to be uniform and setting it equal to zero, the pressure p in the curved part of the liquid film, where intermolecular forces play an insignificant role, is dictated primarily by the Laplace pressure and of order $p = -2\gamma/R_c$. Conversely, the pressure in the thin flat part is dictated by intermolecular forces, which in this paper are considered as attractive van der Waals forces, such that it is of order $p = A/6\pi h^3$, with A being the Hamaker constant. The difference in pressure drains the liquid from the flatter part of the film to the more curved part.

The axisymmetric thin film equation that describes the evolution of non-planar thin films can be derived by applying a long-wave approximation to the incompressible Navier-Stokes equations[31,32]. Considering rigid interfaces characteristic for a surfactant-laden system, which are described by commonly encountered tangentially immobile boundary conditions[19], this yields

$$\frac{\partial h}{\partial t} = \frac{1}{12\mu}\frac{1}{r}\frac{\partial}{\partial r}\left(rh^3\frac{\partial}{\partial r}\left[\frac{A}{6\pi h^3} - \frac{\gamma}{2r}\frac{\partial}{\partial r}\left(r\frac{\partial h}{\partial r}\right)\right]\right), \tag{4.1}$$

with the first term on the right side arising from long-ranged attractive van der Waals forces and the second term from surface tension forces. Since the problem we consider is axisymmetric around $r = 0$, at the left boundary of our domain, gradients in thickness and pressure are zero, i.e.

$$\frac{\partial h}{\partial r}(r=0) = 0, \ \frac{\partial p}{\partial r}(r=0) = 0 \tag{4.2}$$

Using $p = A/6\pi h^3 - \gamma/2r\,(\partial/\partial r\,(r\partial h/\partial r))$, the boundary condition for pressure becomes $\frac{A}{2\pi h^4}\frac{\partial h}{\partial r} + \frac{\gamma}{2}\frac{\partial}{\partial r}\left(\frac{1}{r}\frac{\partial h}{\partial r} + \frac{\partial^2 h}{\partial r^2}\right) = 0$ at $r = 0$, which simplifies to $\partial^3 h/\partial r^3(r = 0) = 0$ when using the first boundary condition $\partial h/\partial r(r = 0) = 0$ together with the notion that the two principal curvatures are the same at $r = 0$ due to axisymmetry. A Plateau border of constant curvature is obtained by imposing its shape, i.e. curvature $(2/R_c)$ and corresponding height, at the other domain boundary $(r = R_{film} + R_{pb})$, i.e.

$$\left.\begin{aligned} \frac{1}{2r}\frac{\partial}{\partial r}\left(r\frac{\partial h}{\partial r}\right)(r = R_{film} + R_{pb}) &= \frac{2}{R_c}, \\ h(r = R_{film} + R_{pb}) = h_o + \frac{(r^2 - R_{film}^2)}{R_c} &+ \frac{2R_{film}^2}{R_c}\ln\left(\frac{R_{film}}{r}\right). \end{aligned}\right\} \tag{4.3}$$

This height is obtained by integrating the expression for constant curvature in the curved meniscus and imposing that the height and its first derivative match the planar part of the film at $r = R_{film}$, i.e. $h(r = R_{film}) = h_o$ and $\partial h/\partial r(r = R_{film}) = 0$.

The initial film profile is described by a flat film connected to a Plateau border of constant curvature, i.e.

$$\left.\begin{aligned} h(0 < r \leq R_{film}, t = 0) &= h_o, \\ h(R_{film} < r \leq R_{film} + R_{pb}, t = 0) &= h_o + \frac{(r^2 - R_{film}^2)}{R_c} \ldots \\ &+ \frac{2R_{film}^2}{R_c} \ln\left(\frac{R_{film}}{r}\right). \end{aligned}\right\} \tag{4.4}$$

While the height and its first derivative smoothly connect the flat and the curved parts, we note that the second derivative is discontinuous. Although the corresponding pressure profile is discontinuous at the connection, we confirm from checking the pressure profiles that this discontinuity equilibrates very quickly, i.e. in less than 0.01 % of the lifetime. Additionally, eliminating the pressure discontinuity by using an initial condition that connects the flat part to the curved part using a transition region, we see that the resulting profiles (see Fig. 4.2) overlap those without the transition region soon after the start (for $t \gtrapprox t_r/8$). Furthermore, the addition of a significant perturbation representative of hydrodynamic non-homogeneities in the initial condition, as indicated by the red dashed curves in Fig. 4.2, also proves to be inconsequential in determining the lifetime and the film profile at the instant of rupture. This initial condition independency study ensures that the film dynamics during almost the entire process and the resulting lifetime are not affected by the choice of our initial condition.

The governing equation, boundary and initial conditions are provided in dimensional form and show that the problem is governed by six parameters, which include three material properties, i.e., μ, γ and A, and three geometric parameters, i.e., h_o, R_c and R_{film}. The solution is insensitive to the chosen value of R_{pb} (see Fig. 4.1) as long as it lies between an upper and a lower bound. The upper bound is dictated by the validity of lubrication approximation, i.e., $R_{pb} \ll R_c/4\left(1 + \sqrt{(1 + 16R_{film}^2/R_c^2)}\right) - R_{film}$, while the lower bound is dictated by the region where curvature goes from practically zero in the flat part to $2/R_c$ in the curved part. This leads to $R_{pb} \gg \sqrt{h_o R_c}$, as discussed in more detail in Shah et al. [18].

We now perform a scaling analysis to demonstrate that the problem is governed by two dimensionless parameters. Using a height scale $h^* = h_o$, a radial scale $r^* = \sqrt{h_o R_c/4}$ (obtained from the constant curvature boundary condition at far right, i.e., Eq. 4.3) and a time scale $t^* = 3\mu R_c^2/2\gamma h_o$, we obtain the dimensionless variables $\tilde{h} = h/h^*$, $\tilde{r} = r/r^*$ and $\tilde{t} = t/t^*$ together with the following dimensionless

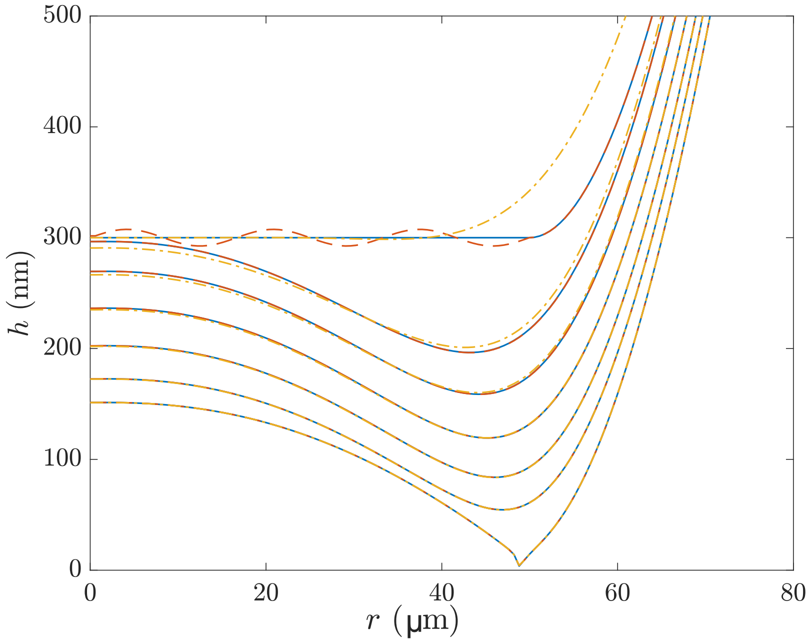

Figure 4.2 Evolution of a film with initial thickness, $h_o = 300$ nm, and radius, $R_{film} = 50\,\mu$m, with three different initial conditions. Blue solid lines correspond to the initial condition prescribed in Eq. 4.4. Red dashed lines correspond to an initial condition where a small sinusoidal perturbation with an amplitude of 25 nm and a wavelength of 16.7 µm is added to the flat part of the initial condition in Eq. 4.4. Yellow dashed-dot lines correspond to a film that has a transition region from the flat portion of the film to the curved portion, with transition region as determined in Eq. 1 in the supplementary material. Besides the initial profiles at $t = 0$, profiles are shown for $t_r/2^n$ with $n = 5 \ldots 0$, with the rupture times, t_r being 15.74 s, 15.74 s and 15.69 s for these three initial conditions respectively.

governing equation

$$\frac{\partial \tilde{h}}{\partial \tilde{t}} = \frac{1}{\tilde{r}}\frac{\partial}{\partial \tilde{r}}\left(\tilde{r}\tilde{h}^3\frac{\partial}{\partial \tilde{r}}\left(\frac{1}{12\kappa}\frac{1}{\tilde{h}^3} - \frac{1}{\tilde{r}}\frac{\partial}{\partial \tilde{r}}\left(\tilde{r}\frac{\partial \tilde{h}}{\partial \tilde{r}}\right)\right)\right), \tag{4.5}$$

where $\kappa = \pi h_o^3\gamma/AR_c$ is the relative strength of drainage. It signifies the ratio of the Laplace pressure and the initial van der Waals pressure. Additionally, we obtain the dimensionless boundary conditions

$$\left.\begin{aligned}
\frac{\partial \tilde{h}}{\partial \tilde{r}}(\tilde{r}=0)=0,\ \frac{\partial^3 \tilde{h}}{\partial \tilde{r}^3}(\tilde{r}=0)=0, \\
\frac{1}{\tilde{r}}\frac{\partial}{\partial \tilde{r}}\left(\tilde{r}\frac{\partial \tilde{h}}{\partial \tilde{r}}\right)(\tilde{r}=\tilde{R}_{film}+\tilde{R}_{pb})=1, \\
\tilde{h}(\tilde{r}=\tilde{R}_{film}+\tilde{R}_{pb})=1+\frac{(\tilde{r}^2-\tilde{R}^2_{film})}{4}+\frac{\tilde{R}^2_{film}}{2}\ln\left(\frac{\tilde{R}_{film}}{\tilde{r}}\right),
\end{aligned}\right\} \tag{4.6}$$

and dimensionless initial condition

$$\left.\begin{aligned}
\tilde{h}(0<\tilde{r}\leq\tilde{R}_{film},\tilde{t}=0)=1, \\
\tilde{h}(\tilde{R}_{film}<\tilde{r}\leq\tilde{R}_{film}+\tilde{R}_{pb},\tilde{t}=0)=1+\frac{(\tilde{r}^2-\tilde{R}^2_{film})}{4}... \\
+\frac{\tilde{R}^2_{film}}{2}\ln\left(\frac{\tilde{R}_{film}}{\tilde{r}}\right),
\end{aligned}\right\} \tag{4.7}$$

with R_{film} and R_{pb} made dimensionless using r^*. With $\tilde{R}_{pb}$ chosen such that the solution is insensitive to its value, this scaling analysis shows that the problem is fully governed by two dimensionless control parameters, i.e., the relative strength of drainage, κ and the film radius, $\tilde{R}_{film}$. We explore the parameter space by varying these two dimensionless parameters. As the main aim of this work is to understand how film dynamics depend on the initial features of the film, i.e. the film radius and its thickness, we translate the dimensionless representation back to the dimensional one. This is done by fixing μ, γ, A and R_c, as is for example the case when performing experiments with a given set of working fluids in a capillary of given radius in a so-called Scheludko cell. Motivated by the experiments from Manev et al.[25], we use $\mu = 0.00089$ Pa s, $\gamma = 0.0445$ N/m, $A = 1.5 \cdot 10^{-20}$ J and $R_c = 1.8$ mm. The dimensional parameter space is then spanned by the initial film thickness h_0 from 300 nm - 2000 nm and the film radius R_{film} from 40 µm - 4000 µm. Note that in our simulations, we are able to control these parameters independently, while they are coupled in experiments through the flow rate at which liquid is withdrawn between two bubbles prior to the start of the film rupture experiments[7].

We conclude our problem formulation with a note on thermal fluctuations at the gas-liquid interface. These fluctuations do significantly influence film dynamics and rupture time in case of weak drainage ($\kappa \ll 1$), as shown in our previous work [18]. The focal point in this work is on cases with $\kappa \gg 1$, such that we have not included thermal fluctuations in our problem description. This is also further corroborated with the notion that films with a small radius are stable against waves, because the unstable ones have wavelengths that exceed the radius of the film[9,19].

4.3 Numerical implementation

We numerically solve [*] the axisymmetric thin film equation (Eq. 4.5) along with its boundary and initial conditions (Eqs. 4.6 - 4.7) using a finite difference scheme. We discretize the domain into an equidistant mesh of size, $\Delta\tilde{r}$, using a second-order central differencing scheme for spatial discretization. Time discretization is performed using an implicit-explicit scheme of a constant time step size, $\Delta\tilde{t}$, wherein the fourth-order term describing capillary forces is discretized implicitly and the second-order term describing the nonlinear van der Waals forces is discretized explicitly. The mobility term ($\tilde{r}\tilde{h}^3$) is discretized as per the positivity-preserving scheme discussed in Diez et al.[33]. Based on our previous work[34], we use $\Delta\tilde{r} = 0.05$ and $\Delta\tilde{t} = \Delta\tilde{r}^{2.25}$, and confirm that the presented simulation results for lifetimes are grid and time step size independent.

4.4 Results

4.4.1 Characterisation of the film evolution for the governing parameter space

We start by characterising the thinning dynamics for the governing parameter space. As explained, we fix μ, γ, A and R_c such that the parameter space is spanned by the initial film thickness h_0 and film radius R_{film}. The lower limit of the film radius (40 µm) was chosen based on the experimentally observed values[25,35], while the upper limit (4000 µm) was chosen to approach the semi-infinite film asymptote[29,34,36]. The range of initial film thicknesses studied in this work is representative of the drainage experiments reported in the literature[7,35].

We start with a description of films with the largest radius ($R_{film} = 4000$ µm) considered in this work, connecting their behaviour to the well-known behaviour of semi-infinite films[29,34,36]. The features of thinning of large films are the same for thin ($h_0 = 300$ nm) and thick ($h_0 = 2000$ nm) films. They are characterized by the formation of a local depression, called a dimple, near the connection between the flat and curved part of the film, while the film at the center, i.e. at $r = 0$, remains unaffected, see Figs. 4.3a, 4.3b. With the thinning being a localised phenomenon, the evolution of the film is insensitive to the film radius itself, given it is sufficiently large. Later in this paper, we quantitatively show that the large film radius limit considered in this work indeed approaches the behaviour observed for semi-infinite films sometimes referred to as marginal pinching[29]. Having confirmed the behaviour for such large films, we

---

[*] MATLAB files used for simulations available at github.com/mss01

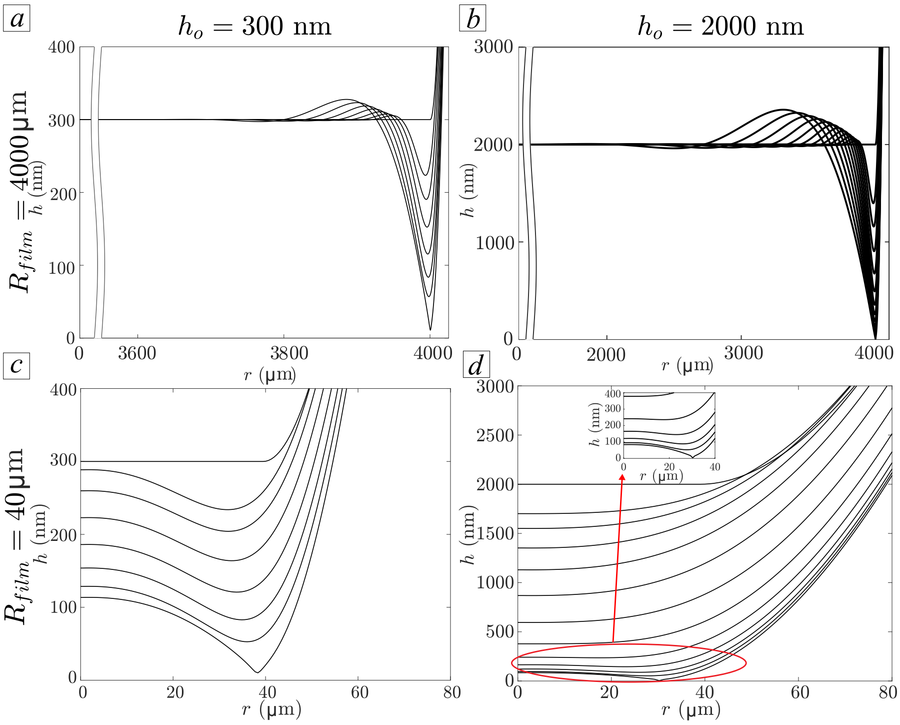

Figure 4.3 Film evolution in space and time at the boundaries of our parameter space. Large films $R_{film} = 4000\,\mu\text{m}$ of $h_0 = 300\,\text{nm}$ (a) and $h_o = 2000\,\text{nm}$ (b) initial thickness. The abscissa were made discontinuous to better illustrate the localized dimple for large film radius. Small films $R_{film} = 40\,\mu\text{m}$ of $h_0 = 300\,\text{nm}$ (c) and $h_o = 2000\,\text{nm}$ (d) initial thickness. (c) and (d): Film evolution in space and time for $R_{film} = 40\,\mu\text{m}$ at $h_o = 300\,\text{nm}$ in (c) and $h_o = 2000\,\text{nm}$ in (d). Inset in (d): Zoomed view of the film evolution at $t = t_r/2^n$ with $n = 5 \ldots 0$. Besides the initial profiles at $t = 0$, profiles are shown for $t_r/2^n$, with $n = 6 \ldots 0$ in (a) and (c) and $n = 11 \ldots 0$ in (b) and (d), with $t_r = 22.87$ s, 150.48 s, 12.91 s and 11.12 s for (a), (b), (c) and (d) respectively.

now continue with the focal point of the paper: the behaviour of films with small radii.

The thinning behaviour for the smallest film radius considered in this work ($R_{film} = 40\,\mu\text{m}$) is deliberately different from that for the largest films: film thinning initially occurs across the entire film as evident for thin and thick films in Figs. 3c and 3d, respectively. Shortly prior to rupture, the films do develop a dimple. A prediction for the transition from uniform thinning to dimpled thinning was first developed by Joye et al [7], who evaluated the ratio between the order of magnitude of the curvature at the center of the film, $2h(t)/R_{film}^2$, and at the bubble, $1/R_c$. Using numerical simulations, they found that films develop a dimple when this ratio decreases below a value of 0.7. For the here considered case with $R_c = 1.8$ mm and R_{film} at the time of rupture [†] being 38 µm and 30 µm for $h_o = 300$ nm and 2000 nm respectively, Joye's criterion predicts a transition around $h(t) = 286$ nm and $h(t) = 175$ nm, respectively, which is in good agreement with those found in Figs. 4.3c and 4.3d.

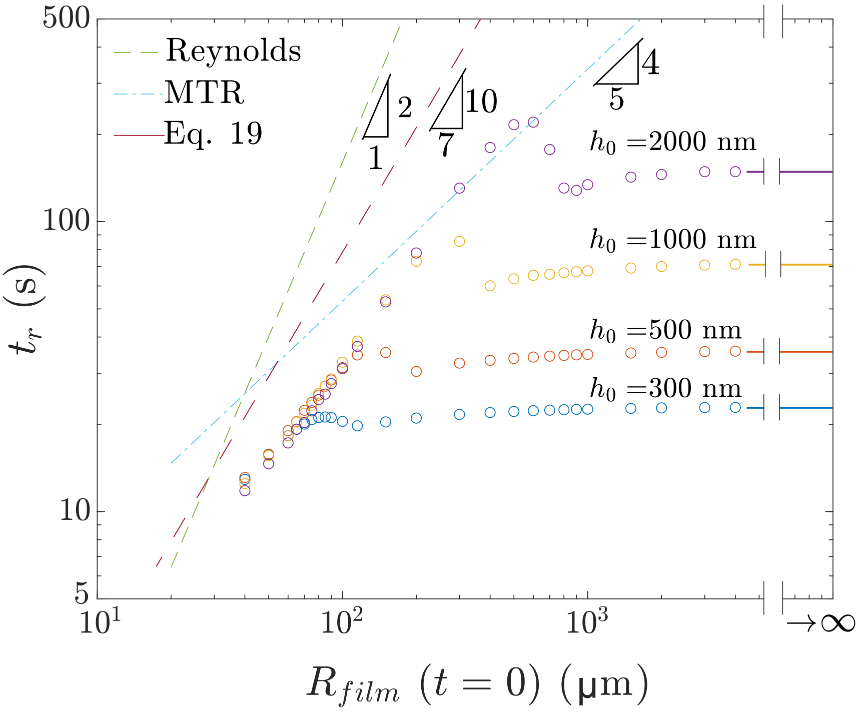

Figure 4.4 Lifetime of the film as a function of the initial film radius, for different initial film thicknesses. Green and blue dashed line corresponds to the lifetimes calculated based on Reynolds'[1] and MTR theory[26], respectively. The red dashed line corresponds to lifetime calculated based on Eq. 4.19. The horizontal solid lines at the right of the figure signify the plateauing values of film lifetimes at large radius. These values are further used in Fig. 4.9 to compare with the mechanistic model developed for large films in Appendix 4.5.

[†] The dimple does not necessarily remain at the location determined by the initial film radius during the film evolution. Once the interface relaxes from the discontinuous initial condition, the dimple initially moves towards the center, and then moves outward, with the final film radius at the instant of rupture in Figs. 4.3c and 4.3d being 38.34 µm and 30.22 µm respectively, as compared to the initial film radius $R_{film} = 40$ µm.

4.4.2 Influence of initial film radius and film thickness on film lifetime

Having studied the film evolution at the boundaries of our parameter space, we now study how film lifetime depends on the initial film radius and film thickness. As anticipated, we observe two regimes with distinctly different behaviour for small and large radii films as shown in Fig. 4.4.

For large radii films, the lifetime of a film is independent of the initial film radius and depends solely on the initial film thickness, confirming what is well established for semi-infinite films[36]. Briefly, the independence on film radius is explained by the thinning process being a localized phenomena, such that the radius of the film plays no role. Lifetimes are well described by our earlier developed model for semi-infinite 2D films[36], after modification to account for the radial geometry considered in this work leading to $t_r \sim R_{film}^0 h_o^{5/7}$, as detailed in Appendix 4.5.

For small radii films, film lifetime solely depends on the initial film radius and not on the initial film thickness, in qualitative agreement with the work by Malhotra and Wasan[23]. Our numerical data show t_r to scale with R_{film}^n, with the power n being smaller than 2 from classical Reynolds' theory[1] and greater than $4/5$ from MTR theory[23,25]. The thin film simulations as done in this work with h_o and R_{film} being direct input parameters hence clarify the variety of different exponents reported in literature that were obtained under various simplifying assumptions. In order to develop a better understanding on key simplifying assumptions and provide mechanistic insights in the numerically obtained scaling relation between t_r, R_{film} and h_o, we combine two known analytical solutions[6,30]. Full details on this model are provided in the next section §4.4.3. For the reader mainly interested in the outcome, the analytical description yields $t_r \sim h_o^0 R_{film}^{10/7}$, in fair agreement with the numerical data, as shown in Fig. 4.4.

We close the discussion on Fig. 4.4 by briefly commenting on the observation that film lifetime does not monotonically reach the plateauing value observed for large radii film. We observe that the thinning behaviour in the transition region is qualitatively different from that for the large radii films, with the dimple shifting to the centre of the film and growing beyond the initial film thickness (see Appendix 4.5, Fig. 4.10). Since the focal point of this paper has been to study small films, a deeper analysis of this behavior is beyond the scope of the present study.

4.4.3 Analytical model for dynamics of films with small radius

In this section, we develop a mechanistic model that combines two known analytical solution that were obtained for the early and late stage dynamics through simplifications of the thin film equation. We start our analysis by (re)examining the two mechan-

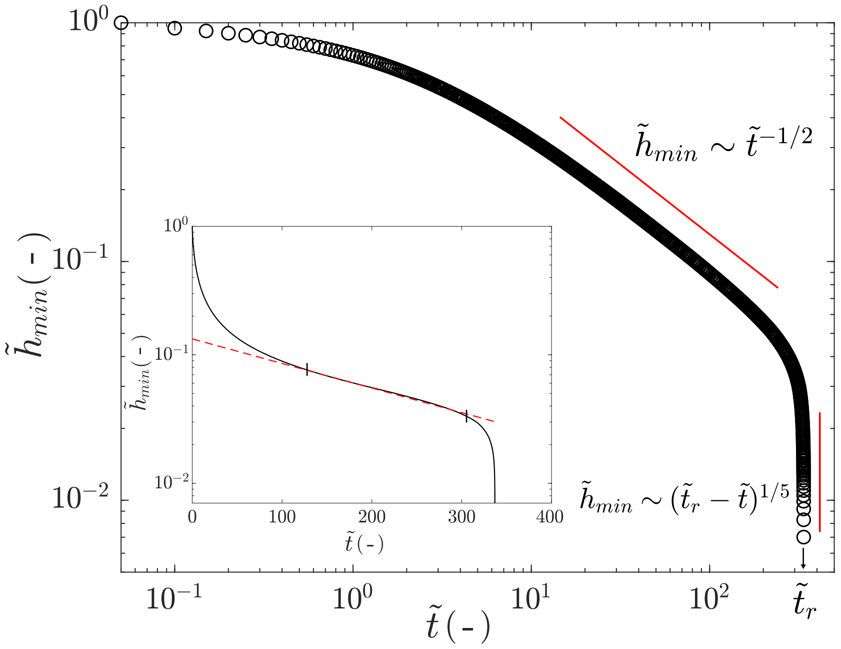

Figure 4.5 (colour online) Film dynamics for a prototypical small film ($R_{film} = 100\,\mu\text{m}$), with initial thickness $h_o = 1000$ nm illustrating how the dimensionless minimum film thickness extracted from the numerical simulations evolves in time. The film evolution shows an early and a late stage, both governed by power law dynamics (further detailed in §4.4.3 and §4.4.3). The inset shows the same data in a log-lin plot. The red dashed line shows an exponential fit from $0.03 < \tilde{h}_{min}(t) < 0.08$ as used in Manev et al.[25]. When we recast the fitting parameters $\tilde{a}$ and $\tilde{b}$ to their dimensional equivalents we find these parameters as $a = 133$ nm and $b = 0.046$ Hz. While the value of a is not available to compare with in the paper by Manev et al.[25], the value of b is within 15% of their experimentally determined values.

isms in these two stages. In the early stage, thinning is primarily governed by capillary drainage, while van der Waals forces govern the late stage. These stages are clearly evident from a plot of the minimum film thickness as a function of time, as shown for a prototypical small film ($R_{film} = 100\,\mu\text{m}$) in Fig. 4.5. Some previous works [12,13] captured the dynamics using a single exponential function, fitted to, (and currently found to describe,) only a part of the evolution ($0.03 < \tilde{h}_{min} < 0.08$) as shown in the inset of Fig. 4.5. Other works studied the early and late stage separately[6,30]. In the subsequent sections §4.4.3 and §4.4.3, we characterize these two stages. In section §4.4.3, we combine them to develop a theoretical model that describes how the lifetime of films depend on their initial features.

Scaling rule for the early stage

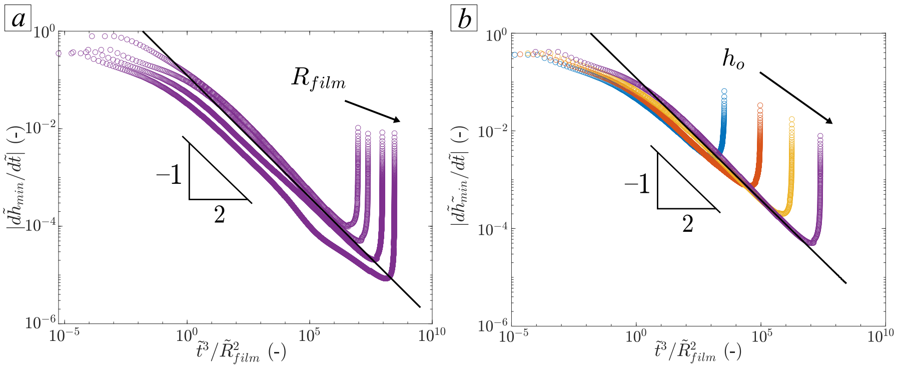

Figure 4.6 Dimensionless thinning rate as a function of the rescaled time axis (based on Eq. 4.12) illustrating early stage film dynamics for a fixed initial film thickness of $h_o = 2000$ nm and different $R_{film} = 50$ µm, 100 µm, 200 µm and 400 µm in (a); and for a fixed film radius of $R_{film} = 100$ µm and different $h_0 = 300$ nm, 500 nm, 1000 nm and 2000 nm in (b). The black solid lines correspond to Eq. 4.12.

Frankel and Mysels[6] developed scaling rules for the evolution of the film thickness at the center, h_c, and at the minimum of the dimple, h_{min}. They arrived at these rules by first determining the shape of a dimple close to rupture based on a self-similar solution of Eqs. 4.1-4.4 after applying the following simplifying assumptions: (i) a quasi-steady flow, (ii) $h_{min} \ll h_c$[5], (iii) negligible influence of van der Waals forces (iv) inner far-field constant slope and (v) outer far-field constant curvature. They then connect the dimple to the central part of the film by assuming it to be described by a parabola, $h(r,t) = ar^2 + br + c$, and infer the dynamics of h_c and h_{min} by solving the continuity equation. On substituting the boundary conditions, $h(r = 0, t) = h_c$, $\partial h/\partial r(r = 0, t) = 0$ and $h(r = R_{film}, t) = h_{min}$ in the afore-mentioned parabola, along with the assumption of $h_{min} \ll h_c$, results into a film profile, $h(t) = h_c(1 - r^2/R^2_{film})$. Using the two-dimensional flow rate $\left(Q = \frac{1}{2\pi R_{film}} \frac{\partial}{\partial t}\left(2\pi \int_0^{R_{film}} hrdr\right)\right)$ through the dimple, an inner far-field constant slope, $-2h_c/R_{film}$ and a constant far-field outer curvature $2/R_c$, Frankel and

Mysels[6] show[‡] that h_c and h_{min} scale as

$$h_c = \left(\frac{3\mu R_{film}^6}{c_1 2^4 \gamma R_c t}\right)^{1/4} \tag{4.8}$$

and

$$h_{min} = \frac{2c_1 c_2 h_c^2 R_c}{R_{film}^2} \tag{4.9}$$

respectively. Here $c_1 = 1.22$ and $c_2 = 1.25$ as determined by Frankel and Mysels[6] are the numerical solution for the asymptotic curvature at the far-right boundary of the dimple and the minimum value of the film thickness at the dimple, respectively. On substituting for h_c from Eq. 4.8, in Eq. 4.9, we obtain

$$h_{min} = \left(\frac{3\mu c_1 c_2^2 R_{film}^2 R_c}{2^4 \gamma t}\right)^{1/2}. \tag{4.10}$$

Non-dimensionalizing Eq. 4.10, using $\tilde{R}_{film} = R_{film}/\sqrt{h_o R_c/4}$, $\tilde{t} = t/(3\mu R_c^2/2\gamma h_o)$ and $\tilde{h}_{min} = h_{min}/h_o$ as discussed in section §4.2, we obtain

$$\tilde{h}_{min} = \left(\frac{c_1 c_2^2}{2^5}\frac{\tilde{R}_{film}^2}{\tilde{t}}\right)^{1/2}. \tag{4.11}$$

We note that the starting point in the model derived by Frankel and Mysels[6] is the occurrence of a dimple, such that this equation holds near rupture. We hence expect this relation to describe the simulations, which start from a finite value of $\tilde{h}_{min}$ at $\tilde{t} = 0$, after an initial transient. As commonly done in literature[7,24], rather than considering $\tilde{h}_{min}$ in a comparison between theory and simulations, we compare the thinning rate

$$\frac{\partial \tilde{h}_{min}}{\partial \tilde{t}} = -\frac{1}{2}\left(\frac{c_1 c_2^2}{2^5}\right)^{1/2}\left(\frac{\tilde{R}_{film}^2}{\tilde{t}^3}\right)^{1/2}. \tag{4.12}$$

This expression shows that the dimensionless thinning rate scales with time as $\tilde{t}^{-3/2}$, with film radius as $\tilde{R}_{film}^1$, and with film thickness as h_o^0. Comparing our simulations for different R_{film} and fixed h_o, we see a reasonable collapse of the curves when plotting the dimensionless rate against $\tilde{t}^3/\tilde{R}_{film}^2$ (Fig. 4.6a). Furthermore, for different h_o and fixed $\tilde{R}_{film}$, we see that the early stage dynamics indeed does not depend on the initial film thickness (Fig. 4.6b).

[‡] The numerical factors in Eqs. 4.8 and 4.9 are adjusted to account for the difference in the definition of film thicknesses between our work (see, section §4.2) and Frankel and Mysels[6]. More specifically, the constant 2^4 instead of 2^8 in Eq. 4.8, and the constant 2^0 instead of 2^1 in Eq. 4.9 stems from considering the upper half of an axisymmetric film between two bubbles in our work as compared to the full film thickness considered between the gas-liquid interface and the solid substrate in Frankel and Mysels[6].

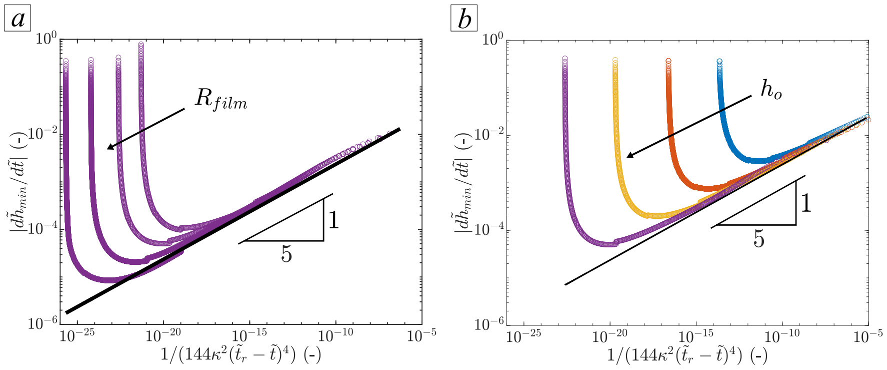

Figure 4.7 Dimensionless thinning rate as a function of the rescaled time axis (based on Eq. 4.14) illustrating late stage film dynamics for a fixed initial film thickness of h_o = 2000 nm and different R_{film} = 50 µm, 100 µm, 200 µm and 400 µm in (a); and for a fixed film radius of R_{film} = 100 µm and different h_0 = 300 nm, 500 nm, 1000 nm and 2000 nm in (b). The black solid lines correspond to Eq. 4.14.

As mentioned earlier, van der Waals forces are not included in the model by Frankel and Mysels[6]. Consequently, the film approaches rupture asymptotically, i.e. $\tilde{h}_{min} = 0$ does not occur in a finite time. Thus Eq. 4.12 on its own, could not be used to predict the lifetime of the film. In the next section, we therefore consider the late stage governed by van der Waals forces separately.

Scaling rule for the late stage

Van der Waals forces induce a rapid rupture once the film is thinned sufficiently to a certain critical thickness, h_{cr}. Considering the evolution of the dimple close to rupture where it is known to be independent of initial and boundary conditions[37], Zhang and Lister[30] developed a similarity solution for Eq. 4.1 to arrive at the following scaling

$$\tilde{h}_{min} = a_v \left(\frac{\tilde{t}_r - \tilde{t}}{144\kappa^2}\right)^{1/5}, \tag{4.13}$$

where a_v is an O(1) constant. Here, $144\kappa^2$ is a factor that relates $\tilde{t}_r$ and $\tilde{t}$ to a dimensionless time relevant for this late stage[30] [§]. The thinning rate is then given by

$$\frac{\partial \tilde{h}_{min}}{\partial \tilde{t}} = -\frac{a_v}{5}\left(\frac{1}{144\kappa^2(\tilde{t}_r - \tilde{t})^4}\right)^{1/5}. \tag{4.14}$$

[§] Note that the ratio $(1/144\kappa^2)$ arises from the translation from the time scale based on the growth of unstable waves to the time scale based on drainage as used throughout this paper. More specifically, the length scale pertaining to the unstable waves is $h_o^2\sqrt{3\pi\gamma/A}$, which translates into a time scale $216\pi^2\gamma\mu h_o^5/A^2$.

Notably, the thinning rate in the late stage neither depends on the initial film thickness nor on the initial film radius. Replotting the data set shown in Figs. 4.6a and 4.6b, now using the rescaled time axis $1/(144\kappa^2(\tilde{t}_r - \tilde{t})^4)$ all curves indeed collapse close to rupture as shown on the right hand sides of Figs. 4.7a and 4.7b[¶]. The O(1) constant is obtained by fitting the data to obtain $a_v = 1.18$.

Estimate of the film lifetime

To arrive at the total thinning rate, we consider the contribution of the early and the late stage (Eqs. 4.12 and 4.14) as additive[36], to arrive at

$$\left(\frac{\partial \tilde{h}_{min}}{\partial \tilde{t}}\right)_{total} = -\frac{1}{2}\left(\frac{c_1 c_2^2}{2^5}\right)^{1/2}\left(\frac{\tilde{R}_{film}^2}{\tilde{t}^3}\right)^{1/2} - \frac{a_v}{5}\left(\frac{1}{144\kappa^2(\tilde{t}_r - \tilde{t})^4}\right)^{1/5}. \tag{4.15}$$

On recasting $\tilde{t}$ and $(\tilde{t}_r - \tilde{t})$ in the first and the second term on the right hand side in terms of $\tilde{h}_{min}$ using Eq. 4.11 and 4.13, respectively, we obtain the total thinning rate as,

$$\left(\frac{\partial \tilde{h}_{min}}{\partial \tilde{t}}\right)_{total} = \left(\frac{-2^4}{c_1 c_2^2 \tilde{R}_{film}^2}\right)\tilde{h}_{min}^3 - \frac{a_v^5}{720\tilde{h}_{min}^4\kappa^2}, \tag{4.16}$$

which is independent of time. An estimate for the lifetime can then be obtained as

$$\tilde{t}_r = \int_0^{\tilde{t}_r} \partial\tilde{t} = \int_1^0 \frac{\partial \tilde{h}_{min}}{\left(\frac{-2^4}{c_1 c_2^2 \tilde{R}_{film}^2}\right)\tilde{h}_{min}^3 - \frac{a_v^5}{720\tilde{h}_{min}^4\kappa^2}} \tag{4.17}$$

The solution of the above integral[‖] at the limit $\tilde{R}_{film} \to 0$, for any value of κ, gives

$$\tilde{t}_r = 0.65\ \tilde{R}_{film}^{10/7}\kappa^{4/7}, \tag{4.18}$$

On substituting back the relevant length and time scales from section §4.2, we get

$$t_r = 0.65\left(\frac{R_{film}}{r^*}\right)^{10/7}\left(\frac{\pi h_o^3\gamma}{AR_c}\right)^{4/7} t^* = 5.05 R_{film}^{10/7}\gamma^{-3/7}A^{-4/7}R_c^{5/7}. \tag{4.19}$$

This analysis shows that the dimensional lifetime is independent of the initial thickness, h_o and scales with the radius, R_{film} with an exponent of 10/7. This result is plotted in Fig. 4.4 as the dashed red line. Given the simplifying assumptions used to derive the similarity solutions for the early and late stage, Eq. 19 fairly well describes the numerical data, as shown in Fig. 4.4. The here presented analytical model hence provides mechanistic insights on the numerically established scaling relation, and the comparison shows the extent to which film thinning of small radii films can be described through the used simplifications.

[¶] We note that the non-smooth connection between the early and late stage arises from a shift in the location of the dimple (as for instance seen in Fig. 3). In our simulations, this shift occurs by one grid point such that it appears as a non-continuous jump.

[‖] The exact solution is an impractically long solution and hence we solve it at limit $R_{film} \to 0$ and $R_{film} \to \infty$ to arrive at an approximate, but compact solution. The relative difference between the actual solution and the approximate solution Eq. 4.18 is approximately 1%.

4.5 Conclusions

The aim of this work is to understand how the thinning dynamics and lifetime of films between two bubbles depend on the extent to which the bubbles have deformed upon close contact, as characterized by the initial radius and thickness of the flattened film. Numerical solutions of a hydrodynamic thin film model show that the thinning dynamics are distinctly different for films of large and small initial radius. Large films thin locally through the formation of a dimple at the edge of the film[29], while small films initially thin across the entire film, then develop a dimple, and eventually rupture at the minimum of this dimple. For large films, our simulations confirm earlier theoretical work on films of semi-infinite radius[36] that predicts that the lifetime t_r scales with initial film radius R_{film} and thickness h_0 as: $t_r \sim R_{film}^0 h_0^{5/7}$. As opposed to this scaling for large films, we found the lifetime of small films, which was the focus of the current work, to be independent of the initial film thickness and dependent on film radius. To understand the scaling for small films, we combined earlier-reported analytical solutions for dimpled thinning in the early stage[6] and van der Waals rupture in the late stage[30]. While these analytical solutions were obtained through simplification of the full thin film equation, the predicted scaling $t_r \sim h_0 R_{film}^{10/7}$ captures the trend in the numerical data reasonably well.

Acknowledgements

This work is supported by the Netherlands Organization for Scientific Research (NWO) and the Dutch Institute for Sustainable Process Technology (ISPT) as part of the project COFILM.

Appendix

Theoretical model for large axisymmetric films

In this section, we adapt our earlier model developed for semi-infinite films in a 2D Cartesian geometry to the axisymmetric geometry considered in the present paper. We begin the model description by studying the early stage dynamics that follows the scaling rule developed by Aradian et al.[29],

$$\tilde{h}_{min} = a_r \tilde{t}^{-1/2}, \tag{4.20}$$

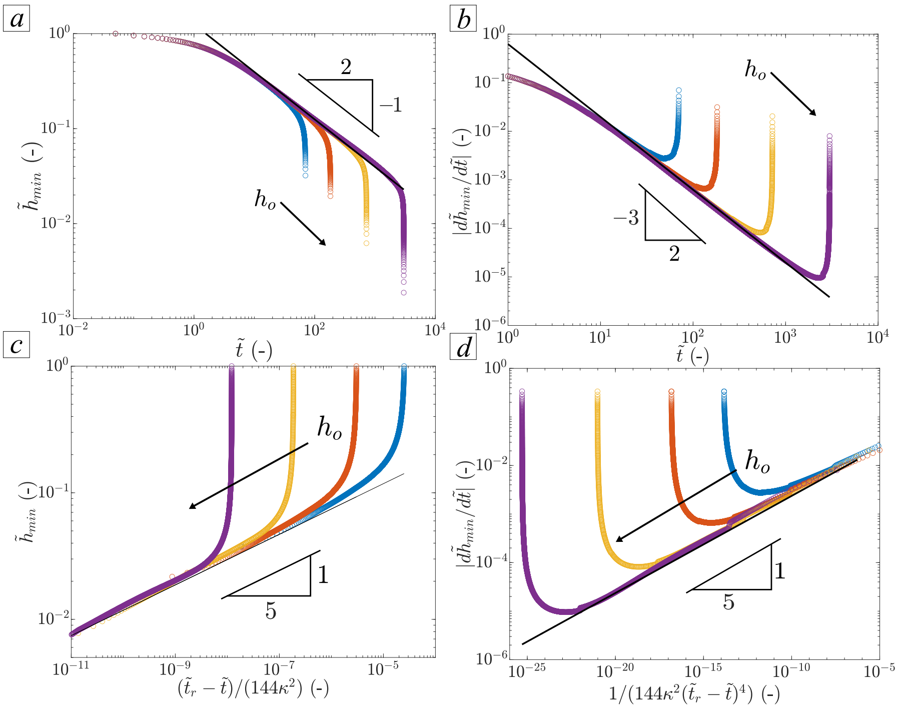

Figure 4.8 Dimensionless film thickness and thinning rate as a function of time illustrating the early stage in (a) and (b) respectively and the late stage film dynamics in (c) and (d) respectively for a fixed film radius of $R_{film} = 4000\,\mu\text{m}$ and different initial film thicknesses of $h_o = 300$, 500, 1000 and 2000 nm. The black solid lines in (a), (b), (c) and (d) correspond to Eqs. 4.20, 4.21, 4.13 and 4.14, respectively.

which on taking the time derivative leads to,

$$\frac{\partial \tilde{h}_{min}}{\partial \tilde{t}} = -\frac{a_r}{2\tilde{t}^{3/2}}. \tag{4.21}$$

Figs. 4.8a and 4.8b show how the early stage film dynamics from numerical simulations for these large films compare for different initial film thicknesses for a fixed large $R_{film} = 4000\,\mu\text{m}$. The data is well described by the model, after a first initial transient. The O(1) constant obtained from a fit of the data is $a_r = 1.2$.

The late stage evolution for these large axisymmetric films follows the model by Zhang and Lister[30] presented in Eqs. 4.13 and 4.14, with the earlier reported O(1) constant $a_v = 1.18$. Figs. 4.8c and 4.8d show how our numerical simulations follow the late stage dynamics for different h_o and for $R_{film} = 4000\,\mu\text{m}$.

Considering the contribution of the early and the late stages as additive and using the same approach as presented in the main body of the paper, we arrive at the total thinning rate

$$\left(\frac{\partial \tilde{h}_{min}}{\partial \tilde{t}}\right)_{total} = -\frac{a_r}{2\tilde{t}^{3/2}} - \frac{a_v}{5}\left(\frac{1}{144\kappa^2(\tilde{t}_r - \tilde{t})^4}\right)^{1/5}, \tag{4.22}$$

which, when represented in terms of $\tilde{h}_{min}$, reads

$$\left(\frac{\partial \tilde{h}_{min}}{\partial \tilde{t}}\right)_{total} = -\frac{\tilde{h}^3_{min}}{2a_r^2} - \frac{a_v^5}{720\tilde{h}^4_{min}\kappa^2}. \tag{4.23}$$

An estimate for the film rupture time can then be obtained as

$$\tilde{t}_r = \int_0^{\tilde{t}_r} \partial \tilde{t} = -\int_1^0 \frac{\partial \tilde{h}_{min}}{\frac{\tilde{h}^3_{min}}{2a_r^2} + \frac{a_v^5}{720\tilde{h}^4_{min}\kappa^2}}. \tag{4.24}$$

The solution of the above integral at the limit $\kappa \to \infty$ gives

$$\tilde{t}_r = 6.32\kappa^{4/7}. \tag{4.25}$$

Fig. 4.9 shows how large film asymptotes from Fig. 4.4 agrees well with the theoretical model Eq. 4.25. On substituting the scales in Eq. 4.25 to determine the dimensional lifetime, we obtain

$$t_r = 18.2\mu R_c^{10/7}\gamma^{-3/7}A^{-4/7}h_o^{5/7}R^0_{film}. \tag{4.26}$$

For large film radii, we hence find that the dimensional lifetime of the film depends on the initial film thickness and is independent of the film radius.

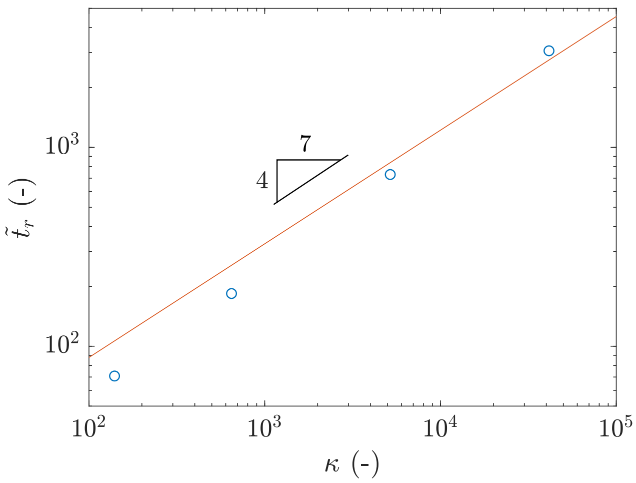

Figure 4.9 (colour online) Dimensionless film rupture times as a function of dimensionless curvature for the large film asymptotes at the extreme right in Fig. 4.4. The blue circles correspond to the numerical simulations whereas the red line corresponds to the theoretical expression as described in Eq. 4.25.

Film evolution at the transition region

The thinning behaviour at the transition region is illustrated for a thin (h_o = 300 nm) and thick (h_o = 2000 nm) film in Fig. 4.10, for which the transition occurs around $R_{film} = 80\,\mu\text{m}$ and $R_{film} = 600\,\mu\text{m}$, respectively. As expected, the film thinning is observed to proceed via the formation of a dimple at the connection between the planar and the curved portion of the film. Qualitatively, the difference in the film thinning at this transition region from that at the large radii films is that the film thickness at the centre of the film increases beyond the initial film thickness. The physics behind film dynamics for films in this transition region is beyond the scope of this work.

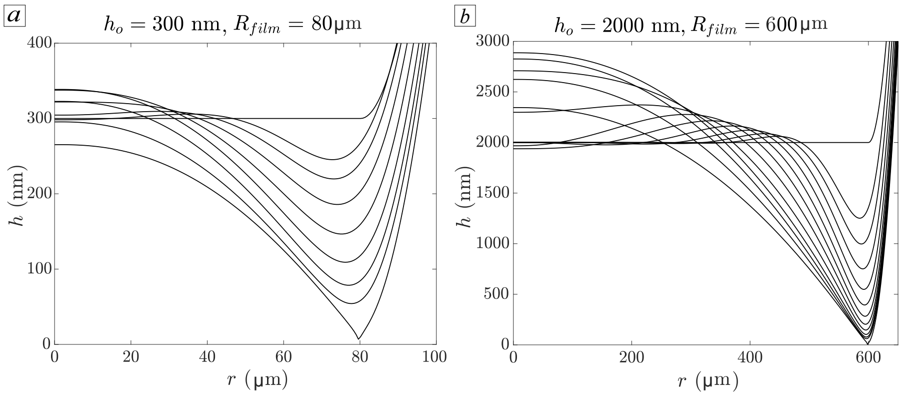

Figure 4.10 Film evolution in the transition regime for two examples: (a) a thin film ($h_0 =$ 300 nm), which has the transition around $R_{film} = 80$ µm and (b) a thick film ($h_0 = 2000$ nm), with the transition around $R_{film} = 600$ µm. Besides the initial profiles at $t = 0$, profiles are shown for $t_r/2^n$, with $n = 7 \ldots 0$ in (a) and $n = 11 \ldots 0$ in (b), with $t_r = 11.0$ s and 220.4 s for (a) and (b) respectively.

Bibliography

[1] Osborne Reynolds. On the theory of lubrication and its application to mr. beauchamp tower's experiments, including an experimental determination of the viscosity of olive oil. Phil. Trans. Roy. Soc. Lon., 177:157–234, 1886. doi: 10.1098/rstl.1886.0005.

[2] A. Vrij. Possible mechanism for the spontaneous rupture of thin, free liquid films. Discuss. Faraday Soc., 42:23–33, 1966. doi: 10.1039/DF9664200023.

[3] PS Prokhorov. The effects of humidity deficit on coagulation processes and the coalescence of liquid drops. Discuss. Faraday Soc., 18:41–51, 1954. doi: 10.1039/DF9541800041.

[4] R.S Allan, G.E Charles, and S.G Mason. The approach of gas bubbles to a gas/liquid interface. J. Colloid Sci., 16(2):150 – 165, 1961. doi: 10.1016/0095-8522(61)90014-9.

[5] D Platikanov. Experimental investigation on the "dimpling" of thin liquid films. J. Phys. Chem., 68 (12):3619–3624, 1964. doi: 10.1021/j100794a030.

[6] Stanley P Frankel and Karol J Mysels. On the "dimpling" during the approach of two interfaces1. J. Phys. Chem., 66(1):190–191, 1962. doi: 10.1021/j100807a513.

[7] Jean Luc Joye, George J Hirasaki, and Clarence A Miller. Dimple formation and behavior during axisymmetrical foam film drainage. Langmuir, 8(12):3083–3092, 1992. doi: 10.1021/la00048a038.

[8] Gurmeet Singh, C.A. Miller, and G.J. Hirasaki. On dimple formation in foam films. J. Colloid Interface Sci., 187(2):334 – 337, 1997. doi: 10.1006/jcis.1996.4703.

[9] Ivan U. Vakarelski, Rogerio Manica, Xiaosong Tang, Sean J. O-Shea, Geoffrey W. Stevens, Franz Grieser, Raymond R. Dagastine, and Derek Y. C. Chan. Dynamic interactions between microbubbles in water. Proc. Nat. Acad. Sci., 107(25):11177–11182, 2010. doi: 10.1073/pnas.1005937107.

[10] B. Liu, R. Manica, Q. Liu, E. Klaseboer, Z. Xu, and G. Xie. Coalescence of bubbles with mobile interfaces in water. Phys. Rev. Lett., 122:194501, 2019. doi: 10.1103/PhysRevLett.122.194501.

[11] E. Klaseboer, J. Ph. Chevaillier, C. Gourdon, and O. Masbernat. Film drainage between colliding drops at constant approach velocity: Experiments and modeling. J. Colloid Interface Sci., 229(1): 274 – 285, 2000. doi: 10.1006/jcis.2000.6987.

[12] R. Manica, E. Klaseboer, and D. Y. C. Chan. Dynamic interactions between drops—a critical assessment. Soft Matter, 4:1613–1616, 2008. doi: 10.1039/B806741D.

[13] L. R. Fisher, D. Hewitt, E. E. Mitchell, J. Ralston, and J. Wolfe. The drainage of an aqueous film between a solid plane and an air bubble. Adv. Colloid Interface Sci., 39:397 – 416, 1992. doi: 10.1016/0001-8686(92)80067-8.

[14] R. Manica, L. Parkinson, J. Ralston, and D. Y. C. Chan. Interpreting the dynamic interaction between a very small rising bubble and a hydrophilic titania surface. J. Phys. Chem. C, 114(4):1942–1946, 2010. doi: 10.1021/jp911104b.

[15] R. F. Tabor, R. Manica, D. Y. C. Chan, F. Grieser, and R. R. Dagastine. Repulsive van der waals forces in soft matter: Why bubbles do not stick to walls. Phys. Rev. Lett., 106:064501, 2011. doi: 10.1103/PhysRevLett.106.064501.

[16] J. N. Connor and R. G. Horn. The influence of surface forces on thin film drainage between a fluid drop and a flat solid. Faraday Discuss., 123:193–206, 2003. doi: 10.1039/B204500C.

[17] R. Manica, J. N. Connor, L. Y. Clasohm, S. L. Carnie, R. G. Horn, and D. Y. C. Chan. Transient responses of a wetting film to mechanical and electrical perturbations. Langmuir, 24(4):1381–1390, 2008. doi: 10.1021/la701562q.

[18] D. Exerowa and P. M. Kruglyakov. Foam and foam films: theory, experiment, application. Elsevier, 1997.

[19] Derek Y. C. Chan, Evert Klaseboer, and Rogerio Manica. Film drainage and coalescence between deformable drops and bubbles. Soft Matter, 7:2235–2264, 2011. doi: 10.1039/C0SM00812E.

[20] R. K. Prud'homme. Foams: theory, measurements, and applications. Routledge, 2017.

[21] Dimitr Stanchev Dimitrov and Ivan Boyanov Ivanov. Hydrodynamics of thin liquid films. on the rate of thinning of microscopic films with deformable interfaces. J. Colloid Interface Sci., 64(1):97 – 106, 1978. doi: 10.1016/0021-9797(78)90338-7.

[22] A Sharma and E Ruckenstein. Stability, critical thickness, and the time of rupture of thinning foam and emulsion films. Langmuir, 3(5):760–768, 1987. doi: 10.1021/la00077a033.

[23] AK Malhotra and DT Wasan. Effect of film size on drainage of foam and emulsion films. AIChE J., 33(9):1533–1541, 1987. doi: 10.1002/aic.690330913.

[24] Boryan P Radoev, Alexei D Scheludko, and Emil D Manev. Critical thickness of thin liquid films: Theory and experiment. J. Colloid Interface Sci., 95(1):254 – 265, 1983. doi: 10.1016/0021-9797(83)90094-2.

[25] Emil Manev, Roumen Tsekov, and Boryan Radoev. Effect of thickness non-homogeneity on the kinetic behaviour of microscopic foam film. J. Dispersion Sci. Technol., 18(6-7):769–788, 1997. doi: 10.1080/01932699708943771.

[26] Roumen Tsekov. The r4/5-problem in the drainage of dimpled thin liquid films. Colloid Surf. A: Physicochem. Eng. Asp., 141(2):161 – 164, 1998. doi: 10.1016/S0927-7757(97)00253-7.

[27] E Ruckenstein and A Sharma. A new mechanism of film thinning: Enhancement of Reynolds' velocity by surface waves. J. Colloid Interface Sci., 119(1):1 – 13, 1987. doi: 10.1016/0021-9797(87)90239-6.

[28] A.N Zdravkov, G.W.M Peters, and H.E.H Meijer. Film drainage between two captive drops: Peo–water in silicon oil. J. Colloid Interface Sci., 266(1):195 – 201, 2003. ISSN 0021-9797. doi: 10.1016/S0021-9797(03)00466-1.

[29] A. Aradian, E. Raphael, and P. G. de Gennes. Marginal pinching in soap films. Europhys. Lett., 55

(6):834–840, 2001. doi: 10.1209/epl/i2001-00356-y/fulltext/.

[30] W. W. Zhang and J. R. Lister. Similarity solutions for van der waals rupture of a thin film on a solid substrate. Phys. Fluids, 11(9):2454–2462, 1999. doi: 10.1063/1.870110.

[31] A. Oron, S. H. Davis, and S. G. Bankoff. Long-scale evolution of thin liquid films. Rev. Mod. Phys., 69(3):931–980, 1997. doi: 10.1103/RevModPhys.69.931.

[32] G. K. Batchelor. An Introduction to Fluid Dynamics. Cambridge Mathematical Library. Cambridge University Press, 2000.

[33] Javier A Diez, Lou Kondic, and Andrea Bertozzi. Global models for moving contact lines. Phys. Rev. E, 63(1):011208, 2000. doi: 10.1103/PhysRevE.63.011208.

[34] Maulik S. Shah, Volkert van Steijn, Chris R. Kleijn, and Michiel T. Kreutzer. Thermal fluctuations in capillary thinning of thin liquid films. J. Fluid Mech., 876:1090–1107, 2019. doi: 10.1017/jfm.2019.595.

[35] E.D Manev, S.V Sazdanova, and D.T Wasan. Emulsion and foam stability—the effect of film size on film drainage. J. Colloid Interface Sci., 97(2):591 – 594, 1984. doi: 10.1016/0021-9797(84)90334-5.

[36] Michiel T. Kreutzer, Maulik S. Shah, Pravien Parthiban, and Saif A. Khan. Evolution of nonconformal landau-levich-bretherton films of partially wetting liquids. Phys. Rev. Fluids, 3:014203, Jan 2018. doi: 10.1103/PhysRevFluids.3.014203.

[37] L Gary Leal. Advanced transport phenomena: fluid mechanics and convective transport processes. Cambridge University Press, 2007.

[38] S. Hartland, B. Yang, and S.A.K. Jeelani. Dimple formation in the thin film beneath a drop or bubble approaching a plane surface. Chem. Eng. Sci., 49(9), 1994. doi: 10.1016/0009-2509(93)E0006-X.

[39] H. Wong, C. J. Radke, and S. Morris. The motion of long bubbles in polygonal capillaries .1. thin films. J Fluid. Mech., 292:71–94, 1995. doi: '10.1017/S0022112095001443'.

Supplementary Material

Initial condition with a transition region

The pressure discontinuity arising in the initial film profile at the connection between the flat and curved part is eliminated by adding a transition region between $\tilde{R}_{film} - \tilde{R}_{tr} < \tilde{r} < \tilde{R}_{film} + \tilde{R}_{tr}$ and connecting the flat and the curved part by including a third order polynomial. Adjusting Eq. 4.7 in this way, we obtain

$$h = \begin{cases} 1, & \text{for } \tilde{r} < \tilde{R}_{film} - \tilde{R}_{tr} \\ 1 + \alpha_1 \tilde{r}^3 + \alpha_2 \tilde{r}^2 + \alpha_3 \ln(\tilde{r}) + \alpha_4, & \text{for } \tilde{R}_{film} - \tilde{R}_{tr} < \tilde{r} < \tilde{R}_{film} + \tilde{R}_{tr} \\ 1 + \frac{\tilde{r}^2}{4} + \alpha_5 \ln(\tilde{r}) + \alpha_6, & \text{for } \tilde{r} > \tilde{R}_{film} + \tilde{R}_{tr} \end{cases} \tag{4.27}$$

The constants α_1, α_2, α_3, α_4, α_5 and α_6, are obtained by matching the height, its first and its second derivative at the two boundaries of the transition region. This gives

$$\alpha_1 = \frac{1}{18\tilde{R}_{tr}}; \ \alpha_2 = \frac{1}{4} - \frac{(\tilde{R}_{film} + \tilde{R}_{tr})}{8\tilde{R}_{tr}} \tag{4.28}$$

$$\alpha_3 = -(\tilde{R}_{film} - \tilde{R}_{tr}) \left(\frac{(\tilde{R}_{film} - \tilde{R}_{tr})^2/3 - (\tilde{R}_{film} + \tilde{R}_{tr})(\tilde{R}_{film} - \tilde{R}_{tr})/2}{2\tilde{R}_{tr}} \right) - (\tilde{R}_{film} - \tilde{R}_{tr}) \left(\frac{\tilde{R}_{film} - \tilde{R}_{tr}}{2} \right) \tag{4.29}$$

$$\alpha_4 = -\frac{(\tilde{R}_{film} - \tilde{R}_{tr})^2}{4} - \frac{(\tilde{R}_{film} - \tilde{R}_{tr})^3/9 - (\tilde{R}_{film} + \tilde{R}_{tr})(\tilde{R}_{film} - \tilde{R}_{tr})^2/4}{2\tilde{R}_{tr}} - \alpha_3 \ln(\tilde{R}_{film} - \tilde{R}_{tr}) \tag{4.30}$$

$$\alpha_5 = \alpha_3 - \frac{(\tilde{R}_{film} + \tilde{R}_{tr})^2}{12\tilde{R}_{tr}}; \ \alpha_6 = \frac{-5}{72a}(\tilde{R}_{film} + \tilde{R}_{tr})^3 + (\alpha_3 - \alpha_5)\ln(\tilde{R}_{film} + \tilde{R}_{tr}) + \alpha_4 \tag{4.31}$$

Derivation of scaling rules from Frankel and Mysels[6] paper

Assume a parabolic profile of the film, i.e., $h = ar^2 + br + c$, with the boundary conditions at the time of the rupture being $r = 0, h = h_c$; at $r = 0, \partial h/\partial r = 0$ and at $r = R_{film}, \partial h/\partial r = -k$, where $k > 0$ is a constant. The first condition gives $c = h_c$, the second one gives $b = 0$ and the third one gives $a = -k/2R_{film}$. The film profile then is given by $h = h_c - kr^2/2R_{film}$. Assuming $h(r = R_{film}) = h_{min} \ll h_c$, we get $k = 2h_c/R_{film}$.

Now, volume of fluid in a cylindrical film is given by $V = 2\pi \int_o^{R_{film}} hrdr$, which gives $V = 2\pi h_c R_{film}^2/4$. The two dimensional flow rate, Q, can be given by the following balance,

$$2\pi R_{film} Q = -\frac{\partial V}{\partial t} \tag{4.32}$$

which leads to

$$Q = -\frac{R_{film}}{4}\frac{\partial h_c}{\partial t} \tag{4.33}$$

We now focus in the vicinity of the dimple. We start with the governing equation for the flow through the film, i.e.,

$$\frac{1}{\mu}\frac{\partial p}{\partial r} = \frac{\partial^2 u_r}{\partial z^2} \tag{4.34}$$

Applying no-slip boundary condition (i.e. $u_r = 0$) at the surfactant-rich gas-liquid interface (at $z = h/2$) and symmetry boundary condition (i.e. $\partial u_r/\partial r = 0$) at $z = 0$ (geometry described in schematic Fig. 1 in the main text), we obtain,

$$u_r = \frac{1}{2\mu}\frac{\partial p}{\partial r}\left(z^2 - \frac{h^2}{4}\right) \tag{4.35}$$

The two-dimensional flow rate through the dimple is given by the continuity as,

$$\left(\int_0^{h/2} u_r \partial z\right) = \frac{Q}{2}, \tag{4.36}$$

which simplifies to

$$\frac{h^3}{12\mu}\frac{\partial p}{\partial r} = Q \tag{4.37}$$

With the pressure contribution solely from the surface tension forces, we obtain**,

$$\frac{\gamma}{24\mu} h^3 \frac{\partial^3 h}{\partial r^3} = Q \tag{4.38}$$

The governing equation 4.38 has a different numerical pre-factor than that found in the work of Frankel and Mysels[6] due to the difference in the geometry under consideration. In our work, we consider an axisymmetric film with the film thickness between the rigid gas-liquid interface (no-slip) and the axis of symmetry (no-shear) being $h/2$, as shown in the schematic Fig. 1 in the main text, whereas in the work of Frankel and Mysels[6], the film thickness between the free gas-liquid interface (no-shear) and the solid subtrate (no-slip) is h.

Frankel and Mysels[6] show that the inner far-field of the dimple is represented by a constant slope. We derive the slope of the film at $r = R_{film}$ from the above-derived parabolic profile of the film, thereby leading to the inner far-field slope given by $(\partial h/\partial r)|_{(r-R_{film})\to -\infty} = -2h_c/R_{film}$ (also shown in Hartland et al.[38]). Frankel and Mysels[6] also show that the curvature at the outer far-field can be expressed as a constant curvature, thereby leading to, $1/2r(\partial^2 h/\partial r^2)|_{(r+R_{film})\to\infty} = 2/R_c$.

Applying O(1) scaling for the governing Eq. 4.38 and the afore-mentioned inner far-field slope, using $\tilde{h} = h/[h]$ and $\tilde{r} = (r - R_{film})/[r]$, gives,

$$[h] = 2\left(\frac{h_c}{R_{film}}\right)[r]; [r] = \left(\frac{3\mu Q R_{film}^4}{2\gamma h_c^4}\right). \tag{4.39}$$

Here the scale of [h] is the same as that found in Frankel and Mysels[6], whereas [r] is a factor 2^3 larger and is due to the difference in choice of the geometry that is considered in our work and in that of Frankel and Mysels[6].

On substituting these scales in the outer far-field curvature, i.e..,

$$\frac{[h]}{[r]^2}\frac{\partial^2 \tilde{h}}{\partial \tilde{r}^2} = \frac{4}{R_c} \tag{4.40}$$

we obtain,

$$\frac{\partial^2 \tilde{h}}{\partial \tilde{r}^2} = \frac{3\mu Q R_{film}^5}{R_c \gamma h_c^5} = c_1 \tag{4.41}$$

Here, $c_1 = 1.22$ is a constant determined numerically. Altogether, we have the following set of dimensionless equations

$$\tilde{h}^3 \frac{\partial^3 \tilde{h}}{\partial \tilde{r}^3} = 1 \tag{4.42}$$

[**] More accurate approach would to use axisymmetric set of equations for the curvature and hence the governing equation. Here, we use the Cartesian equivalents to keep the analysis simple, in line with the work of Frankel and Mysels[6].

$$\left(\frac{\partial \tilde{h}}{\partial \tilde{r}}\right)_{\tilde{r}\to-\infty} = -1 \tag{4.43}$$

and

$$\frac{\partial^2 \tilde{h}}{\partial \tilde{r}^2}_{\tilde{r}\to\infty} = c_1 \tag{4.44}$$

Using Eq. 4.33 to substitute for Q in Eq. 4.41, we get,

$$\frac{3\mu(-R_{film})R_{film}^5}{4R_c\gamma h_c^5}\frac{\partial h_c}{\partial t} = c_1 \tag{4.45}$$

$$-\int_{\infty}^{h_c}\frac{\partial h_c}{h_c^5} = \int_0^t \frac{c_1 2^2\gamma R_c \partial t}{3\mu R_{film}^6} \tag{4.46}$$

which upon integration gives

$$h_c = \left(\frac{3\mu R_{film}^6}{c_1 2^4 \gamma R_c t}\right)^{1/4} \tag{4.47}$$

which is a factor 2 larger than what we find in the paper by Frankel and Mysels[6].

Having determined h_c, we set out to determine the scaling rule for h_{min}. Substituting for Q in Eq. 4.39 from Eq. 4.41, we get,

$$[r] = \frac{c_1 h_c R_c}{2R_{film}} \tag{4.48}$$

This gives the scale of film thickness as

$$[h] = \frac{c_1 h_c^2 R_c}{R_{film}^2} \tag{4.49}$$

Using $[h] = h_{min}/c_2$, where c_2 is the minimum value of the film thickness obtained numerically, we get,

$$h_{min} = \frac{c_1 c_2 h_c^2 R_c}{R_{film}^2} \tag{4.50}$$

The above Eq. for h_{min} is a factor 2 smaller than that obtained in Frankel and Mysels[6], with $c_1 = 1.22$ and $c_2 = 1.25$[††]. On substituting for h_c from Eq. 4.47, in Eq. 4.50, we obtain,

$$h_{min} = \left(\frac{3\mu c_1 c_2^2 R_{film}^2 R_c}{2^4\gamma t}\right)^{1/2} \tag{4.51}$$

[††] These constants $c_1 = 1.22$ and $c_2 = 1.25$ are also obtained in Wong et al.[39].

5. Epilogue

The purpose of this chapter is (i) to provide a brief summary of the work discussed in this thesis, (ii) to briefly discuss the extensibility of the current work and (iii) to discuss future research opportunities. We first start with providing conclusions from the previous three chapters. Thereafter, we discuss the extensibility of the results obtained in this thesis when we allow for different functional forms of the disjoining pressure between the two interfaces. We conclude by discussing further research opportunities in the context of (a) using the theoretical and numerical framework developed in this thesis to study metastable thin films between foam bubbles and (b) developing a theoretical framework to study chaos in planar thin liquid films.

5.1 Conclusions

The overall goal of this thesis was to (i) develop scaling rules to predict lifetimes of semi-infinite, non-planar thin liquid films as a function of the fluid properties and the process conditions, (ii) reveal whether and when thermal fluctuations are relevant in determining film lifetimes and (iii) characterize how lifetimes of finite size thin films depend on the initial geometrical features of the film, i.e. radius and thickness. In the following three paragraphs, we briefly discuss the conclusions of the three research questions that were outlined in the Introduction chapter, and answered in the previous three chapters.

Research question 1: We started our work by developing scaling rules for films that are semi-infinite in their lateral dimension, through the development of a model that combines the dynamics of dimple formation due to drainage and of the rapid collapse due to van der Waals forces in order to answer the question: What scaling rule govern the lifetime of semi-infinite non-planar films as a function of the fluid properties and the process conditions?

To this end, we simulated the dynamics of a non-planar film geometry by numerically integrating the well-known thin film equation[1], in which we included both surface tension and van der Waals forces. We amended the commonly used initial condition of a planar film by adding a curved portion of constant curvature, akin to a Plateau border, to the planar film. Furthermore, we amended the commonly used periodic boundary conditions by using a constant curvature and film height at the far-field curved portion and a constant film thickness and zero gradient of the film height and pressure on the far-field planar portion of the film.

Upon non-dimensionalization of the governing thin film equation, and its initial and boundary conditions, we found that the entire problem was governed by a single dimensionless parameter, κ. Here, κ signifies the relative strength of drainage, resulting from the non-planar nature of the films, to the strength of van der Waals forces that drive the rupture. For all κ's studied, we observed that the film evolution consists of two stages, viz. the early and the late stages. In the early stage of film evolution, these films drain due to lower pressure in the curved portion of the film, which results in the formation of a well-known dimple at the connection between the planar and the curved portion of the film. Once the film is thinned sufficiently, we observed a crossover from the early stage dynamics due to dimpling to the late stage dynamics, wherein a rapid collapse due to van der Waals forces occurs. We described the early and the late stages with self-similar solutions, which were studied earlier in the literature in the limiting cases of only drainage (no van der Waals forces)[2] and only surface tension forces and van der Waals forces (no drainage)[3] in the literature. Furthermore, we developed a theoretical framework by matching these two self-similar solutions for the early and the late stage dynamics. This yielded a scaling rule that relates dimensionless film lifetimes, t_r to κ as $t_r \sim \kappa^{-10/7}$, which was in good agreement with our numerical results.

Research question 2: What role do thermal fluctuations play in determining lifetimes of non-planar films? Are there any distinct regimes where thermal fluctuations are relevant, and if so, what are the bounds of those regimes? What are the observable differences in film evolution and final rupture as thermal fluctuations become more relevant?

We answered this question using the stochastic thin film equation originally developed in the literature to study film dewetting[4] and droplet spreading[5] on solid substrates. We modified the problem description used in these works by changing the initial and boundary conditions. For the initial conditions, we used a semi-infinite non-planar film geometry (i.e. a large planar film connected to a curved film of constant curvature) as considered in chapters 2 and 3. We used the far-field boundary conditions discussed in detail in chapters 2 and 3. Upon non-dimensionalization of the governing stochastic thin film equation and its initial and boundary conditions, we found that its dynamics is then governed by two key dimensionless parameters: the strength of drainage, κ and the strength of thermal noise, θ. For strong drainage ($\kappa \gg \kappa_{tr}$), with κ_{tr} being a temperature dependent dimensionless parameter (for which we provide an estimate), our simulations indicated the following: (a) the film ruptures deterministically due to rupture in the thinnest part of the dimple, and (b) film lifetimes depend solely on κ, based on the earlier predicted scaling rule[6], regardless of the noise strength. By contrast, for weak drainage ($\kappa \ll \kappa_{tr}$), the film ruptures through the spontaneous growth of waves originating from thermal fluctuations. Our work in this chapter explains whether it is important to include thermal fluctuations in the dynamics of draining thin films to predict when they rupture, and if so, when and why to include them.

Research question 3: How do film lifetimes depend on the initial film radii and film thicknesses when all the relevant physics, i.e. drainage due to dimple formation, surface tension and van der Waals forces, is included in the problem description?

We demonstrated that a simple hydrodynamic thin film model that includes surface tension and van der Waals forces and that allows for film drainage by incorporating a curvature at the edge of the film, is sufficient to predict the dependency of the film dynamics and lifetime dependencies on the initial geometric features of the film. Our simulations revealed that the dynamics are distinctly different for films of small and large initial radii. The thinning dynamics of the latter are akin to that of semi-infinite films, evolving with a characteristic localized dimple. The film lifetimes for such films solely depend on the initial film thickness as per the scaling rule developed in chapter 2. For small radii films, which were the focal point of study in chapter 4, the film initially thins uniformly across the entire film radius, before developing a dimple, with the lifetime depending solely on the initial film radius. For such small radii films, we combined the early-stage dimple formation based on the self-similar scaling rules proposed by Frankel and Mysels[7] and a late-stage accelerated thinning that leads to rupture through van der Waals forces based on the self-similar scaling rules of Zhang and Lister[3]. We developed a theoretical model that describes the film lifetime as a function of initial radius, being independent of the initial film thickness. Our work in chapter 4 shows the drainage behaviour for a given initial film radius and film thickness, and relates these features to its lifetime.

5.2 Extensibility

In this section, we briefly discuss the extensibility of our work in a broader context. We mainly discuss how the current framework can be extended to include additional (repulsive) disjoining pressures in the film.

Inclusion of multiple disjoining pressures

For the discussion that follows, we re-iterate the central thin film equation that we have used in this thesis (for simplicity, we consider Cartesian coordinates):

$$\frac{\partial h}{\partial t} = -\frac{1}{3\mu}\left(\frac{\partial}{\partial x}\left(h^3\frac{\partial P}{\partial x}\right)\right) \tag{5.1}$$

with,

$$P = P_{\mathrm{st}} - P_{\mathrm{vdW}} = \gamma\frac{\partial^2 h}{\partial x^2} - \frac{A}{6\pi h^3}, \tag{5.2}$$

with μ, γ and A the fluid viscosity, interfacial tension and Hamaker constant, respectively. P, P_{st} and P_{vdW} correspond to total pressure, pressure due to surface tension forces and due to van der Waals forces in the thin liquid film, respectively. In this thesis, we have only used an attractive van der Waals component of the disjoining pressure in the theoretical and numerical description. We have used a power law to describe the dependency of the intermolecular forces between the two interfaces of the film on the film thickness. Other than this commonly used power law[8,9], several other functional forms of van der Waals pressure exist that consist of an exponential dependency[10,11], or a combination of power-law and exponential dependency on film thickness[12–14]. It is relatively straightforward to include one or a combination of these functional forms in the thin film equation in the pressure term. It would then lead to a different definition of κ than the one we have found (i.e. $\kappa = \pi h_o^3\gamma/Ar$) in this thesis.

Furthermore, in addition to van der Waals attraction forces, other interaction forces that include electrostatic repulsion and steric repulsion forces also exist when electrolytes and surfactants are present in the film and at the film interface. The contribution of these forces can also be added in the thin film equation, with their respective functional forms (exponential and power-law) that are available in the literature[15–17]. The pressure in the film is then given by

$$P = P_{\mathrm{st}} - P_{\mathrm{vdW}} + P_{\mathrm{el}} + P_{\mathrm{steric}} = \gamma \frac{\partial^2 h}{\partial x^2} - \frac{A}{6\pi h^3} + c_1 e^{-c2h} + \frac{c3}{h^9} \tag{5.3}$$

where P_{el} and P_{steric} correspond to the repulsive contribution to the disjoining pressure, arising from electrostatic and steric repulsion, respectively, with c_1, c_2 and c_3 being constants that depend on the surface charge and electrolyte concentration, and for which closed form expressions are available in the literature[17,18]. The addition of these two new disjoining pressures, followed by subsequent non-dimensionalization (using the scales used in chapters 2 and 3), results in the following two dimensionless parameters,

$$\alpha_1 = \frac{c_1}{A/2\pi h_o^3}; \ \alpha_2 = \frac{c_3}{Ah_o^6/2\pi} \tag{5.4}$$

in addition to the dimensionless parameter κ introduced earlier in this thesis. These new dimensionless parameters, α_1 and α_2 signify the relative contribution of these individual repulsion forces with respect to the attractive van der Waals forces, thereby making it possible to study this system for different process conditions.

5.3 Research opportunities

We conclude this chapter by discussing further research opportunities in (both planar and non-planar) thin liquid films.

5.3.1 Thermal nucleation in metastable films

As discussed in section §5.2, we can, in a relatively straightforward manner, add the contribution of electrostatic and steric repulsions in the pressure term in the thin film equation. Due to repulsive forces, these films do not rupture, but instead have equilibrium states. The balance between attractive van der Waals forces and repulsive electrostatic forces results in the formation of a thicker (≈ 30 nm) equilibrium state of the film. This equilibrium state is metastable. If sufficient energy is provided to overcome the energy barrier associated with this metastable state, the film thins further to an even thinner equilibrium state of the film (≈ 5 nm). These thicker and thinner equilibrium films are referred to as ‘Common black film’ (CBF) and ‘Newton black film’ (NBF), respectively in the literature[19,20].

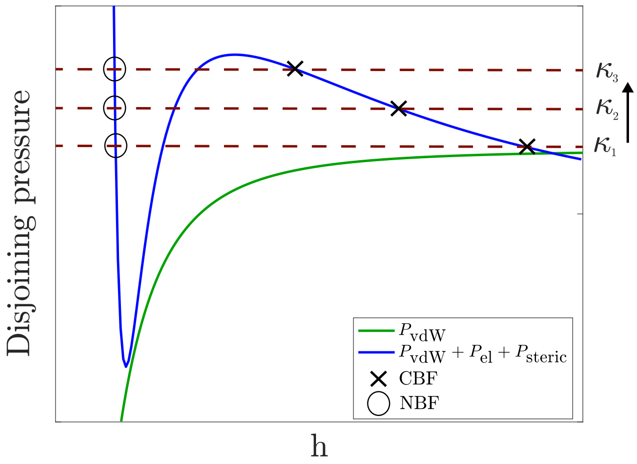

Figure 5.1 Disjoining pressure as a function of film thickness when only van der Waals forces (blue line) are included as the disjoining pressure and when all three contributions, viz., attractive van der Waals, repulsive electrostatic and repulsive steric forces are included in the disjoining pressure. Red dashed lines correspond to different values of suction pressure, κ. For three different suction pressures, there are three different set of film thicknesses where Common black films (crosses) and Newton black films (circles), respectively, are formed.

One of the common experimental techniques used to study the transition between CBF and NBF is a thin film balance technique, wherein an external suction pressure is applied to a film in CBF state[16]. This external pressure can be casted into the capillary pressure in the curved portion of the film that enables drainage of the film from the planar portion. This capillary pressure can in turn be expressed in dimensionless form as κ. The intersection of a certain value of κ with the disjoining pressure isotherm shown in Fig. 5.1[*] corresponds to equilibrium states of the film with CBF and NBF forming at larger and smaller film thickness, respectively. Increasing the external suction pressure, increases κ, and in turn decreases the energy barrier required to overcome the transition from CBF to NBF. The stochastic thin film framework developed in chapter 3 can be used to study how thermal fluctuations can cause nucleation events to enable this transition from CBF to NBF for different values of external pressure, κ. These findings could then be compared[21] to the experimental data-set from Casteletto et al.[16], and thereby provide a theoretical framework to describe these transitions from

---

[*] The equilibrium stable states are formed at the negative slopes of the disjoining pressure isotherm, i.e. when d(Disjoining pressure)/dh < 0. The third intersection which is at a positive slope of disjoining pressure isotherm is an unstable equilibrium state, and has, in fact, a higher energy state than either of the other two stable equilibrium states.

CBF to NBF.

5.3.2 Fundamental topics in planar thin liquid films

Here we discuss some of the interesting research opportunities in the context of planar thin liquid films that have not been covered in this thesis.

Planar thin films as a chaotic systems

Chaos is a certain behaviour of a system wherein infinitesimally small changes in the initial conditions lead to finite (significant) changes in the output[23]. Recent simulations[22] of planar thin liquid films (Eqs. 5.1 and 5.2, subjected to an initial condition of uniform thickness and to periodic boundary conditions) show conclusive evidence of such a chaotic behaviour. Multiple realizations of the film evolutions in which a planar film is perturbed with a white noise (of amplitude O($10^{-10}h_o$)), show that infinitesimally small changes in the initial condition can lead to finite significant changes in the final output (rupture time and morphology) at the instant of rupture. Fig. 5.2a shows different morphologies resulting from two such realisations of a planar film evolution. Although conclusive, this first study on the chaotic nature of planar thin film system is qualitative in nature. A quantitative analysis (for instance, using bifurcation theory and period-doubling analysis) that further substantiates chaotic nature of planar thin liquid films is yet to be conducted and seems to be an exciting research opportunity.

External forcing: facilitating order in chaos

Significant research[24] has been done to study planar thin film evolution in the presence of an external forcing in the last decade with an intent to better control the dynamics of planar thin films. Pattern formation, in the presence of periodic oscillations in lateral and vertical direction on the free interface of a planar thin film, has been a subject of study, albeit, for relatively thicker films (O (0.1 mm))[25,26]. For such thick films, van der Waals forces were neglected. Shklyaev et al.[27] demonstrated that the instability in the planar film can be controlled by the vertical oscillations on the film, when the time scale of oscillations is small in comparison to the time scale of the system. Additionally, many recent studies[28–30] have further substantiated the notion that an external forcing can be used to control the morphology of the planar films on solid substrates.

In order to evaluate whether an external forcing brings order to the chaotic behaviour of planar thin film system, a controlled external forcing term was added to the thin

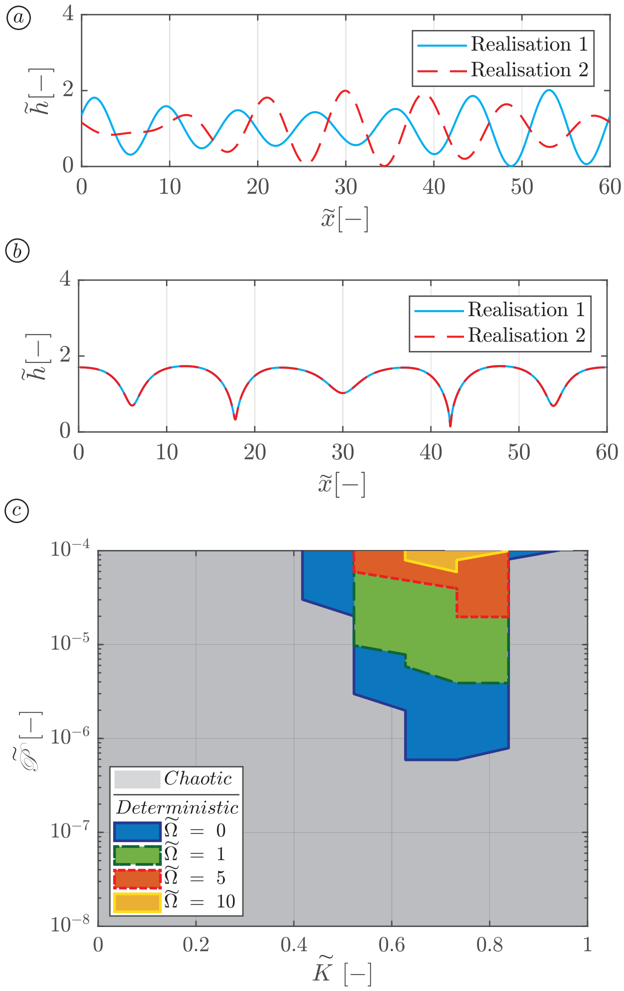

Figure 5.2 (a) and (b) Non-dimensional film thickness, $\tilde{h}$ as a function of the axial position $\tilde{x}$ for two different realisations of a planar film subjected to a (pseudo-)white noise (amplitude 10^{-10} smaller than the initial film thickness) as an initial condition. Evidence of (a) chaos in planar thin film systems without any external forcing and (b) deterministic morphology in planar thin films subjected to an external forcing. (c) Chaos elimination map delineating chaotic and deterministic regime for a particular choice of dimensionless forcing parameters. Figure from Pari[22].

film equation (Eq. 5.1 and 5.2). The resulting thin film equation is given by[22]

$$\frac{\partial h}{\partial t} + \frac{1}{3\mu}\left(\frac{\partial}{\partial x}\left(h^3\frac{\partial}{\partial x}\left(\gamma\frac{\partial^2 h}{\partial x^2} - \frac{A}{6\pi h^3}\right)\right)\right) = \frac{1}{3\mu}\frac{\partial}{\partial x}\left(h^3\frac{\partial}{\partial x}\left(F_{\text{ext}}\right)\right), \tag{5.5}$$

with,

$$F_{\text{ext}} = \mathscr{P} cos(Kx + \Omega t + \phi), \tag{5.6}$$

where F_{ext}, $\mathscr{P}$, K, Ω and ϕ are external forcing, amplitude, wavenumber, frequency and the original phase of the forcing, respectively. It was found (see Figs. 5.2b and 5.2c) that with the addition of an external forcing, the system became deterministic for a certain range of parameter space[22]. Determining such a parameter space enables better control of the film morphology for the same initial amplitude of a (pseudo-)random perturbation, thereby making the film evolution truly deterministic. Pari[22] studied the influence of the afore-mentioned forcing parameters in further eliminating chaos. To substantiate these results, the mathematical treatment of the elimination of chaos using dynamical systems and chaos theory[23] would be an interesting research opportunity.

Lastly, it would be interesting to explore whether it is possible to bring different cases of thin film systems subjected to external forcing, such as, chemically patterned substrates with periodic variation of heterogeneity on the solid substrate[31,32], or even films subjected to drainage (the subject of this thesis), under one broad generalized problem description and show equivalence between these specific cases.

Bibliography

[1] A. Oron, S. H. Davis, and S. G. Bankoff. Long-scale evolution of thin liquid films. Rev. Mod. Phys., 69(3):931–980, 1997. doi: 10.1103/RevModPhys.69.931.

[2] A. Aradian, E. Raphael, and P. G. de Gennes. Marginal pinching in soap films. Europhys. Lett., 55 (6):834–840, 2001. doi: 10.1209/epl/i2001-00356-y/fulltext/.

[3] W. W. Zhang and J. R. Lister. Similarity solutions for van der waals rupture of a thin film on a solid substrate. Phys. Fluids, 11(9):2454–2462, 1999. doi: 10.1063/1.870110.

[4] G. Grün, K. Mecke, and M. Rauscher. Thin-film flow influenced by thermal noise. J. Stat. Phys., 122(6):1261–1291, 2006. doi: 10.1007/s10955-006-9028-8.

[5] B. Davidovitch, E. Moro, and H. A. Stone. Spreading of viscous fluid drops on a solid substrate assisted by thermal fluctuations. Phys. Rev. Lett., 95:244505, 2005. doi: 10.1103/PhysRevLett.95.244505.

[6] M. T. Kreutzer, M. S. Shah, P. Parthiban, and S. A. Khan. Evolution of nonconformal landau-levich-bretherton films of partially wetting liquids. Phys. Rev. Fluids, 3:014203, 2018. doi: 10.1103/PhysRevFluids.3.014203.

[7] S. P. Frankel and K. J. Mysels. On the dimpling during the approach of two interfaces. J. Phys. Chem., 66(1):190–191, 1962. doi: 10.1021/j100807a513.

[8] V. S. Mitlin. Dewetting of solid surface: Analogy with spinodal decomposition. J. Colloid Interface Sci., 156(2):491 – 497, 1993. doi: 10.1006/jcis.1993.1142.

[9] A. L. Bertozzi, G. Grün, and T. P. Witelski. Dewetting films: bifurcations and concentrations. Nonlinearity, 14(6):1569–1592, sep 2001. doi: 10.1088/0951-7715/14/6/309.

[10] L. M. Pismen and Y. Pomeau. Disjoining potential and spreading of thin liquid layers in the diffuse-interface model coupled to hydrodynamics. Phys. Rev. E, 62:2480–2492, 2000. doi: 10.1103/PhysRevE.62.2480.

[11] M. Bestehorn and K. Neuffer. Surface patterns of laterally extended thin liquid films in three dimensions. Phys. Rev. Lett., 87(4):046101, 2001. doi: 10.1103/PhysRevLett.87.046101.

[12] A. Sharma and A. T. Jameel. Nonlinear stability, rupture, and morphological phase separation of thin fluid films on apolar and polar substrates. J. Colloid Interface Sci., 161(1):190–208, 1993. doi: 10.1006/jcis.1993.1458.

[13] P. Beltrame, E. Knobloch, P. Hänggi, and U. Thiele. Rayleigh and depinning instabilities of forced liquid ridges on heterogeneous substrates. Phys. Rev. E, 83:016305, 2011. doi: 10.1103/PhysRevE.83.016305.

[14] U. Thiele. Recent advances in and future challenges for mesoscopic hydrodynamic modelling of complex wetting. Colloid Surface A, 553:487–495, 2018. doi: 10.1016/j.colsurfa.2018.05.049.

[15] V. Bergeron. An introduction to forces and structure in individual foam and emulsion films. In Foams and Emulsions, pages 45–72. Springer, 1999.

[16] V. Casteletto, I. Cantat, D. Sarker, R. Bausch, D. Bonn, and J. Meunier. Stability of soap films: Hysteresis and nucleation of black films. Phys. Rev. Lett., 90:048302, 2003. doi: 10.1103/PhysRevLett.90.048302.

[17] J. N. Israelachvili. Intermolecular and surface forces. Academic press, 2015.

[18] H. J. Butt and M. Kappl. Surface and interfacial forces. Wiley Online Library, 2010.

[19] D. Exerowa, A. Nikolov, and M. Zacharieva. Common black and newton film formation. J. Colloid Interface Sci., 81(2):419 – 429, 1981. doi: 10.1016/0021-9797(81)90424-0.

[20] E. Ruckenstein and M. Manciu. On the stability of the common and newton black films. Langmuir, 18(7):2727–2736, 2002. doi: 10.1021/la011569w.

[21] D. Salaheddine. The influence of thermal fluctuations on the destabilization of thin liquid films. Master's thesis, Delft University of Technology, the Netherlands, 2018.

[22] A. Pari. Dynamics of thin liquid films subjected to an external forcing. Master's thesis, Delft University of Technology, the Netherlands, 2019.

[23] S. H Strogatz. Nonlinear dynamics and chaos with student solutions manual: With applications to physics, biology, chemistry, and engineering. CRC press, 2018.

[24] R. V. Craster and O. K. Matar. Dynamics and stability of thin liquid films. Rev. Mod. Phys., 81: 1131–1198, 2009. doi: 10.1103/RevModPhys.81.1131.

[25] M. Bestehorn. Laterally extended thin liquid films with inertia under external vibrations. Phys. Fluids, 25(11):114106, 2013. doi: 10.1063/1.4830255.

[26] M. Bestehorn, Q. Han, and A. Oron. Nonlinear pattern formation in thin liquid films under external vibrations. Phys. Rev. E, 88:023025, 2013. doi: 10.1103/PhysRevE.88.023025.

[27] S. Shklyaev, M. Khenner, and A. A. Alabuzhev. Enhanced stability of a dewetting thin liquid film in a single-frequency vibration field. Phys. Rev. E, 77:036320, 2008. doi: 10.1103/PhysRevE.77.036320.

[28] E. Sterman-Cohen, M. Bestehorn, and A. Oron. Rayleigh-taylor instability in thin liquid films subjected to harmonic vibration. Phys. Fluids, 29(5):052105, 2017. doi: 10.1063/1.4984082.

[29] E. Sterman-Cohen, M. Bestehorn, and A. Oron. Ratchet flow of thin liquid films induced by a two-frequency tangential forcing. Phys. Fluids, 30(2):022101, 2018. doi: 10.1063/1.5010262.

[30] S. Richter and M. Bestehorn. Direct numerical simulations of liquid films in two dimensions under horizontal and vertical external vibrations. Phys. Rev. Fluids, 4:044004, 2019. doi: 10.1103/PhysRevFluids.4.044004.

[31] A. Pototsky, M. Bestehorn, and U. Thiele. Control of the structuring of thin soft matter films by means of different types of external disturbance. Physica D, 199(1):138 – 148, 2004. doi: 10.1016/j.physd.2004.08.019.

[32] M. Vishal. Dynamics of thin films on chemically patterned substrates and the effect of thermal fluctuations on short-term morphologies. Master's thesis, Delft University of Technology, the Netherlands, 2019.

List of publications

Papers

[1] M. S. Shah, C. R. Kleijn, M. T. Kreutzer and V. van Steijn Influence of initial film radius and film thickness on the rupture of foam films Physical Review Fluids, under review.

[2] M. S. Shah, V. van Steijn, C. R. Kleijn, and M. T. Kreutzer Thermal fluctuations in capillary thinning of thin liquid films. Journal of Fluid Mechanics, 876, 1090-1107. doi: 10.1017/jfm.2019.595

[3] Y. Wang, S. Oldenhof, F. Versluis, M. S. Shah, K. Zhang, V. van Steijn, X. Guo, R. Elkema, and J. van Esch Controlled Fabrication of Micropatterned Supramolecular Gels by Directed Self-Assembly of Small Molecular Gelators. Small, 15 (8), 1804154. doi: 10.1002/smll.201804154

[4] M. T. Kreutzer, M. S. Shah, P. Parthiban, and S. A. Khan Evolution of nonconformal Landau-Levich-Bretherton films of partially wetting liquids. Physical Review Fluids, 3 (1), 014203. doi: 10.1103/PhysRevFluids.3.014203

Acknowledgements

As I come to the end of this thesis, I wish to thank all the people who made my PhD journey a wonderful experience.

First of all, I thank you, **Michiel**, **Chris** and **Volkert** for your contributions to my academic and personal growth during this journey. I must admit I was a bit intimidated to have progress meetings with all three of you. But very soon I started looking forward to attending them. These meetings did not only help me navigate through this thesis, but were also a lesson on different leadership styles. Thank you for providing me with opportunities to grow, both professionally and personally.

Michiel, I feel immensely fortunate to have you in my supervisory team because of your energy, ability to ask sharp questions and a strong grasp on the literature of thin films. Your analytical bent of mind and hypothesis-driven methodology has helped me tremendously in developing into a sound researcher. I will highly cherish our extensive brainstorming sessions during the last two summers, spontaneous meetings at the coffee machine and discussions on health and fitness over lunch.

Chris, thanks to your expertise in numerical methods, rigorous sanity checks have been incorporated in the numerical framework of this thesis. Your enthusiasm towards research and the pursuit to help young researchers grow, has been invaluable during this journey. Your timely feedback and constructive criticism, especially in the last few months, helped me bring my work to fruition and finish my thesis.

Volkert, the prospect of working with you was pivotal for me in choosing this project. From your very first MTP lecture during my MSc to the last meeting we had, my admiration and respect for you as a researcher and a kind human has only kept on increasing. I have enjoyed our weekly Tuesday morning meetings and discussions on MTP for preparing innovative exam questions. I highly value and aspire to emulate your subtle art of meting constructive criticism with a positive spin.

A special thanks to **Luis** and **Dries** for creating an inspiring research atmosphere during my MSc that also led me on the path to pursue a PhD. **Luis**, I have high regard for your ability to ask fundamental questions, as a result of which I had a chance to collaborate with you again during my PhD. Although it did not become a part of this thesis, I am very proud of what we learnt and discovered about planar thin films during our collaboration. Your penchant for providing guidance to students is second to none. I know that I can still count on you for any advice, be it my career or even taking a trip to Lisbon.

I would like to thank **Prof. Uwe Thiele**, **Prof. Jacco Snoeijer**, **Prof. Johan Padding** and **Prof. Kees Vuik** for their willingness to be in my committee and for their critical evaluation and approval of my thesis. I am grateful to you, **Prof. Thiele** for hosting me at your lab at the University of Muenster, and for discussions on planar thin liquid films. One of the ideas that originated from our discussions culminated into a MSc thesis. I am also thankful to **Prof. Jacco Snoeijer** for our fruitful discussions during FOM Physics 2019.

I wish to thank you, **Prof. Arnold Heemink**, for your guidance on how to numerically solve stochastic differential equations in the first year of my PhD. I am also very grateful to you, **Dr. Murali Ghatkesar**, for your collaboration and efforts in performing bubble coalescence experiments in Atomic Force Microscopy (AFM).

Getting things to work seamlessly would not have been possible if not for the support staff of **Astrid**, **Elly**, **Anita**, **Jennifer**, **Karin**, **Sandra** and **Leslie**. **Astrid**, had it not been for your efforts in organizing meetings with Michiel, Chris and Volkert, my PhD journey would not have been as smooth. **Elly**, thank you for organizing biweekly meets with Volkert and students. I will never forget your patience in listening to my Dutch, in all its spaghetti-*esque* syntactic glory. I would also like to take this opportunity to thank **Wim**, **Stefan**, **Marcel** and **Ruben** for their help in the brief time I spent doing experiments in the lab. Special thanks to **Marcel** for teaching me how to conduct AFM experiments. I would also like to thank **Edwin** and **Hans** at the ICT team for making sure our systems work seamlessly.

Over the years, I have had the opportunity and privilege to mentor many students. **Vincent**, I admire your enthusiasm in trying out a new numerical scheme for our stochastic simulations. **Djalil**, **Chih-Chia** and **Hongyu**, you joined the thin-films team together and it was an absolute pleasure to work with all three of you. **Djalil**, you carried the baton from Vincent and elevated the research on metastable thin films beyond our expectations. Your clarity of thought and intent to help others in the team is remarkable. **Chih-Chia**, you are extremely gifted in your coding skills, and I hope you are benefitting from it in your PhD. Thanks for inviting me over to Taiwanese cultural nights and for the special pineapple cakes from Taiwan! **Hongyu**, you took on the most difficult project I had to offer. I admire your skills in the lab and your persistence to understand how a process worked. **Manu** and **Arvind**, you joined the thin-films team during my final year. **Manu**, it was great to see your passion for dancing and the way you balanced and excelled at your thesis alongside it. **Arvind**, your project was a result of our collaboration with Luis. What a ride it was! With your curiosity, persistence and the ability to present complex concepts to a wider audience, an extremely rare and a historic perfect 10 as your thesis grade was very well deserved!

During my PhD, I had the privilege of being a part of two research groups - PPE and TP, and was always surrounded by great colleagues who also became good friends over the years. **Lea**, your dedication and focus towards research and for things that you care about, is so inspirational. **Serhii**, your steadfast Ukranian brand of *isms* will stay with me for a long time, most notably, the 5 minute rule. Thank you for helping me investigate the series of experimental papers on Scheludko-cells. **Dominik**, if not for you, how would I have completed the survival run! Thank you for keeping the group atmosphere lively. **Aswin**, it was always great to discuss theory with you. Also, thanks to you, we never needed a ChemE newsletter. **Damiano**, your warm personality and unbridled laughter were good company during those long weekend hours at the university. **Abhay**, I will always remember your voracious appetite for reading books and the *Band on the run* renditions when working on our assignments. **Hamid**, thank you for your help in guiding me with job applications. **Afshin**, your comments on writing good scientific papers were quite valuable. **Durgesh**, thank you for your help with interview preparations and introducing me to the golden ratio of butter to *pav bhaaji*. **Dayinta**, your help and guidance with AFM experiments were insightful to say the least. Also, thanks to you, *theplas* became the talk of the town. **Fabio**, your sense of humour stood out amongst all of us, and so did the lovely Christmas dinners! **Feilong** and **Fuweng**, thank you for the amazing dumplings that you cooked for us! **Erik**, thank you for taking the lead to represent PPE at the PhD council. **Samir**, **Hao**, **Georg**, **Isabell**, **Ruben**, **Zaid**, **Alvaro**, **Alessandro**, **Qian**, **Fatemeh**, **Albert**, **Aris**, **Aptem** and **Saeed**, our group was so much more vibrant because of you.

Ruud, thank you for providing a stimulating research environment at PPE and for being highly competitive at all the PPE outings. **Pouyan**, your friendly personality at group meetings and the funny anecdotes you shared at PPE outings were always refreshing. **Gabrie**, your ability to guide young researchers who wish to start a career in industry, is immensely helpful, thank you for sharing your wisdom. **Henk**, it inspires me how you keep fit with long bike rides to the university. **Peter**, it was always interesting to get Dutch history lessons from you. Thank you all for keeping PPE a cohesive group!

To all my friends at TP, coffee breaks and VriMiBo were always a treat. **Hrushi**, you were my go-to person for any thesis related questions in my first year of PhD. Thank you for always being ready to help out. **Chirag**, you are as helpful now, as you were back then when our times overlapped at Delft. Spending time at your place meant home-like comfort. The *sabzis* that you made have definitely kept up my spice tolerance. **Manas**, you are the most enterprising person I have met in my life. In your time away from all the travel, its amazing to see how you keep yourself busy learning something new. I will fondly remember our adventures at Cologne. **Manu**, I admire your helpful, humble and down to earth nature. **Elin**, thank you for the smart tips, particularly, in using the cluster. **Wenjie**, thank you for introducing me to *hua jiao* pepper at Sansan in Rotterdam. **Rudi**, thank you for helping me move my stuff back in 2015. **Annekatrien**, thank you for the speculaas, and for always being available to help. **Jorrit**, thank you, teaching ATP became a lot more fun and easier because of you. **Christiaan**, thank you for organizing board games and for helping me with my Dutch every now and then. **Kevin**, **Romana**, **Iman**, **Snehal**, **Fei**, **Saeid**, **Xiolin**, **Amin**, **Saidah**, **Peng**, **Pranav** and **Evert**, thank you for the amazing times at TP Christmas dinners and summer outings. **Lorenz**, **Matheus**, **Debashish**, **Kostas**, **Artem**, **Brice**, **Rose**, thank you for all the initiatives that you take to keep the TP group lively and vibrant.

Harry, it is very inspiring to see your enthusiasm towards research and education. **Rob**, I used to look forward to your puzzles during TP lunches. **David**, it was great to sometimes converse with you in Hindi and Dutch during ATP TA-ship. **Sasa**, **André** and **Valeria**, thank you for keeping our spirits high in TP at various group outings.

Shaurya, **Kartik** and **Prachi**, thank you for being my family away from home. **Shaurya**, from the times of *nasha* and *Science* to you becoming a health freak, I was happy to witness an inspiring story evolve right in front of me. Your passion for research and your *nasha*, be it food, books, music, even fitness, is contagious. I fondly remember our laid-back evenings at Bal-pol, legendary breakfasts and comfort dinners at Caspar Fagelstraat! Your presence all these years were a source of immense strength, belief to keep calm and motivation to carry on. That to me meant a lot. **Kartik**, I still remember the first time I met you in Pune at NCL, where you had a child-like researcher fervour to work on microfluidics. From being room-mates and then office-mates, we have always been together through thick and thin; thank you for being there. I will miss your characteristic squeak to call me and all the comedy references from the Indian stand-up scene. **Prachi**, please don't be too *jasbaati* when I say that you dragged us out of our departments to enjoy life outside. You are someone who goes the extra mile to get your close friends together to celebrate life. Your perceptive sense of humour and spot on imitations of Indian uncles and aunties will always bring a smile to my face.

Siddhartha, **Dries**, **Cees** and **Anand**, my book-club comrades, it's been a pleasure to discuss literature with you. **Siddhartha**, thanks for your persistent support and all the beautiful recommendations over the years, be it books, music, food and pursuits to follow. I will fondly cherish our times exploring chaos at the ever so calm *uit de kunst* cafe, and our love for Toko Idola that never subsides. Thank you for creating the beautiful artwork for the cover of my thesis. **Dries**, I feel incredibly lucky that I had you as my supervisor during my MSc, and as a friend during my PhD. I fondly remember your speech during my MSc graduation ceremony. I would like to believe that you are not bored of the *pav bhaaji* that I make, for I am not tired at all of the vegetarian *erwtensoep*, *stamppot* and the delicious cakes that you have fed me over the years. Many thanks for being so patient in teaching me Dutch, and for helping me out with the Dutch translation of my summary. **Cees**, your sense of humour made sure we always had fun along-side our "hard-core" literature discussion. Thanks for redefining *metre* for me at Ecast, and for the amazing pumpkin risotto at our very first literature club meets. **Anand**, thanks to you, uncle and aunty, I have missed home a little less all these years. I feel lucky to have spent so many enjoyable evenings at your house talking about everything under the sun and having a delicious South Indian dinner. Your characteristic laughter has always uplifted me.

Thomas, your passion for a sustainable lifestyle and being connected to nature is highly inspiring. Thank you for the spontaneous outings - bike rides during our MSc, walking Maja in the forests and miso night with your Japanese friends. Your enthusiasm for *chai* and creativity in bringing *suikerbuik* in an exam question is pretty cool. Thank you for introducing us to **Maja**. **Gijs**, I miss our boisterous evenings at Ecast. You were the perfect teammate during our MSc and I wish we could have continued that later as well. **Pieter**, your wit, ability to challenge and question established methods inspire me.

Rajat, **Rupali**, **Purvil** and **Sumit**, thank you for being so patient and selfless, and for being a great support system over the years. Those birthday parties and Indian festivities were so much more enjoyable owing to your efforts and enthusiasm to celebrate. **Lalit** and **Trinath**, it is always fun listening to all the anecdotes that you keep sharing. **Navin**, thank you for all your help in guiding me with the *inburgeringstoets*. **Robert**, your "hows the josh?" always made me smile. **Vaishnavi**, thanks for the amazing dinners and the *piece de resistance dal makhani*. **Chiara** and **Alexander**, thank you for keeping our, otherwise quiet office, quite entertained. Thanks **Chiara** for your tapas recommendations in Barcelona. Thank you, **Pavithra** and **Meera**, for some good humour during our encounters at the corridors of ChemE, and for inviting me to the Christmas dinner at your house. **Mogre** and **Swej**, thank you for keeping in touch after our MSc. **Tomasz**, I cannot thank you enough (and **Dominik**, thank you again!) for helping me make it to the finish line of the survival race and for keeping all of ours spirits high. **Samiya**, **Aparna** and **Aruna**, thank you for good memories from our MSc, and for taking the initiatives to keep in touch after our MSc.

Anne, thanks to you, I have found someone with whom I can enjoy watching and discussing test cricket. Thank you, for organizing the amazing road trip to the UK to watch the Champions Trophy semis and for the spectacular hike. **Aurélie**, thanks for keeping in touch and for your friendship over the years. **Ali**, thank you for teaching me best practices in numerical codes and for our collaboration over the years. **Nathan**, you are the best cook that I met during my stay at CF51. Thank you for teaching me how to make tarte tatin, vegetarian sushi, falafel, and most importantly, for the amazing dosas that you made for dinner. **Andrea**, thank you for being so patient while giving me piano lessons. Now that you are back to the Netherlands, I look forward to attending your concerts. **Tristan** and **Kostas**, thanks for being amazing buddies for our gardening adventures at the TU Delft greenhouse.

To my friends from UD, **Hersh**, **Mitesh**, **Prathamesh**, **Ashwini**, **Prachi** and **Manali**, thank you for being there by my side all these years. **Hersh**, thank you, for standing beside me like a brother in some very difficult times. **Mitesh**, you have an uncanny ability to spew words of wisdom after 4 am in the night. **Prathamesh**, there is never a dull moment when you are around. **Ashwini**, thank you for being so patient with me all these years in teaching me to move my hands and feet in coordination at *sangeets* of our friends. **Prachi**, thanks for giving sound advice for PhD, career and life. **Manali**, thank you for rooting for me all these years.

I would like to thank you, **Dhiren Sir**, **Chetan Sir** and **Meena Teacher**, for your unconditional love and teachings which have made me who I am. I am extremely grateful that I have the privilege to be one of your students. Thank you **Satish masa** and **Naina masi** for introducing me to *Pathshala*, and for the many kind conversations we have had. **Dhimant bhai**, thank you for the push to help me grow spiritually and for sharing your experiences. Thank you, **Atman** and **Vishal**, for your unwavering support. **Atman**, it is because of you and your planning that all of our trips are a source of happy memories for me. **Vishal**, thank you for being an epitome of kindness, and a source of wisdom, be it career or life itself. **Dilip**, thank you for being there to listen, and for your help in exploring different perspectives at critical junctures in my life. **Chintan**, thank you for organizing box cricket all these years, your commitment towards your pursuits is inspirational. **Ankur**, thank you for leading our *FAUJIS* group from the front, and for keeping our spirits high. **Jubin**, your gladiator-like cricketing shots always bring a smile to my face. Thank you **Kirtan**, **Suchit bhai**, **Dhilan bhai** and all the **Faujis** for the soothing conversations whenever we have met over these years. Special thanks to **Suchit bhai** for sharing your beautiful poems. **Unnati didi**, thank you for sharing all the fun stories in your school, and all the amusing acts that **Jinisha** comes up with.

Rajiv sir, **Manoj sir**, **Jagad sir**, **Sarla teacher** and to all my teachers from school, I am eternally grateful for your efforts in laying a strong foundation. **Ranade Sir**, **Pandit Sir** and **Bhagwat Sir**, thank you very much for being a huge source of inspiration over the years. Your work ethics and values will always stay with me. **Ranade Sir** and **Pandit Sir**, thank you for your recommendation to study in Delft, and to also providing me with a push to pursue a PhD.

Nisarg, thanks for your creative videos of our family gatherings; they always bring a smile to my face. **Moonmoon**, your contagious laughter and the funny nicknames you come up with, are so refreshing. **Darshil** and **Rajvi**, it is because of you, that I was assured that mummy and papa were having a good time back home. Thanks for being so perceptive and for keeping a positive atmosphere back home. **Divya**, thank you for being so kind to send me *raakhis* all these years. **Mankuvar Ba**, your resolve and grit in raising a huge family on your own is highly inspirational. Any trip to India

without spending time with you is incomplete. **Ba** and **dada**, you would have been the happiest, among all, to hold this thesis. All of your blessings have shaped me into what I am today.

Bhavyank, not many people are aware of the strength behind your eternally calm and ever smiling face. Without your emotional and moral support and deeply caring personality, I would not have come this far. You are a great younger brother and I look up to you. **Bhakti**, thank you for your love and support and for the constant reassurance that I was never alone in this obsession of thin films. I admire your ability to diffuse seemingly tough situations, it gives me immense courage to face them. **Mummy**, **Papa**, I am not equipped with words to express how grateful I am for you. Thank you for leading by example and teaching me that a good measure of realizing meaning in life is to live for someone else's happiness. This thesis is no less an outcome of your sacrifices and prayers and I would like to dedicate this thesis to both of you.

Curriculum Vitae

Maulik Shah was born on 10th of September 1988, in Mumbai, India. He finished his primary and secondary education from Pune Vidya Bhavan in 2004 and higher secondary education from Ramnarian Ruia College in 2006, both in Mumbai. He went on to do a Bachelors in Chemical Engineering from the Institute of Chemical Technology (ICT), in Mumbai, graduating in 2010. He then worked as a technical (CFD) consultant at Tridiagonal Solutions Pvt. Ltd. in Pune, India.

Thereafter, he went back to the university at TU Delft in 2013 for a Masters in Chemical Engineering. During his Masters, he worked in the Transport Phenomena research group for his MSc thesis on the experimental determination of the rheology of aqueous foams and graduated with honours in June, 2015. Maulik then joined the Product and Process Engineering and Transport Phenomena research groups as a PhD student in October 2015, in the Department of Chemical Engineering, TU Delft. Here he worked on the dynamics of non-planar thin liquid films, that are for instance, found between bubbles in foams, under the supervision of his promotors Prof. Michiel Kreutzer and Prof. Chris Kleijn and Dr. Volkert van Steijn as his daily supervisor.